High Latitude Influences on Eastern Equatorial Pacific Climate Evolution Since the Pliocene

By

Kristin M. Kimble

M.Sc. Brown University, Providence, RI, 2021

B.A. Middlebury College, Middlebury, VT, 2019

A dissertation submitted in partial fulfillment of the requirements for the degree of Doctor of Philosophy in the Department of Earth, Environmental, and Planetary Sciences at Brown University

Providence, Rhode Island, USA

October 2024

© Copyright 2024 by Kristin M. Kimble

This dissertation by Kristin Kimble is accepted in its present form by the Department of Earth, Environmental, and Planetary Sciences as satisfying the dissertation requirement for the degree of Doctor of Philosophy.

Date 8/20/24

Timothy Herbert, PhD, Advisor

Recommended to the Graduate Council

Date 8/20/24

James Russell, PhD, Reader

Date 8/20/24

Steven Clemens PhD, Reader

Date 8/20/2024

Colleen Dalton, PhD, Reader

Date 20 Aug 2024

Heather Ford, PhD, External Reader

Approved by the Graduate Council

Date

Thomas Lewis, Dean of the Graduate School

CURRICULUM VITAE

Kristin M. Kimble

EDUCATION

Ph.D. in Earth, Environmental, and Planetary Sciences, Brown University, 2024
Advisor: Timothy Herbert

M.Sc. in Earth, Environmental, and Planetary Sciences, Brown University, 2021
Advisor: Timothy Herbert

B.A. in Geology high honors, **B.A. in Biology**, summa cum laude, Middlebury College, 2019
Advisor: Jeffrey Munroe

PUBLICATIONS

1. **Kimble, K. M.**, Herbert, T. D., & Jones, C. A. (2024). Pliocene weakening of gradients in temperature but not in productivity in the eastern equatorial Pacific. *Paleoceanography and Paleoclimatology, 39*(3), e2023PA004711. https://doi.org/10.1029/2023PA004711.
2. Munroe, J., **Kimble, K.**, Spötl, C., Marks, G. S., McGee, D., & Herron, D. (2021). Cryogenic cave carbonate and implications for thawing permafrost at Winter Wonderland Cave, Utah, USA. *Scientific Reports, 11*(1) 1-9. https://doi.org/10.1038/s41598-021-85658-9.

MANUSCRIPTS IN PREPARATION

1. **Kimble, K. M.** & Herbert, T. D. High latitude oceanic tunnel controls of eastern equatorial Pacific surface temperature and productivity since the Pliocene. In preparation, *Geophysical Research Letters*.
2. **Kimble, K. M.** & Herbert, T. D. Thermocline steepening and shoaling in the eastern equatorial Pacific since 3.5 Ma. In preparation.

CONFERENCE ABSTRACTS (* denotes presenting author)

1. Wilk, K. A.*, Prilipko Huber, O., Razionale, D., Bowers, S., Shabtian, H., **Kimble, K.**, Lo Piccolo, A., Mason, A. Krueger, H. Garelick, S., & Sully, C. (2024). DEEPS CORES: Bridging the Gaps of Earth and Planetary Science Education in Providence Public School District. *LPSC 2024 (The Woodlands, TX)*, poster presentation.
2. **Kimble, K. M.*** & Herbert, T. D. (2023). Plio-Pleistocene Development of Strong Sea Surface Temperature Gradients Across the Eastern Equatorial Pacific Influenced by High-Latitude Forcings. *AGU 2023 (San Francisco, CA)*, oral presentation.
3. **Kimble, K. M.*** & Herbert, T. D. (2023). Organic Proxy- and Satellite-Derived Estimates of Ocean Temperature and Productivity. *Rhode Island Space Grant Consortium 2023 (Newport, RI)*, poster presentation.
4. **Kimble, K. M.*** & Herbert, T. D. (2022). Pliocene Weakening of Gradients in Temperature but not in Productivity in the Eastern Equatorial Pacific. *AGU 2022 (Chicago, IL)*, oral presentation.
5. Garelick, S.*, **Kimble, K.**, Russell, J. B., Lark, L., Mason, A., Muñoz, S., & Prilipko Huber, O. (2022). Introducing High School Students in Providence, Rhode Island to Research and Careers in Earth Science. *AGU 2022 (Chicago, IL)*, poster presentation.

6. **Kimble, K. M.*** & Herbert, T. D. (2021). Eastern Equatorial Pacific Surface Temperatures and Productivity Gradients During the Warmer Pliocene. *AGU 2021 (New Orleans, LA)*, poster presentation.
7. **Kimble, K.***, Munroe, J., Walcott, C., & Herron, D. (2019). Investigation of Cryogenic Cave Carbonates from Winter Wonderland Cave, Uinta Mountains, Utah, USA. *EGU 2019 (Vienna, Austria)*, poster presentation.
8. Munroe, J.*, Marks, G. S., **Kimble, K.**, McGee, D., Spötl, C., & Herron, D. (2019). A Preliminary Stable Isotope Record of Six Interglaciations from Whiterock Cave, Utah, USA. In *EGU 2019 (Vienna, Austria)*, poster presentation.

INVITED ORAL PRESENTATIONS

1. **Kimble, K.** (2024). Polar Influences on Tropical Pacific Climate Evolution over the Last Three Million Years. *Earth and Climate Sciences Seminar, Middlebury College (Middlebury, VT)*, invited oral presentation.

FIELD EXPERIENCE AND WORKSHOPS

Gulf of Papua Workshop on Scientific Ocean Drilling (March 14 - 18, 2023)
U.S. Science Support Program, University of Arizona Biosphere 2
Alpha Crucis (April 29 - May 6, 2022)
IODP Training on board the Alpha Crucis, University of São Paulo, Brazil

TEACHING EXPERIENCE

Lead Instructor, Fire and Ice: A Journey Through Rhode Island's Climate History (STEM for Rising 9th and 10th Graders, Pre-College Programs, Brown University), Summer 2023
Teaching Assistant, Spring Break Field Trip to Death Valley, CA (DEEPS, Brown University), March 2023
Teaching Assistant, Earth Processes (DEEPS, Brown University), Fall 2021
Teaching Assistant, Stratigraphy and Sedimentation (DEEPS, Brown University), Fall 2020
Teaching Assistant, Geology of Climate Change (Geology Department, Middlebury College), Spring 2019
Teaching Assistant, Bedrock Geology of Vermont (Geology Department, Middlebury College), Fall 2018

TEACHING CERTIFICATES

Certificate II: Sheridan Course Design Seminar (Sheridan Center for Teaching and Learning, Brown University), Spring 2023
Certificate I: Sheridan Teaching Seminar in Reflective Teaching (Sheridan Center for Teaching and Learning, Brown University), Fall 2020

HONORS, AWARDS, AND GRANTS

2023 Graduate Student Council Conference Travel Fund, Brown University ($300)
2023 Graduate School Conference Funding, Brown University ($650)
2023 IBES Research, Training, and Travel Award, Brown University ($2,800)
2023 Presidential Award for Excellence in Teaching, Brown University ($500)

2022 Graduate Student Council Conference Travel Fund, Brown University ($300)
2022 Graduate School Conference Funding, Brown University ($650)
2022 NASA Rhode Island Space Grant Consortium (summer stipend funding)
2022 Doctoral Research International Travel Grant, Brown University ($700)
2021 Graduate Student Council Conference Travel Fund, Brown University ($300)
2021 Graduate School Conference Funding, Brown University ($650)
2021 GSA Graduate Student Research Grant ($2,400)
2020 IBES Research, Training, and Travel Award, Brown University ($5,557)
2019 Award for Excellence in Student Research, Council on Undergraduate Research
2019 Student Academic Conference Travel Fund, Middlebury College
2019 Senior Research Project Supplement, Middlebury College ($1,000)
2017-9 All-Academic list, New England Small College Athletic Conference
2016 First-Year Explore Grant, Middlebury College ($1,000)
2016-9 College Scholar, Middlebury College

MENTORING

Claire Xu (Brown ’27), Spring - Summer 2024
Liam Johnson (Brown ’26) Fall 2023 - Spring 2024
Max Ferguson (Brown ’24), *senior thesis student*, Fall 2022 - Spring 2024
Jonathan Zhao (Brown ’27), Fall 2023 - Spring 2024
Rocky Mattos-Canedo (Brown ’26), Fall 2023 - Spring 2024
Anjali Shah (Brown ’25), Fall 2022 - Summer 2023
Omeed Siadati (UC Berkeley ’27), Summer 2022
Duncan Jurayi (Brown ’24), Fall 2021 - Spring 2022

SERVICE TO THE DEPARTMENT AND COMMUNITY

Representative Department Faculty Meetings, 2022 - 2024
Mentor First-Year Graduate Students, 2022 - 2024
Co-coordinator Department High School Research and Outreach Program, 2021 - 2024
Co-coordinator Department Elementary School Outreach Program, 2021 - 2023
Representative Sheridan Center for Teaching and Learning, 2021 - 2023
Speaker Research Matters, Brown University, 2022
Panelist and presenter, A Look at the UN IPCC Climate Report, Brown Family Weekend, 2021
Treasurer Department Graduate Student Geology Club, 2020 - 2021

OTHER PROFESSIONAL EXPERIENCE

Undergraduate Research Assistant, Department of Geology, Middlebury College, Advisor: Dr. Jeffrey Munroe, 2018 - 2019
Undergraduate Researcher, Department of Earth, Atmospheric and Planetary Sciences, Massachusetts Institute of Technology, Advisor: Dr. David McGee, 2018
Intern with State Aquatic Ecologist, Massachusetts Division of Fisheries and Wildlife, Advisor: Dr. Peter Hazelton, 2018 and 2016
Undergraduate Research Assistant (REU), Department of Biology, University of Massachusetts Boston, Advisor: Dr. Jarrett Byrnes, 2017

ACKNOWLEDGEMENTS

I received significant scientific and moral support from many people over the course of my PhD. I would first like to thank my advisor, Tim Herbert, for sharing his expertise and enthusiasm for paleoceanography and for his constant encouragement. He has advocated for me in large and small ways that have proved invaluable as I begin my scientific career. I also would like to thank the members of my dissertation committee, Jim Russell, Colleen Dalton, Steve Clemens, and Heather Ford, as well as past members of my advisory and preliminary exam committees, Baylor Fox-Kemper and Jung-Eun Lee. My committee members generously shared their time and resources with me over the last five years, and they provided thoughtful insight and research advice that challenged me to improve my science communication skills.

I have had the privilege of working with several undergraduate student researchers who assisted me in the lab. I owe a big thank you to J.B. Novak, Veronica Gordon, Duncan Jurayi, Anjali Shah, Max Ferguson, Liam Johnson, Rocky Mattos-Canedo, Jonathan Zhao, and Claire Xu for their diligent efforts with lab work. The many hours they spent washing, picking, and cleaning foraminiferal samples made the fourth and fifth dissertation chapters possible.

I have found myself thinking countless times over the last five years how lucky I was to end up at Brown, surrounded by incredible people and opportunities. Thank you to the many people who have made my PhD so rewarding, including TDH lab members Anson Cheung, Bryce Mitsunaga, Jared Nirenberg, Brianna Hoegler, Allison Jacobel, Weimin Si, Jamie Pahigian, and Nuri van Dommelen. I have benefited from their camaraderie while confronting lab work challenges, and from their thoughtful feedback during lab meetings.

I am grateful for the wonderful colleagues and friends I have met through the DEEPS community, including the office staff, lab managers, graduate students, and professors I have had

the pleasure of working with. I extend special thanks to Olga Prilipko Huber for introducing me to the rewards and challenges of teaching in the earth sciences, and for being a compassionate pedagogical mentor. Meredith Parish was a fantastic officemate, and she cheerfully served as my sounding board for myriad research and life questions. I appreciate the continuing friendship of other DEEPS graduate students, and I look forward to seeing them thrive at Brown and beyond.

Finally, I would like to thank my family for their everlasting support and investment in my goals. My parents encouraged me to expand my ambitions and gave me the freedom and tools to follow my passions. My sisters, Sara and Kathryn, have been lifelong confidants and kept me focused on the bigger picture. I thank my extended family for supporting me from around the country. A final thanks to my husband, Thomas, for his unwavering dedication as he saw me through the highs and lows of graduate school.

TABLE OF CONTENTS

LIST OF TABLES

LIST OF FIGURES

CHAPTER 1

Introduction

Kristin M. Kimble[1]

[1]Department of Earth, Environmental, and Planetary Sciences, Brown University, Providence, Rhode Island, 02912, USA.

Overview

This dissertation comprises a paleoceanographic study of the evolution of the eastern equatorial Pacific Ocean from the Late Miocene to the present. This time span saw considerable global climate evolution from a warmer world that sustained permanent ice cover on a single pole to the colder world of the Late Pleistocene marked by bipolar glaciation. The work presented here evaluates processes that changed ocean surface and subsurface temperature, east-west temperature gradients, surface and subsurface biological productivity and nutrient gradients, and deep water properties.

1. Ocean's role in regulating global climate

Earth's oceans possess over 1,000 times the heat capacity of the atmosphere (Schmitt, 2018) and have absorbed over 90% of warming generated through anthropogenic carbon dioxide (CO_2) emissions over the last several decades (Rhein et al., 2013). The modern ocean acts as a sink for up to 30% of anthropogenic carbon, and the ocean's ability to regulate atmospheric CO_2 in past climate states has resulted in glacial-interglacial climate variability (Fischer et al., 2010). In tropical upwelling zones like the eastern equatorial Pacific Ocean (EEP), cold subsurface water outcrops at the surface, producing a net transfer of heat from the atmosphere into the ocean. The heat uptake and CO_2 regulation capabilities of upwelling zones are particularly important as global climate warms in the coming decades (Marshall & Zanna, 2014).

The influx of colder subsurface water rich in dissolved nutrients upwelled to the EEP surface fuels among the highest surface primary productivity of photosynthetic marine organisms in the global oceans (Chavez & Barber, 1987). Although primary productivity removes dissolved CO_2 in the surface ocean, deeper decomposition of large volumes of sinking organic matter and

warming of recently ventilated subsurface waters releases CO_2, making the high-nutrient low-chlorophyll EEP region responsible for the largest yearly marine CO_2 flux into the atmosphere relative to other areas of the ocean (Takahashi et al., 1997). In addition to global carbon cycle contributions, phytoplankton also comprise the base of the marine food web, serving as food sources for higher trophic level organisms important to EEP fisheries (Pennington et al., 2006). The herring, anchovy, and tuna fisheries support over a million jobs in countries bordering the eastern Pacific and make up ~10% of global fisheries (Clarke et al., 2021). The future of EEP fisheries remains uncertain in the face of anthropogenic climate change which has altered surface temperature, upwelling, and primary productivity (Clarke et al., 2021).

There is no precedent within the history of human civilization for global average temperature projected by the end of the 21st century (Noguer et al., 2002). We look to paleoceanographic records to locate analogs for Earth's projected future climate like the Pliocene Epoch (5.3-2.6 Ma), given that anthropogenic climate change will drastically alter global climate over the next generation. The historical record of marine conditions is spatially and temporally limited relative to terrestrial records (Lundstad et al., 2023), so we rely on proxy reconstructions of ocean temperature and biological productivity from a warmer period in Earth's history to inform future climate projections. Constraining eastern tropical Pacific temperature and productivity changes over the last several million years is critical given the region's ability to counteract anthropogenic warming as well as its globally important fisheries (Clarke et al., 2021; Rhein et al., 2013).

2. Modern tropical Pacific setting

2.1 Eastern equatorial Pacific oceanography

The modern EEP is marked by strong east-west (zonal) gradients in sea surface temperature (SST) and surface primary productivity. Easterly winds drive water away from coastal South America and allow cold and nutrient-rich water to upwell from intermediate depths in the eastern EEP, supporting high biological productivity in a tongue of cold water that extends into the central Pacific. As upwelling increases toward the eastern EEP, the thermocline shoals to a depth of ~50 m relative to the ~100 m thermocline depth of the western Pacific (Jakob et al., 2018). The asymmetry of the EEP thermocline and upwelling generates large modern gradients in temperature, nutrients, and productivity that enhance the signal to noise ratio of climate parameters measured on either side of the EEP.

El Niño-Southern Oscillation (ENSO) dominates modern tropical Pacific temperature and upwelling patterns on 2-7 year timescales (Cane, 2005; Wang et al., 2017). The significantly weakened easterly winds, reduced EEP upwelling velocity, flattened and deepened EEP thermocline, reduced east-west SST gradient, and diminished EEP productivity characteristic of El Niño events affect not only local tropical climate, but extratropical regions as well (Stan et al., 2017). Weakened Walker circulation results in eastern Pacific convection while the western Pacific experiences drought, and global atmospheric reorganization influences weather patterns as far as the eastern USA through teleconnections (Pielke & Landsea, 1999; Yu et al., 2012).

Water upwelling in the EEP originates in high southern and northern latitudes where average conditions are colder and nutrient concentrations are higher because phytoplankton cannot utilize all preformed nutrients brought to the euphotic zone through weak vertical density gradients (Sigman & Hain, 2012). Remineralized nutrients also accumulate on the transit from the high latitudes to the EEP as sinking organic matter decomposes in the water column (Rafter et al., 2012). Most EEP upwelled water comes from the South Pacific and Southern Ocean

(**Figure 1**) in the form of nitrate- and phosphate-rich (but silicate-deplete) Subantarctic Mode Water (SAMW) and Antarctic Intermediate Water (AAIW). SAMW forms in a band in the Subantarctic Zone when late winter temperatures cool surface water enough to subduct (McCartney, 1979). It flows northwest from its formation regions at water depths between ~300-600 m before traveling eastward across the equatorial Pacific subsurface and upwelling in the EEP (McCartney, 1979; Qu et al., 2009; Rintoul & England, 2002; Toggweiler et al., 1991). AAIW also forms in the Southern Ocean, with the main formation region positioned west of the Drake Passage where the coldest and densest SAMW mix with Antarctic Surface Waters (Bostock et al., 2010). AAIW then flows northwest from its formation region at depths greater than ~600 m before contributing to Equatorial Pacific Intermediate Water and flowing eastward along the equator to upwell in the EEP (Bostock et al., 2010, 2013; Herraiz-Borreguero & Rintoul, 2011; McCartney, 1979). A smaller portion of upwelled EEP water comes from North Pacific Intermediate Water (NPIW) forming east of Japan (Talley, 1993; Yasuda, 1997). In addition to being nitrate- and phosphate-rich, NPIW almost exclusively supplies silicate to the EEP (Sarmiento et al., 2004).

The process of transporting physical and biogeochemical water properties that formed at high latitudes to the tropics is oceanic tunneling (Liu & Alexander, 2007; Liu & Yang, 2003), where SAMW, AAIW, and NPIW flow at intermediate water depths eastward across the equator and shape the temperature and nutrient concentrations of upwelled EEP waters (**Figure 1**).

2.2 Top-down and bottom-up climate forcings

Several local and distal climate processes influence EEP temperature and productivity gradients. Note that over Plio-Pleistocene timescales, these processes are equilibrated and play

out over longer time spans than modern ENSO variability, which dominates tropical Pacific climate dynamics today. Following Bolton, Gibbs, et al. (2010), we have characterized these processes into top-down forcings, which affect EEP conditions through the atmosphere, and bottom-up forcings, which govern surface patterns through the EEP subsurface.

Amongst the top-down controls, decreasing atmospheric CO_2 concentrations since the Pliocene have cooled local ocean surface temperatures through the greenhouse effect (de la Vega et al., 2020; Foster et al., 2012). Zonal wind stress may have increased over the Plio-Pleistocene as zonal SST gradients strengthened, which would have increased upwelling velocity and intensified Walker circulation by linking atmospheric gradients to SST gradients through the Bjerknes feedback (Ravelo et al., 2004). Increasing meridional gradients in cloud albedo may have accompanied greater high-low latitude SST gradients that developed over several million years of global cooling, which could have strengthened zonal SST gradients across the EEP (Burls & Fedorov, 2014). Orbital variations govern insolation received in the tropics and alter global energy distribution, making orbital changes ultimately responsible for global ice volume (Hays et al., 1976). Obliquity cycles occurring at 41-kyr intervals are mostly associated with high latitude changes because high latitude insolation variability increases significantly with a larger obliquity while tropical seasonality remains small (Liu & Herbert, 2004). Changes in 23- and 19-kyr precession cycles prompt atmospheric circulation and hydrologic responses at low latitudes, altering zonal and meridional atmospheric heating gradients (Clement et al., 2004).

Bottom-up processes that influence EEP temperature and productivity include high latitude source water properties transmitted through the oceanic tunnel to the EEP subsurface (Bolton, Lawrence, et al., 2010; Dekens et al., 2007; Fedorov et al., 2006; Lee & Poulsen, 2005; Philander & Fedorov, 2003). This dissertation discusses how Plio-Pleistocene cooling of high

latitude formation regions of SAMW, AAIW, and NPIW may have allowed the oceanic tunnel to transport cooler water to the base of the EEP thermocline. Likewise, changes in source water nutrient concentrations or the proportions of different water bodies feeding nutrients to the EEP subsurface may have governed EEP productivity and nutricline evolution. Paleo-proxy reconstructions are best explained by high latitude oceanic tunnel forcings of tropical Pacific climate, rather than top-down forcings that affect local variability.

This dissertation assesses the top-down and bottom-up controls on EEP SST and productivity evolution over the last several million years using geochemical signals preserved in marine sediment cores in a transect along the modern EEP cold tongue.

3. Eastern equatorial Pacific paleoclimate

3.1 Existing paleoclimate reconstructions

Although several paleoclimate records reconstructing SST gradients between the eastern and western tropical Pacific exist (Dekens et al., 2007; Fedorov et al., 2006; Ravelo et al., 2006; Wara et al., 2005), they rely on different proxies to estimate temperatures in the western Pacific warm pool versus the EEP. Mixing proxies at different sites often results in contradictory paleoclimate interpretations: i.e., whether Pacific zonal SST gradients weakened (Ford et al., 2015; Ravelo et al., 2004, 2006; Wara et al., 2005) or remained stable (O'Brien et al., 2014; Zhang et al., 2014) during the Pliocene. Cross-Pacific productivity reconstructions spanning the Pliocene to modern are even more rare, especially at orbital resolution (Dekens et al., 2007). Few studies synthesize temperature and productivity data from an equatorial transect of sites in the EEP, despite the strong zonal gradients eliciting high signal to noise in measurements. The reconstructions in this dissertation reflect long downcore records with high temporal and spatial

resolution of EEP SST using the same proxy, surface productivity, and subsurface temperature and nutrient availability spanning the Pliocene to modern. The work presented here contributes novel insights into EEP zonal surface and subsurface temperature and productivity gradient evolution in the context of high latitude controls on tropical climate. All newly generated data will be archived through an online data publisher so they are publicly available.

3.2 Ocean surface paleo-reconstructions

This doctoral dissertation examines how EEP temperature and productivity gradients evolved from the Pliocene to modern. We first constrained EEP SST and productivity patterns during the Pliocene to assess if our proxies agreed with other tropical Pacific paleoclimate reconstructions during a globally warmer time in Earth's past. We used alkenone palaeothermometry to reconstruct SST, which relies on biomarkers synthesized by phytoplankton in the ocean mixed layer (Herbert, 2014). The alkenone $U^{k'}_{37}$ index measures the degree of unsaturation of alkenone molecules, which is strongly correlated with temperature where more saturated alkenones with fewer double bonds between carbon atoms are produced under warmer conditions (Herbert, 2014; Müller et al., 1998). The total concentration of C_{37} alkenones (C_{37} total) shares strong positive correlations with both surface chlorophyll and marine export productivity (Raja & Rosell-Melé, 2021), and we interpret the C_{37} total index as a productivity proxy. Before assessing the forcings that drove EEP climate change over the last several million years, we first reconstructed mean state conditions during the Pliocene and modern.

Chapter 2 presents alkenone biomarker and X-ray fluorescence (XRF) elemental reconstructions of Pliocene (3.0-3.6 Ma) SST and productivity relative to modern from four

Ocean Drilling Program sites in a transect across the EEP (Kimble et al., 2024). Analyses of core top sediments from 44 EEP sites and comparison to observed modern ocean conditions supported the use of alkenone proxies for EEP paleoclimate reconstructions because the proxies successfully captured modern zonal gradients: core top alkenone SST strongly correlated with observed modern SST and alkenone C_{37} total mass accumulation rates (MAR) reflected satellite chlorophyll estimates. We applied the alkenone proxies to Pliocene sediments to reconstruct downcore records at ~3-kyr resolution. We found that although Pliocene zonal gradients were greatly reduced (0.9°C as compared to 1.8°C today), productivity gradients remained as strong or stronger than modern, based on XRF calculations of biologically produced silicate and alkenone C_{37} total MAR. The Pliocene warming and increased productivity was most noticeable in the eastern EEP in the heart of the upwelling zone with the closest high latitude connections. This Pliocene pattern of decoupled temperature and productivity is opposite the modern El Niño pattern of tight coupling between warm and unproductive waters, suggesting that high latitude source waters were both warmer in the globally warmer Pliocene and more nutrient-rich, which could occur if source water initial nutrient content were higher and/or if older water upwelled.

After constraining SST and surface productivity gradients across the Pliocene EEP, we sought to identify the timing of the surface gradient evolution over the last 3.6 Ma in Chapter 3. We also considered the oceanographic processes and external climate forcings responsible for the transition from the decoupled SST and productivity of the Pliocene EEP to the modern tight coupling. Chapter 3 presents new orbitally resolved alkenone biomarker reconstructions of SST and productivity spanning four time windows of >300 kyr through the Plio-Pleistocene from four sites arrayed in an east-west EEP transect. We record continuous strengthening of zonal SST gradients throughout the Plio-Pleistocene as eastern EEP waters cooled, which supports previous

equatorial Pacific gradient reconstructions (Dekens et al., 2007; Lawrence et al., 2006; Ravelo et al., 2006; Wara et al., 2005). However, alkenone C_{37} total MARs indicate that the surface productivity gradient weakened from the Late Pliocene to modern, despite progressive cooling of upwelled water, suggesting that high latitude water sources delivered progressively more nutrient-depleted water though the oceanic tunnel over time. Obliquity cycles paced eastern EEP SST until the dominant 100-kyr cycles of the Late Pleistocene, providing further evidence of high latitude controls on EEP upwelling. The Pliocene decoupling of SST and productivity persisted into the Late Pleistocene as productivity gradients appeared to have evolved independently from SST gradients, indicating that warm waters could support high primary productivity (Dekens et al., 2007) and complicating the current understanding of both the Pliocene permanent El Niño and future changes to ENSO in the face of anthropogenic warming.

3.3 Ocean subsurface and deep water paleo-reconstructions

Surface temperature and productivity reconstructions only partially capture subsurface thermocline and nutricline dynamics, which prompted the exploration of subsurface water properties using planktic foraminiferal stable isotopic data presented in Chapter 4 and benthic isotopes in Chapter 5. Single-celled foraminifera live in the ocean surface and subsurface (planktic foraminifera) and on the seafloor (benthic foraminifera) and record water chemistry in their tests. More enriched foraminiferal oxygen isotope ratios ($\delta^{18}O$) correspond to globally colder conditions with greater ice volume (Spero et al., 2003), and more depleted planktic carbon isotopes ($\delta^{13}C$) reflect greater upwelling of water rich in nutrients and respired carbon (Claret et al., 2021; Spero et al., 2003). Combining planktic foraminiferal isotopic data with alkenone SST and productivity reconstructions provides independent estimates of surface and subsurface

temperature and nutrients, which we use to assess our Chapter 1 and 2 conclusions that high latitude cooling and depleted nutrient concentrations resulted in decoupled EEP SST and productivity.

In Chapter 4, we present planktic foraminiferal $\delta^{18}O$ and $\delta^{13}C$ measured on paired surface- and thermocline-dwelling species from two EEP sites spanning four time windows of >250 kyr through the Plio-Pleistocene. The combination of alkenone SST with surface and subsurface planktic $\delta^{18}O$ reveals signs of initial Northern Hemisphere high latitude glaciation beginning at ~2.72 Ma outcropping in the eastern EEP. A trend toward more enriched subsurface planktic $\delta^{13}C$ suggests that EEP nutrient availability diminished over the last 3.5 Ma, which is consistent with alkenone surface productivity records showing greater Pliocene EEP productivity decreasing toward modern (Kimble et al., 2024). Progressively enriched planktic $\delta^{18}O$ in the eastern EEP subsurface implies oceanic tunnels transferred cool high latitude waters to the EEP subsurface since 3.5 Ma, which shoaled and tilted the thermocline. Weakening vertical $\delta^{13}C$ gradients between surface- and subsurface-dwelling foraminifera suggest diminished available nutrients transported within the upwelled waters, which may have caused the EEP nutricline to deepen toward its modern position. The surface temperature and productivity gradient decoupling reported in previous chapters is mimicked in the subsurface based on the decoupled thermocline and nutricline evolution recorded in the planktic isotope data. A common thread in the surface and subsurface reconstructions is that high latitude ocean changes exert critical controls on EEP temperature, nutrients, and productivity.

Chapter 5 re-evaluates the Shackleton et al. (1995) benthic foraminiferal stable isotope record from the historically important Ocean Drilling Program Site 846, recognized as the gold standard of chronological correlations. However, we were unable to replicate the often-cited

structure in the original benthic isotope record, possibly due to analytical shortcomings, instrument malfunctions, reproducibility issues, and interspecies isotopic offsets in the original benthic isotope measurements. In Chapter 5, we present new benthic oxygen and carbon stable isotope analyses from Site 846 over a Late Miocene to Pliocene interval (~4.0-6.2 Ma), resolved to ~3-kyr to capture orbital variability. The new record was measured using updated analytical techniques (i.e., individual vial acidification rather than a common acid bath) and a single foraminifera genus (*Cibicidoides spp.*) instead of a dozen species. The new records exhibit roughly half the variance of the original data for both $\delta^{18}O$ and $\delta^{13}C$. Our updated benthic $\delta^{18}O$ record displays considerable intermittent offsets relative to the Shackleton et al. (1995) record (our record was 0.18‰ more enriched from 5.1-5.5 Ma but < 0.05‰ more enriched throughout the rest of the Late Miocene to Early Pliocene), but the two $\delta^{13}C$ records were within analytical error. Other global benthic records align more closely with the newly generated $\delta^{18}O$ and $\delta^{13}C$ reconstructions than the original estimates, and substituting the new data for the Shackleton et al. (1995) values in global benthic $\delta^{18}O$ stacks would substantially reduce the uncertainty in the benthic stacks. Inter-lab analytical artifacts may introduce significant uncertainty in global benthic isotope reconstructions, and we argue that revisiting historically important benthic records is worthwhile.

4. Conclusion

The data presented in this dissertation are united in the interpretation that high latitude processes have shaped EEP upwelling over the last several million years. We record high latitude signals through several proxies applied to marine sediment core paleoclimate archives, and we offer mechanisms to explain why bottom-up forcings with high latitude origins overwhelm local

tropical processes and top-down forcings. As global climate warms in the coming decades, the high latitudes are expected to experience the greatest change (Holland & Bitz, 2003). The results outlined in this dissertation indicate that the EEP will be far from immune to high latitude changes because oceanic tunneling connects tropical and high latitude regions. If the Pliocene does serve as an appropriate analog for global climate by the year 2100, then we expect the EEP thermocline would become deeper, warmer, and flatter due to upwelling of warmer waters, reducing the EEP's ability to absorb atmospheric heat. Warmer EEP waters may still support high surface primary productivity, as we observed in the equilibrated Pliocene mean state, but the crucial difference between anthropogenic climate change and the Pliocene lies in the exorbitant rate of modern warming.

Figures

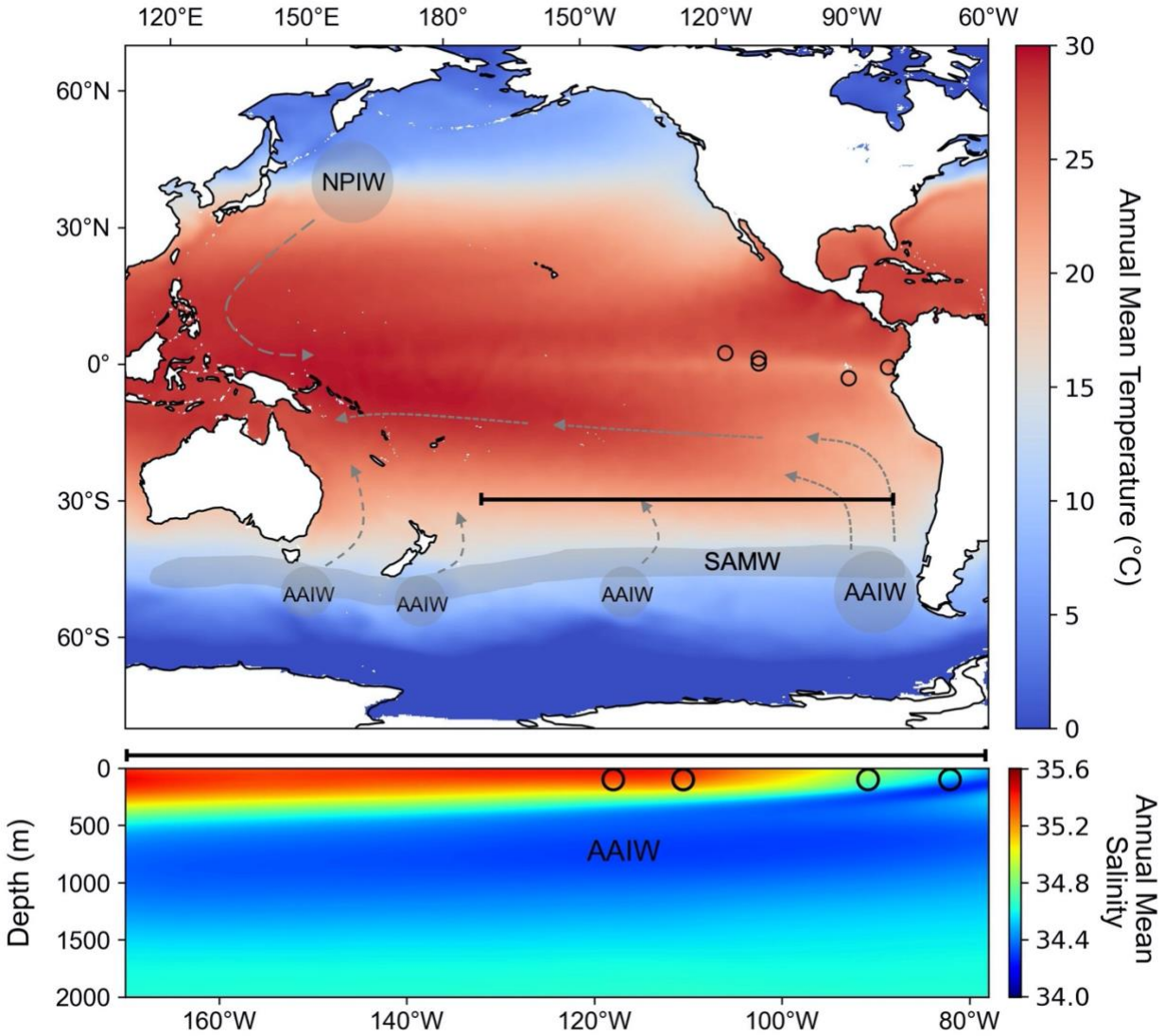

Figure 1. Approximate formation regions of intermediate waters that upwell in the EEP (top panel), after Bostock et al. (2013). Subantarctic Mode Water (SAMW) and Antarctic Intermediate Water (AAIW) supply a greater contribution of modern EEP water relative to North Pacific Intermediate Water (NPIW; Bostock et al., 2013). The salinity depth profile of an east-west transect at 30°S (black bar on map) shows the cool and relatively low salinity AAIW flowing northwest at >600 m water depth (bottom panel). Temperature data are from the World Ocean Atlas 2018 (Boyer et al., 2018; Locarnini et al., 2019) and salinity data are from the World Ocean Atlas 2023 (Reagan et al., 2024). Black circles in the EEP are the five downcore sites discussed in this dissertation.

References

Bolton, C. T., Gibbs, S. J., & Wilson, P. A. (2010). Evolution of nutricline dynamics in the equatorial Pacific during the late Pliocene. *Paleoceanography*, *25*(1). https://doi.org/10.1029/2009PA001821

Bolton, C. T., Lawrence, K. T., Gibbs, S. J., Wilson, P. A., Cleaveland, L. C., & Herbert, T. D. (2010). Glacial–interglacial productivity changes recorded by alkenones and microfossils in late Pliocene eastern equatorial Pacific and Atlantic upwelling zones. *Earth and Planetary Science Letters*, *295*(3–4), 401–411. https://doi.org/10.1016/j.epsl.2010.04.014

Bostock, H. C., Opdyke, B. N., & Williams, M. J. M. (2010). Characterising the intermediate depth waters of the Pacific Ocean using δ13C and other geochemical tracers. *Deep Sea Research Part I: Oceanographic Research Papers*, *57*(7), 847–859. https://doi.org/10.1016/j.dsr.2010.04.005

Bostock, H. C., Sutton, P. J., Williams, M. J. M., & Opdyke, B. N. (2013). Reviewing the circulation and mixing of Antarctic Intermediate Water in the South Pacific using evidence from geochemical tracers and Argo float trajectories. *Deep Sea Research Part I: Oceanographic Research Papers*, *73*, 84–98. https://doi.org/10.1016/j.dsr.2012.11.007

Boyer, T. P., García, H. E., Locarnini, R. A., Zweng, M. M., Mishonov, A. V., Reagan, J. R., Weathers, K. A., Baranova, O. K., Paver, C. R., Seidov, D., & Smolyar, I. V. (2018). *World Ocean Atlas 2018. Temperature* [Dataset]. NOAA National Centers for Environmental Information. https://www.ncei.noaa.gov/archive/accession/NCEI-WOA18

Burls, N. J., & Fedorov, A. V. (2014). Simulating Pliocene warmth and a permanent El Niño-like state: The role of cloud albedo. *Paleoceanography*, *29*(10), 893–910. https://doi.org/10.1002/2014PA002644

Cane, M. A. (2005). The evolution of El Niño, past and future. *Earth and Planetary Science Letters*, *230*(3), 227–240. https://doi.org/10.1016/j.epsl.2004.12.003

Chavez, F. P., & Barber, R. T. (1987). An estimate of new production in the equatorial Pacific. *Deep Sea Research Part A. Oceanographic Research Papers*, *34*(7), 1229–1243. https://doi.org/10.1016/0198-0149(87)90073-2

Claret, M., Sonnerup, R. E., & Quay, P. D. (2021). A Next Generation Ocean Carbon Isotope Model for Climate Studies I: Steady State Controls on Ocean 13C. *Global Biogeochemical Cycles*, *35*(4), e2020GB006757. https://doi.org/10.1029/2020GB006757

Clarke, T. M., Reygondeau, G., Wabnitz, C., Robertson, R., Ixquiac-Cabrera, M., López, M., Ramírez Coghi, A. R., del Río Iglesias, J. L., Wehrtmann, I., & Cheung, W. W. L. (2021). Climate change impacts on living marine resources in the Eastern Tropical Pacific. *Diversity and Distributions*, *27*(1), 65–81. https://doi.org/10.1111/ddi.13181

Clement, A. C., Hall, A., & Broccoli, A. J. (2004). The importance of precessional signals in the tropical climate. *Climate Dynamics*, *22*(4), 327–341. https://doi.org/10.1007/s00382-003-0375-8

de la Vega, E., Chalk, T. B., Wilson, P. A., Bysani, R. P., & Foster, G. L. (2020). Atmospheric CO 2 during the Mid-Piacenzian Warm Period and the M2 glaciation. *Scientific Reports*, *10*(1), Article 1. https://doi.org/10.1038/s41598-020-67154-8

Dekens, P. S., Ravelo, A. C., & McCarthy, M. D. (2007). Warm upwelling regions in the Pliocene warm period. *Paleoceanography*, *22*(3). https://doi.org/10.1029/2006PA001394

Fedorov, A. V., Dekens, P. S., McCarthy, M., Ravelo, A. C., deMenocal, P. B., Barreiro, M., Pacanowski, R. C., & Philander, S. G. (2006). The Pliocene Paradox (Mechanisms for a

Permanent El Niño). *Science*, *312*(5779), 1485–1489. https://doi.org/10.1126/science.1122666

Fischer, H., Schmitt, J., Lüthi, D., Stocker, T. F., Tschumi, T., Parekh, P., Joos, F., Köhler, P., Völker, C., Gersonde, R., Barbante, C., Le Floch, M., Raynaud, D., & Wolff, E. (2010). The role of Southern Ocean processes in orbital and millennial CO2 variations – A synthesis. *Quaternary Science Reviews*, *29*(1), 193–205. https://doi.org/10.1016/j.quascirev.2009.06.007

Ford, H. L., Ravelo, A. C., Dekens, P. S., LaRiviere, J. P., & Wara, M. W. (2015). The evolution of the equatorial thermocline and the early Pliocene El Padre mean state. *Geophysical Research Letters*, *42*(12), 4878–4887. https://doi.org/10.1002/2015GL064215

Foster, G. L., Lear, C. H., & Rae, J. W. B. (2012). The evolution of pCO2, ice volume and climate during the middle Miocene. *Earth and Planetary Science Letters*, *341–344*, 243–254. https://doi.org/10.1016/j.epsl.2012.06.007

Hays, J. D., Imbrie, J., & Shackleton, N. J. (1976). Variations in the Earth's Orbit: Pacemaker of the Ice Ages. *Science, New Series*, *194*(4270), 1121–1132.

Herbert, T. D. (2014). Alkenone Paleotemperature Determinations. In *Treatise on Geochemistry* (pp. 399–433). Elsevier. https://doi.org/10.1016/B978-0-08-095975-7.00615-X

Herraiz-Borreguero, L., & Rintoul, S. R. (2011). Subantarctic mode water: Distribution and circulation. *Ocean Dynamics*, *61*(1), 103–126. https://doi.org/10.1007/s10236-010-0352-9

Holland, M. M., & Bitz, C. M. (2003). Polar amplification of climate change in coupled models. *Climate Dynamics*, *21*(3), 221–232. https://doi.org/10.1007/s00382-003-0332-6

Jakob, K. A., Pross, J., Scholz, C., Fiebig, J., & Friedrich, O. (2018). Thermocline state change in the eastern equatorial Pacific during the late Pliocene/early Pleistocene intensification of Northern Hemisphere glaciation. *Climate of the Past*, *14*(7), 1079–1095. https://doi.org/10.5194/cp-14-1079-2018

Kimble, K. M., Herbert, T. D., & Jones, C. A. (2024). Pliocene Weakening of Gradients in Temperature but Not in Productivity in the Eastern Equatorial Pacific. *Paleoceanography and Paleoclimatology*, *39*(3), e2023PA004711. https://doi.org/10.1029/2023PA004711

Lawrence, K. T., Liu, Z., & Herbert, T. D. (2006). Evolution of the Eastern Tropical Pacific Through Plio-Pleistocene Glaciation. *Science*, *312*(5770), 79–83. https://doi.org/10.1126/science.1120395

Lee, S.-Y., & Poulsen, C. J. (2005). Tropical Pacific climate response to obliquity forcing in the Pleistocene: TROPICAL PACIFIC RESPONSE TO OBLIQUITY FORCING. *Paleoceanography*, *20*(4), n/a-n/a. https://doi.org/10.1029/2005PA001161

Liu, Z., & Alexander, M. (2007). Atmospheric bridge, oceanic tunnel, and global climatic teleconnections. *Reviews of Geophysics*, *45*(2). https://doi.org/10.1029/2005RG000172

Liu, Z., & Herbert, T. D. (2004). High-latitude influence on the eastern equatorial Pacific climate in the early Pleistocene epoch. *Nature*, *427*(6976), Article 6976. https://doi.org/10.1038/nature02338

Liu, Z., & Yang, H. (2003). Extratropical control of tropical climate, the atmospheric bridge and oceanic tunnel. *Geophysical Research Letters*, *30*(5). https://doi.org/10.1029/2002GL016492

Locarnini, M., Mishonov, A., Baranova, O., Boyer, T., Zweng, M., Garcia, H., Reagan, J., Seidov, D., Weathers, K., Paver, C., & Smolyar, I. (2019). World Ocean Atlas 2018, Volume 1: Temperature. *A. Mishonov Technical Ed.*, *NOAA Atlas NESDIS 81*, 52 pp.

Lundstad, E., Brugnara, Y., Pappert, D., Kopp, J., Samakinwa, E., Hürzeler, A., Andersson, A., Chimani, B., Cornes, R., Demarée, G., Filipiak, J., Gates, L., Ives, G. L., Jones, J. M., Jourdain, S., Kiss, A., Nicholson, S. E., Przybylak, R., Jones, P., … Brönnimann, S. (2023). The global historical climate database HCLIM. *Scientific Data*, *10*(1), 44. https://doi.org/10.1038/s41597-022-01919-w

Marshall, D. P., & Zanna, L. (2014). A Conceptual Model of Ocean Heat Uptake under Climate Change. *Journal of Climate*, *27*(22), 8444–8465. https://doi.org/10.1175/JCLI-D-13-00344.1

McCartney, M. S. (1979). Subantarctic Mode Water. *Woods Hole Oceanographic Institution*.

Müller, P. J., Kirst, G., Ruhland, G., von Storch, I., & Rosell-Melé, A. (1998). Calibration of the alkenone paleotemperature index U37K′ based on core-tops from the eastern South Atlantic and the global ocean (60°N-60°S). *Geochimica et Cosmochimica Acta*, *62*(10), 1757–1772. https://doi.org/10.1016/S0016-7037(98)00097-0

Noguer, M., van der Linden, P. J., Dai, X., Maskell, K., & Johnson, C. A. (2002). Climate Change 2001: The Scientific Basis. *Cambridge University Press*, *881*(9), 208. https://doi.org/10.2307/20033020

O'Brien, C. L., Foster, G. L., Martínez-Botí, M. A., Abell, R., Rae, J. W. B., & Pancost, R. D. (2014). High sea surface temperatures in tropical warm pools during the Pliocene. *Nature Geoscience*, *7*(8), 606–611. https://doi.org/10.1038/ngeo2194

Pennington, J. T., Mahoney, K. L., Kuwahara, V. S., Kolber, D. D., Calienes, R., & Chavez, F. P. (2006). Primary production in the eastern tropical Pacific: A review. *Progress in Oceanography*, *69*(2), 285–317. https://doi.org/10.1016/j.pocean.2006.03.012

Philander, S. G., & Fedorov, A. V. (2003). Role of tropics in changing the response to Milankovich forcing some three million years ago: TROPICS AND GLACIAL CYCLES. *Paleoceanography*, *18*(2), n/a-n/a. https://doi.org/10.1029/2002PA000837

Pielke, R. A., & Landsea, C. N. (1999). *La Niña, El Niño, and Atlantic Hurricane Damages in the United States*. https://journals.ametsoc.org/view/journals/bams/80/10/1520-0477_1999_080_2027_lnaeno_2_0_co_2.xml

Qu, T., Gao, S., Fukumori, I., Fine, R. A., & Lindstrom, E. J. (2009). *Origin and Pathway of Equatorial 13°C Water in the Pacific Identified by a Simulated Passive Tracer and Its Adjoint*. https://doi.org/10.1175/2009JPO4045.1

Rafter, P. A., Sigman, D. M., Charles, C. D., Kaiser, J., & Haug, G. H. (2012). Subsurface tropical Pacific nitrogen isotopic composition of nitrate: Biogeochemical signals and their transport. *Global Biogeochemical Cycles*, *26*(1). https://doi.org/10.1029/2010GB003979

Raja, M., & Rosell-Melé, A. (2021). Appraisal of sedimentary alkenones for the quantitative reconstruction of phytoplankton biomass. *Proceedings of the National Academy of Sciences*, *118*(2). https://doi.org/10.1073/pnas.2014787118

Ravelo, A. C., Andreasen, D. H., Lyle, M., Olivarez Lyle, A., & Wara, M. W. (2004). Regional climate shifts caused by gradual global cooling in the Pliocene epoch. *Nature*, *429*(6989), 263–267. https://doi.org/10.1038/nature02567

Ravelo, A. C., Dekens, P., & McCarthy, M. (2006). Evidence for El Niño—Like conditions during the Pliocene. *Gsa Today*, *16*. https://doi.org/10.1130/1052-5173(2006)016<4:EFENLC>2.0.CO;2

Reagan, J. R., Seidov, D., Wang, Z., Dukhovskoy, D., Boyer, T. P., Locarnini, R. A., Baranova, O. K., Mishonov, A. V., Garcia, H. E., Bouchard, C., Cross, S. L., & Paver, C. R. (2024). World Ocean Atlas 2023, Volume 2: Salinity. In A. Mishonov (Ed.), *NOAA Atlas NESDIS 90* (p. 52). https://repository.library.noaa.gov/view/noaa/60600

Rhein, M., Rintoul, S. R., Aoki, S., Campos, E., Chambers, D., Feely, R. A., Gulev, S., Johnson, G. C., Josey, S. A., Kostianoy, A., Mauritzen, C., Roemmich, D., Talley, L. D., & Wang, F. (2013). Observations: Oceans. In T. F. Stocker, D. Qin, G.-K. Plattner, M. Tignor, S. K. Allen, J. Boschung, A. Nauels, Y. Xia, V. Bex, & P. M. Midgley (Eds.), *Climate Change 2013: The Physical Science Basis. Contribution of Working Group I to the Fifth Assessment Report of the Intergovernmental Panel on Climate Change*. Cambridge University Press.

Rintoul, S. R., & England, M. H. (2002). *Ekman Transport Dominates Local Air–Sea Fluxes in Driving Variability of Subantarctic Mode Water*. https://journals.ametsoc.org/view/journals/phoc/32/5/1520-0485_2002_032_1308_etdlas_2.0.co_2.xml

Sarmiento, J. L., Gruber, N., Brzezinski, M. A., & Dunne, J. P. (2004). High-latitude controls of thermocline nutrients and low latitude biological productivity. *Nature*, *427*(6969), Article 6969. https://doi.org/10.1038/nature02127

Schmitt, R. W. (2018). The Ocean's Role in Climate. *Oceanography*, *31*(2), 32–40.

Shackleton, N. J., Hall, M. A., & Pate, D. (1995). *15. Pliocene stable isotope stratigraphy of site 846*. *138*, 337–355. https://doi.org/10.2973/odp.proc.sr.138.1995

Sigman, D. M., & Hain, M. P. (2012). The Biological Productivity of the Ocean. *Nature Education Knowledge*, *3*(10), 21.

Spero, H. J., Mielke, K. M., Kalve, E. M., Lea, D. W., & Pak, D. K. (2003). Multispecies approach to reconstructing eastern equatorial Pacific thermocline hydrography during the past 360 kyr. *Paleoceanography*, *18*(1). https://doi.org/10.1029/2002PA000814

Stan, C., Straus, D. M., Frederiksen, J. S., Lin, H., Maloney, E. D., & Schumacher, C. (2017). Review of Tropical-Extratropical Teleconnections on Intraseasonal Time Scales. *Reviews of Geophysics*, *55*(4), 902–937. https://doi.org/10.1002/2016RG000538

Takahashi, T., Feely, R. A., Weiss, R. F., Wanninkhof, R. H., Chipman, D. W., Sutherland, S. C., & Takahashi, T. T. (1997). Global air-sea flux of CO2: An estimate based on measurements of sea–air pCO2 difference. *Proceedings of the National Academy of Sciences*, *94*(16), 8292–8299. https://doi.org/10.1073/pnas.94.16.8292

Talley, L. D. (1993). *Distribution and Formation of North Pacific Intermediate Water*. https://journals.ametsoc.org/view/journals/phoc/23/3/1520-0485_1993_023_0517_dafonp_2_0_co_2.xml

Toggweiler, J. R., Dixon, K., & Broecker, W. S. (1991). The Peru upwelling and the ventilation of the south Pacific thermocline. *Journal of Geophysical Research: Oceans*, *96*(C11), 20467–20497. https://doi.org/10.1029/91JC02063

Wang, C., Deser, C., Yu, J.-Y., DiNezio, P., & Clement, A. (2017). El Niño and Southern Oscillation (ENSO): A Review. In P. W. Glynn, D. P. Manzello, & I. C. Enochs (Eds.), *Coral Reefs of the Eastern Tropical Pacific: Persistence and Loss in a Dynamic*

Environment (pp. 85–106). Springer Netherlands. https://doi.org/10.1007/978-94-017-7499-4_4

Wara, M. W., Ravelo, A. C., & Delaney, M. L. (2005). Permanent El Nino-Like Conditions During the Pliocene Warm Period. *Science*, *309*(5735), 758–761. https://doi.org/10.1126/science.1112596

Yasuda, I. (1997). The origin of the North Pacific Intermediate Water. *Journal of Geophysical Research: Oceans*, *102*(C1), 893–909. https://doi.org/10.1029/96JC02938

Yu, J.-Y., Zou, Y., Kim, S. T., & Lee, T. (2012). The changing impact of El Niño on US winter temperatures. *Geophysical Research Letters*, *39*(15). https://doi.org/10.1029/2012GL052483

Zhang, Y., Pagani, M., & Liu, Z. (2014). A 12-Million-Year Temperature History of the Tropical Pacific Ocean. *Science*, *344*(6179), 84–87. https://doi.org/10.1126/science.1246172

CHAPTER 2

Pliocene weakening of gradients in temperature but not in productivity in the eastern equatorial Pacific

K. M. Kimble[1], T. D. Herbert[1], and C. A. Jones[2]

[1]Department of Earth, Environmental, and Planetary Sciences, Brown University, Providence, Rhode Island, 02912, USA.

[2]Graduate School of Oceanography, University of Rhode Island, Narragansett, Rhode Island, 02882, USA.

Published in 2024 in *Paleoceanography and Paleoclimatology*, 39, e2023PA004711.

Key Points:

- East-west sea surface temperature gradients in the eastern tropical Pacific "cold tongue" were smaller in the Pliocene compared to modern.
- High easternmost equatorial Pacific biogenic opal and alkenone accumulation rates imply stronger productivity gradients than modern.
- Taken together, these observations suggest vigorous upwelling of subsurface waters that were significantly warmer than today.

Abstract

The modern eastern equatorial Pacific Ocean (EEP) exhibits strong upwelling, producing pronounced gradients in sea surface temperature (SST), nutrient concentration, and biological productivity between 80° and 140°W. During the globally warmer late Pliocene (3.0-3.6 Ma), the EEP may have experienced permanent El Niño-like conditions, supported by a reduced SST gradient across the equatorial Pacific. However, the weakened east-west SST gradient has been controversial, with disparate results depending on the proxy used to monitor Western Warm Pool SSTs. We present new Pliocene alkenone-based SST and paleoproductivity records from four Ocean Drilling Program (ODP) cores spanning an east-west transect across the EEP, which present an internally consistent picture of SST and productivity gradients in the modern cold tongue, resolved at orbital-scale variability. Strong agreement between core top reconstructions and satellite estimates indicates that alkenone paleotemperature and paleoproductivity proxies are appropriate for reconstructing Pliocene EEP conditions. The average SST gradient between 90°-120°W was reduced from the modern 1.8°C gradient to 0.9°C in the late Pliocene. Despite the weakened SST gradient, the surface productivity gradient was stronger during the late Pliocene compared to modern, based on calibrated X-ray fluorescence biogenic opal and alkenone average accumulation rates. Contrary to modern El Niño SST and productivity patterns, reduced Pliocene surface productivity did not accompany the weakened SST gradient. Instead, strong Pliocene biogenic opal and alkenone concentration accumulation gradients in the eastern EEP suggest that subsurface tilting of the nutricline and thermocline persisted to supply vigorous upwelling of warm but nutrient-rich subsurface waters in a warmer climate.

Plain language summary

Ocean surface temperature is often related to productivity, or the intensity of biological activity from algae that live in surface waters and use sunlight energy to grow. Colder waters rich in nutrients important to these algae are brought from the deeper ocean to the sunlit zone at specific locations in the ocean, including the eastern tropical Pacific Ocean. Therefore, colder waters are often associated with higher biological productivity. This research assesses the relationship between temperature and productivity in eastern Pacific waters during a period in Earth's history around three million years ago when global temperatures were warmer than modern. We used geochemical tools to reconstruct temperature and productivity from four locations in the eastern Pacific. We found that three million years ago, the easternmost site was significantly warmer than modern, but biological productivity remained similar to today, which contradicts the pattern we observe in the modern Pacific Ocean. As we expect ocean and global temperatures to warm in the coming decades, relationships between temperature and productivity are important to understand. Determining how organisms at the base of the food web respond to warmer waters has implications for fishing, shipping, and other societal and economic activities along the eastern Pacific.

1. Introduction

Ocean upwelling zones are important controls on the global carbon cycle because cold, nutrient-rich, and CO_2-rich bottom waters ascend to the surface and enhance primary productivity (Toggweiler & Sarmiento, 1985). The modern eastern equatorial Pacific Ocean (EEP) exhibits a zonal gradient in sea surface temperature (SST) and productivity due to an asymmetrical upwelling regime: stronger upwelling delivers cooler waters to the eastern EEP and SSTs warm toward the central Pacific (Liu et al., 2019). The east-west SST gradient

contributes to the Walker Cycle and influences the El Niño-Southern Oscillation, which affects interannual climate variability across the globe (Delcroix, 1998; Wang et al., 2017).

Despite its reputation as one of the most productive marine upwelling regions in the world, the modern EEP is a net source of CO_2 to the atmosphere (Diz et al., 2018; Fiedler et al., 1991; Takahashi et al., 2009). The marine biogeochemistry of the EEP represents a leaky valve in the soft-tissue pump because incomplete nutrient utilization limits the amount of surface productivity the region can support (Dugdale & Goering, 1967). The strong modern gradients in surface productivity between the eastern and western EEP imply potential variations in the leverage by which the EEP carbon cycle influences global climate. A change in upwelling or a change in biological efficiency could affect CO_2 outgassing and the export accumulation of carbon from the surface.

The EEP is one of the only locations where waters originating in the Southern Ocean upwell near the equator (Bostock et al., 2010; Lehmann et al., 2018; Rafter et al., 2013; Toggweiler et al., 1991; Toggweiler & Carson, 1995). In the tropical Pacific, surface currents follow the direction of easterly trade winds. However, in the subsurface, the Equatorial Undercurrent flows eastward at a depth of about 200 m and supplies cool, nutrient-rich water to the EEP upwelling zone (Kessler, 2006; Rafter & Sigman, 2016). South Pacific Intermediate Water, which forms at Southern Hemisphere high latitudes, feeds the Equatorial Undercurrent waters and establishes the high latitude-tropics connection between the Southern Ocean and the EEP (Lu et al., 1998). The "atmospheric bridge and oceanic tunnel" hypothesis posits that extratropical temperature changes can be detected at the equator both rapidly through the atmosphere and more slowly through the ocean subsurface (Gu & Philander, 1997; Liu & Yang, 2003). The modern subsurface structure of the EEP functions as a conduit between high latitude

orbital forcings and tropical SST and productivity responses (Lee & Poulsen, 2005). The EEP offers a unique opportunity to study how changes in the global forcings that affect high latitudes propagate throughout the tropics.

The mid-Pliocene warm period (roughly 3.3 to 3.0 Ma) provides a potential analog for 21st century climate change, revealing how an equilibrated EEP upper water column and carbon cycle might respond in a warmer world (Dowsett, 2007; McClymont et al., 2020). The pole-equator temperature gradients that drive easterly winds and upwelling strength in the equatorial Pacific may have been weaker during the Pliocene when high latitudes were significantly warmer than modern. The temperature of waters upwelled via the oceanic tunnel thus may have been relatively warm (Dekens et al., 2007; Ford et al., 2015). Not much is known about EEP nutrient content and utilization during the Pliocene, but more nutrient-rich upwelled waters may have supported higher primary productivity (Zhang et al., 2017). The warmer and wetter Pliocene climate also may have hindered dust deposition in the EEP, which restricted nutrient utilization because phytoplankton were physiologically prevented from using available nutrients when dust-deposited Fe concentrations were low (Behrenfeld et al., 1996).

Previous Pliocene SST investigations compare a combination of the of the $U^{k'}_{37}$ index (organic biomarker), TEX_{86} (organic biomarker), and Mg/Ca (planktonic foraminiferal elemental ratio) SST proxies from the warmer western Pacific to the cool EEP, resulting in two conflicting positions within the paleoceanography community concerning the SST and productivity of the Pliocene EEP (O'Brien et al., 2014; Ravelo et al., 2014; Zhang et al., 2014). One set of SST reconstructions suggests that the equatorial Pacific experienced homogeneously warm ("permanent El Niño") conditions, with very weak SST gradients (Ford et al., 2015; Ravelo et al., 2004, 2006, 2014; Wara et al., 2005). Other SST reconstructions suggest that SST

gradients remained strong during the Pliocene, similar to modern conditions (O'Brien et al., 2014; Zhang et al., 2014). These differing interpretations hinge on the controversial interpretation of western Pacific warm pool (WPWP) temperature proxies.

Here, we present paleotemperature and productivity records sampled at orbital resolution from the EEP spanning 3.0 to 3.6 Ma. We focus on this region for two reasons. First, modern east-west gradients in SST and productivity are intense, enhancing the potential signal to noise ratio of paleoceanographic proxy comparisons to the modern day. Second, we apply the well-validated alkenone proxy for SST to our paleotemperature analyses, allowing us to generate an internally consistent estimate of past SST gradients that avoids the difficulties of comparing different SST proxies between the EEP and the WPWP. We restrict our analysis region to the EEP to avoid the limitation of alkenone saturation at high temperatures typical of the WPWP. Our SST records address the extent to which upwelled high latitude waters controlled EEP SST and productivity during the warmer Pliocene, predating the initiation of cyclic Northern Hemisphere glaciation (Bartoli et al., 2011). We also investigate east-west gradients in the accumulation of organic biomarkers, specifically alkenone concentrations, which are useful productivity proxies for phytoplankton abundance and activity (Raja & Rosell-Melé, 2021; Volkman et al., 1998), in addition to inorganic proxies related to ocean surface production. The ensemble of proxy estimates allows us to investigate the relative importance of upwelling in setting Pliocene SST gradients.

2. Materials and methods

2.1 Study sites and data acquisition

Ocean Drilling Program (ODP) Leg 138 recovered sediment cores from the EEP, including ODP Sites 846 (3°5.696'S, 90°49.078'W, 3296 mbsl), 849 (0°10.983'N, 110°31.183'W, 3837 mbsl), and 850 (1°17.837'N, 110°31.283'W, 3786 mbsl) in 1991. Integrated Ocean Drilling Program (IODP) Leg 320/321 revisited the EEP in 2010 and collected sediment from Site U1338 (2°30.469'N, 117°58.178'W, 4200 mbsl; **Figure 1**). The four sites form a transect spanning the modern Pacific cold tongue, where the shallow thermocline results from the shoaling of the Equatorial Undercurrent and advection of water from the eastern boundary current along the Peru-Chile margin (Lavín et al., 2006; Liu & Herbert, 2004; Toggweiler et al., 1991). Sites along this equatorial transect are ideally situated to capture modern and past gradients in SST and bioproductivity. The reference temperatures used to estimate Pliocene anomalies are the modern SSTs at the 3 Ma backtracked paleo-locations of each downcore site rather than SSTs at the present-day site locations.

An additional 44 sites located between 5°N, 5°S, 80°W, and 140°W containing core top sediments were selected for a modern model-proxy comparison of SST and bioproductivity in the EEP. These sites span the cold tongue and have sufficient satellite-derived and instrumental SST and productivity data for comparison with core top alkenone data. SST data were extracted from the World Ocean Atlas 2018 (WOA18) dataset and compared to alkenone SST reconstructions (Boyer et al., 2018; Locarnini et al., 2019). Alkenone primary productivity reconstructions were compared to modeled coccolithophore phytoplankton productivity (Losa et al., 2017) and Moderate Resolution Imaging Spectroradiometer (MODIS) satellite chlorophyll estimates (NASA Goddard Space Flight Center, 2022).

Sediment data were acquired from several published sources. Calibrated X-ray fluorescence (XRF) data are from Lyle et al. (2019) for Sites 849 and U1338, and from Robinson

et al. (2019) for Site 846. Alkenone SST and productivity data are from Lawrence et al. (2006) for Site 846, and from Herbert et al. (2021) for Site 850. Sites 846 and 850 $\delta^{18}O$ and $\delta^{13}C$ data are from Herbert et al. (2021), and Site 849 isotope data are from Mix et al. (1995). The age model for Site 846 is from Herbert et al. (2021), while the age models for Sites 849, 850, and U1338 are from Lyle et al. (2019). Modern SST and chlorophyll data are from the WOA18 collection (Boyer et al., 2018; Locarnini et al., 2019) and the MODIS satellite (NASA Goddard Space Flight Center, 2022), respectively, while additional core top alkenone productivity data are from Kienast et al. (2012) and modeled coccolithophore productivity data are from Losa et al. (2017).

The Match program (Lisiecki & Lisiecki, 2002) was used to align SST and stable isotopic time series from Sites 849, 850, and U1338 (SST only) to a slightly modified version of the age-depth tuning of Lisiecki & Raymo (2005), updated with a revised composite section spanning the M2 glacial interval at Sites 846 and 850 (Herbert et al., 2021). XRF data from Sites 846, 849, and U1338 were used as secondary alignment records in the Match program for the SST and isotope time series.

2.2 Paleo-SST estimations

The $U^{k'}_{37}$ index is a widely used SST proxy derived from haptophyte phytoplankton (one lineage of coccolithophores) living near the ocean surface. $U^{k'}_{37}$ is calculated based on the degree of unsaturation of alkenones, or the number of double bonds connecting carbon atoms, according to the following equation (Prahl et al., 1988):

$$U_{37}^{k\prime} = \frac{[C_{37:2}]}{[C_{37:2}+C_{37:3}]} \qquad \text{[Equation 1]}$$

Pliocene SSTs are reported using the Müller et al. (1998) global core-top calibration, which reflects the alkenone-SST calibration directly measured from ocean sediment. Although other non-linear (Tierney & Tingley, 2018) and linear (Conte et al., 2006) $U^{k'}_{37}$ calibrations exist, we chose to present the Müller et al. (1998) calibration due to negligible differences between the calibrations (**Figure S1**). Previous work successfully applied alkenone paleotemperature reconstructions to the Pliocene EEP (Etourneau et al., 2013; Lawrence et al., 2006; Rousselle et al., 2013). We validate the faithfulness of the $U^{k'}_{37}$ proxy in estimating modern SST in a later section.

Average sampling resolution differs between sites (1.3 kyr at Site 846, 3.1 kyr at Site 849, 1.7 kyr at Site 850, and 2.8 kyr at Site U1338), so the difference in SST between sites was calculated by resampling the higher-resolution SST data to the age scale of the lower-resolution data to determine an estimated ΔSST for each time step.

2.3 Paleo-productivity estimations

Several proxies, based on both alkenones and inorganic phases (XRF-based), record relative marine productivity. The concentration of C_{37} alkenones ("C_{37} total," the concentration of C_{37} ketones relative to grams of dry sediment extracted) is positively correlated to primary productivity and surface chlorophyll concentration (Raja & Rosell-Melé, 2021; Volkman et al., 1995). High C_{37} total values may indicate high surface primary productivity among photosynthetic algae and presumably strong upwelling (Bolton, Lawrence, et al., 2010; Ko et al., 2018; Rostek et al., 1997; Villanueva et al., 2002).

Calibrated XRF mass accumulation rates can reflect biogenic opal and carbonate surface productivity, provided that dilution by terrigenous material and dissolution at depth do not

overwhelm the surface signal (Gebregiorgis et al., 2020). Lyle et al. (2019) provide the Site 849 raw XRF scanning data and report calibrated weight percentage concentrations of element oxides according to a normalized median-scaled calibration. Robinson et al. (2019) provide the Site 846 raw XRF scanning data and report calibrated weight percentage concentrations of element oxides according to a log-ratio calibration equation. Oxides were converted to elements according to known conversion factors before any element ratio comparisons were undertaken (e.g., the oxide SiO_2 was multiplied by 0.4674 to convert to the element Si).

The XRF element concentrations represent the total combination of biogenic and non-biogenic portions of each of the sediment components. However, SiO_2 in the EEP is composed of both biogenic and non-biogenic (terrigenous) components. Biogenic silica (also called bio-SiO_2 or biogenic opal here) was calculated from the calibrated SiO_2 wt% at each site according to the following:

$$[\text{bio } SiO_2]_{wt\%} = \left([Si_{total}]_{wt\%} - \left(\frac{Si}{Al_{terrigenous}}\right) \times [Al_{total}]_{wt\%}\right) \times (\text{oxide conversion})$$

where $Si/Al_{terrigenous}$ = 2.717 (Li, 2000), and Si oxide conversion = 2.1393 [Equation 2]

Bio-SiO_2 was multiplied by 1.09 because biogenic SiO_2 sediments contain 9% water (Scheinost, 2005). High biogenic opal indicates either strong SiO_2 productivity and upwelling or little silicate dissolution at depth (Koning et al., 2002). Bio-SiO_2 calculated here agrees with Lyle et al. (2019) low-resolution discrete opal measurements (r^2 = 0.652, reduced major axis regression slope = 0.900).

2.4 Sediment accumulation rates

Variations in terrigenous and biogenic inputs cause the sedimentation rates at the sites to change over time. To avoid the confounding effects of dilution due to these changing

sedimentation rates, mass accumulations rates (MAR) of $CaCO_3$, bio-SiO_2, and clays were calculated based on the Site 846, 849, and U1338 XRF data. MARs are calculated as the weight percent (wt%) of each sediment component × dry bulk density (g/cm^3) × linear sedimentation rate (cm/kyr). Dry bulk density (DBD) was calculated based on the shipboard wet bulk density (WBD) measurements for Sites 846, 849, and U1338 according to the sediment density measurement calibration of Herbert and Mayer (1991):

$$\mathrm{DBD} = \left(1 - \frac{2.65 - \mathrm{WBD}}{2.65 - 1.025}\right) \times 2.65 + \left(\frac{2.65 - \mathrm{WBD}}{2.65 - 1.025}\right) \times 0.025 \qquad \text{[Equation 3]}$$

Linear sedimentation rates were calculated based on the individual age models for Site 846 (Herbert et al., 2021) and Sites 849, 850, and U1338 (M. Lyle et al., 2019) according to the following:

$$\text{linear sedimentation rate}_{(i)} = \frac{\mathrm{depth}_{(i+1)} - \mathrm{depth}_{(i)}}{\mathrm{age}_{(i+1)} - \mathrm{age}_{(i)}} \quad \text{[Equation 4]}$$

Note that the MAR is only strictly correct over the entire interval between age control points and should not be taken literally on a point-by-point basis.

C_{37} total MARs for all sites were calculated by multiplying the C_{37} total concentration (in μg/g) by the product of the dry bulk density and the linear sedimentation rate, so C_{37} total MARs are reported in units of μg cm^{-2} kyr^{-1}. The XRF and C_{37} total MARs reported here depend on the validity of the age models and represent averages between age control points (average distance between control points is <3 kyr). Gradients in C_{37} total MAR between sites were deemed more appropriate than C_{37} total concentration gradients to account for the fivefold difference in Pliocene sediment accumulation rates between the eastern part of the transect (3.4 g/cm^2/kyr average MAR) versus the western end (0.6 g/cm^2/kyr).

XRF wt% values were used to approximate the proportions of the major sediment components ($CaCO_3$, bio-SiO_2, and detrital material) to compare sediment accumulation rates

between sites. The normalized wt% values used here have smaller relative errors than raw peak area data (M. Lyle et al., 2012). $CaCO_3$ and bio-SiO_2 are produced at the ocean surface, while detrital material (also called clay or terrigenous material here) is deposited as aeolian dust in this region. Although there are other origins for elements of interest in the sediment, they appear in such minor concentrations that it is assumed that $CaCO_3$, bio-SiO_2, and detrital material are the only components present. Consequently, the individual component wt% estimates were divided by the total sum of the carbonate, bio-SiO_2, and clay wt% estimates to force the sum of sediment components to 100%, as shown in Equations 5-7.

All the carbonate at the three sites is assumed to be biogenic in origin:

$$\text{biogenic } CaCO_3 = \frac{CaCO_{3\ \text{total}}}{\text{wt\%}_{\text{total}}} \times 100 \quad \text{[Equation 5]}$$

The bio-SiO_2 calculation is the same as Equation 2:

$$\text{biogenic } SiO_2 = \frac{\left([SiO_2]_{\text{wt\%}} - \left(\left(\text{Si/Al}_{\text{terrigenous}}\right) \times [\text{Al}_{\text{total}}]_{\text{wt\%}}\right)\right) \times (\text{oxide conversion})}{\text{wt\%}_{\text{total}}} \times 100$$

[Equation 6]

Detrital material is the sum of the remaining MnO, TiO_2, Al_2O_3, Fe_2O_3, Na_2O, K_2O and non-biogenic SiO_2 components. The average hemipelagic shale compositions of Na and K (Li, 2000) were normalized to Al wt% and converted to the oxides Na_2O and K_2O, respectively, in order to estimate detrital material because these oxides were not reported in XRF measurements.

$$\text{detrital} = \frac{\text{MnO} + TiO_2 + Al_2O_3 + Fe_2O_3 + Na_2O + K_2O + (SiO_{2\ \text{total}} - \text{bio } SiO_2)}{\text{wt\%}_{\text{total}}} \times 100 \quad \text{[Equation 7]}$$

Biogenic barium accumulation (Ba_{xs} MAR), a proxy for organic matter export from the surface to the deep ocean (Dymond et al., 1992), was calculated according to the following:

$$[Ba_{xs}]_{wt\%} = \left([Ba_{total}]_{wt\%} - \left(\frac{\text{Ba}}{\text{Al}}_{\text{terrigenous}}\right) \times [\text{Al}_{\text{total}}]_{\text{wt\%}}\right) \times (\text{oxide conversion})$$

[Equation 8]

The average MAR at each time step was multiplied by the normalized weight percentage of biogenic $CaCO_3$, SiO_2, and clay to yield MARs for each sediment component. Note that without point-by-point normalization to a constant flux proxy, MAR should be estimated as a time-averaged quantity. Average MARs and sediment component wt% were calculated for two time periods: 3.0 to 3.6 Ma in the Pliocene and 0 to 10 ka as a modern comparison.

2.5 Spectral analysis

Spectral analyses were conducted on $\delta^{18}O$, SST, and C_{37} total MAR to determine which orbital frequencies, if any, are dominant controls on temporal variability. Data were normalized, detrended, and linearly interpolated to <3-kyr timesteps. A multitaper method Fourier transform was used to calculate spectra (Meyers et al., 2021), which are reported relative to the 90% confidence interval. The ARAND time-series analysis software (Howell et al., 2006) was used to calculate coherence between $\delta^{18}O$, SST, C_{37} total MAR and a normalized average record of eccentricity, tilt (obliquity), and precession (ETP).

3 Results

3.1 Comparison of proxy-satellite SST and productivity estimates

Among the 44 core top sites, there is strong agreement between SST estimated by the $U^{k'}_{37}$ proxy and WOA18 SST and little coherent spatial variability in residual SST (the difference between the two SST estimates) across the modern EEP (**Figure 2a**). Therefore, $U^{k'}_{37}$ SST is a good approximation of modeled and observed SST in the EEP today (**Figure 2b**). As discussed later, our time series results suggest that SST gradients can be recorded more precisely

than suggested by **Figure 2b**; this perhaps results from the benefits of generating alkenone estimates in the same laboratory for this study (unlike the data from multiple laboratories used in the EEP $U^{k'}_{37}$ core top compilation). Note that there is no suggestion of systematic regional offsets of the $U^{k'}_{37}$ proxy relative to modern SST. The correlation between $U^{k'}_{37}$ SST and WOA18 SST reported here supports the regional findings of Kienast et al. (2012) that biomarker- and satellite-derived SST estimates are reliably consistent in the EEP, but this study focuses on a smaller region restricted to 5° north and south of the equator and between 80°W and 140°W.

The strong positive linear correlation between alkenone C_{37} total and satellite estimates of surface chlorophyll in the modern EEP indicate that C_{37} total scales reliably to estimates of surface primary productivity (**Figure 2c**). Alkenone-producing haptophyte productivity and nutrient availability may be partially decoupled in the modern EEP by incomplete N and P utilization, yet C_{37} total is still a good proxy for surface primary productivity as evidenced by the strong positive relationship with chlorophyll. We will interpret C_{37} total MAR reconstructions from the Pliocene as a proxy for surface productivity, consistent with the global relationship calculated in other recent studies (Raja & Rosell-Melé, 2021; **Figure S2**). However, C_{37} total is negatively correlated with coccolithophore carbonate production (**Figure 2d**), possibly because only a small subset of known coccolithophore species produce alkenones.

Recent studies have shown that bottom water oxygenation affects alkenone C_{37} total preservation (Anderson et al., 2019; Jacobel et al., 2020), but the four sites are located at relatively deep water depths (~3300-4200 mbsl) with minimal vertical oxygen gradients in the modern ocean, so any bottom water oxygenation effects on organic proxies would be imparted equally for all sites (**Figure S3**). If oxygen were the major control on C_{37} total preservation at

each site, then C_{37} total would look similar across the transect. Moreover, changes in dissolved inorganic carbon (DIC) on glacial-interglacial time scales account for the main $\delta^{13}C$ signal, and greater respired carbon and lower oxygen results in higher DIC and more depleted $\delta^{13}C$ values. The weak correlations between C_{37} total and $\delta^{13}C$ at each site imply that oxygen had little effect on the C_{37} total signal (**Figure S3**).

3.2 Paleo-SST estimations

The modern zonal SST gradients reported here use the modern SST above the sites' paleo-locations backtracked to 3 Ma, rather than the present day locations of each site. Modern EEP SST gradients depend on both latitude and longitude (or, in the case of longitude, distance from the South American coastline), as both influence winds (upwelling) and exchange of heat with the atmosphere (SST). Over the last 3 Ma, as the Pacific and Nazca plates have moved apart, several sites (849, 850, U1338) that used to be located closer to the equator during the Pliocene are now located up to 1° farther north, and therefore are differently positioned in relation to the heart of the cold tongue upwelling today compared to 3 Ma. These shifts in longitude are important in the EEP where strong zonal and meridional SST gradients exist. Following the practice of the ODP Scientific Results for Leg 138 (Pisias et al., 1995) and other papers concerned with SST change over time (Herbert et al., 2016), the paleo-locations of each site are used to estimate Pliocene SST anomalies.

Ocean temperatures in the EEP were warmer during the Pliocene (3.0-3.6 Ma) compared to modern (**Figure 3d**). Note that SST offsets between the four sites included in this transect covaried closely across a 600-kyr period. The consistent SST offsets between sites seem reliable despite absolute calibration uncertainties of ~1.5°C and analytical error of 0.15°C, particularly

when noting that the differences between mean SSTs are not constant, but oscillate systematically with orbital cycles. These orbital scale changes in gradient are further indications of good signal to noise in the measurements. Error estimates of SST measurements using Gaussian Process modeling (**Figure S4**) show that out of 189 downcore samples, there are no reversals of the expected east-west (Site 846-U1338) colder-warmer gradient (**Figure 4**).

Even with uncertainty in the absolute SST, the Pliocene $U^{k'}_{37}$-SST values are clearly warmer when compared to the modern alkenone-derived SST from core top samples along the transect (**Figure 3d**). The average site-to-site correlation coefficients are strong, with R^2 values greater than 0.73, and the SST differences between sites are maintained over 600 kyr (**Figure S5**). The average SST gradient between the easternmost and westernmost sites in the transect weakened to 0.9°C during the Pliocene, compared to the modern >1.8°C gradient (**Figure 4**). This pattern is consistent with the longer Pliocene-Pleistocene trend of tropical Pacific SST: the eastern EEP (Site 846) experienced the greatest cooling over the Plio-Pleistocene as the Pacific cold tongue developed, while the western and central EEP did not cool as drastically (Lawrence et al., 2006). The SST gradients between the farthest east and west sites, and the farthest east and central sites generally oscillated with similar orbital-scale variability to that recorded in benthic $\delta^{18}O$ (**Figure 4**). During warmer intervals, the SST gradient was reduced (the eastern EEP warmed to match the western EEP), while during colder intervals, the SST gradient became more positive (the western EEP cooled less than the eastern EEP).

3.3 Paleo-productivity estimations

On average, C_{37} total mass accumulation rates were stronger in the eastern EEP than in the western or central EEP during the Pliocene (**Figures 4c, 5d**). Like the Pliocene SST gradient,

the C_{37} total gradient between the western and eastern EEP also oscillated with glacial-interglacial climate variability. There appeared to be a divide between the higher average C_{37} total MAR east of ~100°W (Site 846) and the lower alkenone accumulation west of 100°W (Sites 849, 850, U1338) throughout the mid-Pliocene (**Figure 5d**). Additionally, during warmer intervals (i.e., 3.4-3.5 Ma), the C_{37} total MAR gradient weakened (eastern EEP inferred productivity decreased to match that of the western EEP), while during colder intervals (i.e., the M2 glaciation at ~3.3 Ma), the C_{37} total MAR gradient strengthened (we infer that the eastern EEP primary productivity increase outpaced that of the western EEP). Alternatively, better oxygenated Pacific Deep Water bathing the eastern EEP site (Site 846) during warmer intervals may have decreased C_{37} total preservation (Anderson et al., 2019; Jacobel et al., 2020), although bio-SiO_2 MARs at Site 846 (**Figure 5c**) did not experience the same glacial-interglacial variability as the zonal C_{37} total MAR gradient (**Figure 4c**).

The sediment component accumulation estimates, represented as average MARs from 3.0 to 3.6 Ma, can account for elements of ecosystem productivity that C_{37} total MAR alone cannot capture. Bio-SiO_2 was particularly important in the Pliocene EEP. Not only did biogenic opal comprise a larger proportion of eastern EEP sediment relative to western or central EEP sediment during the Pliocene (**Figure 5c**), but much higher biogenic opal production (and/or preservation) occurred in the Pliocene relative to the modern eastern EEP (**Figure S6**). Higher Ba_{xs} MARs recorded in the eastern EEP relative to the west or central parts of the transect (**Figure 5e**) also support stronger Pliocene eastern EEP productivity compared to modern.

Meanwhile, detrital MARs changed little from the Pliocene to modern, except at Site 846, where detrital MARs were ~40% higher during the Pliocene relative to modern (**Figure 5a**). Likewise, $CaCO_3$ MARs in the eastern EEP were only slightly higher relative to the central and

western EEP during the Pliocene, while the east-west $CaCO_3$ MAR gradient was similarly small in the present day (**Figure 5b, Figure S6**).

XRF ratios clarify the relationship between $CaCO_3$ and bio-SiO_2 and point to increased biogenic opal production in the Pliocene relative to modern **(Figure 6**). $CaCO_3/Fe_2O_3$ and $CaCO_3/BaSO_4$ ratios show slight decreases in carbonate production normalized to dust deposition and export production, respectively, across the EEP from 3.6 to 3.0 Ma (**Figure 6a, 6c**). Meanwhile, high bio-$SiO_2/CaCO_3$ and bio-$SiO_2/BaSO_4$ ratios indicate that biogenic opal accounts for most of the skeletal export production in the eastern EEP, specifically between ~3.2-3.4 Ma (**Figure 6b, 6d**). A possible ecological shift from siliceous to calcareous plankton from the Pliocene to the late Pleistocene may be consistent with the decline in bio-SiO_2 toward the present (**Figure 5c**).

3.4 Spectral structure

Multitaper method Fourier transform spectral analyses were performed to identify the dominant periods of variability in the SST and productivity records at the 90% confidence interval (**Figure 7**). The $\delta^{18}O$ records from Sites 846 and 849 had dominant periodicities at 100 kyr and 41 kyr based on the analysis interval from 3.0 to 3.6 Ma. SST at all sites showed significant sensitivity to the 100 kyr periodicity, as well as the 41 kyr periodicity (**Figure 7c**). Coherence between $\delta^{18}O$, SST, and C_{37} total MAR versus normalized average eccentricity, tilt (obliquity), and precession (ETP) demonstrate strongest coherency in the obliquity band for all variables and across all sites (**Figure 7**).

4. Discussion

4.1 Time-averaged controls on SST and upwelling in the EEP

The data sets presented here address two related questions: how did the background (e.g., super-orbital) EEP near-surface oceanography differ in the Pliocene compared to today, and how did this background state affect variability at the orbital scale? In the modern EEP, a combination of wind strength, upwelling velocity, thermocline tilt, and subsurface water temperature governs SST. These processes of ocean heat and momentum exchange also affect the energy of atmospheric circulation through the Bjerknes feedback, with strengthened zonal SST gradients corresponding to stronger zonal wind stresses. These factors largely determine surface productivity as well, although incomplete nutrient utilization also plays a role.

However, there are several probable differences between the modern oceanographic setting and the background state of the Pliocene EEP. Top-down controls on EEP SST include weaker zonal wind stresses derived from smaller Pliocene pole-equator temperature gradients, as well as higher than pre-industrial CO_2 concentrations (de la Vega et al., 2020; Foster et al., 2017), which warmed surface waters in the tropical Pacific. Reduced meridional gradients in cloud albedo also weakened zonal Pacific SST gradients (Burls & Fedorov, 2014). Pliocene bottom-up controls include warmer subsurface waters delivered from an oceanic tunnel connecting the warmer high latitudes and the tropics (Bolton, Lawrence, et al., 2010; Dekens et al., 2007; Fedorov et al., 2006; Lee & Poulsen, 2005; Philander & Fedorov, 2003), as well as the nutrient content of subsurface waters.

The alkenone SST records reported here avoid the ambiguity of the western equatorial Pacific warm pool proxy discrepancies by restricting SST reconstructions to the EEP and by

using a single proxy. Note that our conclusion that eastern-western EEP SST gradients were reduced significantly does not depend strictly on the absolute calibration of $U^{k'}_{37}$ to SST, as the gradient in Pliocene proxy values (**Figure 4b**) is strongly reduced relative to our core top $U^{k'}_{37}$ transect.

The SST reconstructions reflect a reduced SST gradient between the western and eastern EEP and support other alkenone-based and Mg/Ca paleothermometer records of reduced zonal gradients between the western Pacific warm pool and the EEP (Dekens et al., 2007; Fedorov et al., 2006; Lawrence et al., 2006; Wara et al., 2005). The boundary between warmer western (Site 1338) and cooler eastern (Sites 846 and 849) SSTs persisted during the Pliocene, despite the overall weakening in the Pliocene zonal SST gradient (**Figure S7**).

A combination of both top-down and bottom-up forcings may be responsible for the Pliocene SST and productivity patterns reported here. An increase in atmospheric pCO_2 may produce approximately equal warming across the eastern and western EEP, thereby maintaining the modern strong SST gradient (Heede & Fedorov, 2021; Jia & Wu, 2013; Lee & Poulsen, 2005). However, the alkenone SST record presented here indicates that the eastern EEP experienced greater Pliocene warming than the core of the EEP relative to today (**Figure 3d**), which implies that the top-down forcing is not solely responsible for Pliocene EEP temperature anomalies (Fedorov et al., 2013).

By contrast, warming of subsurface water at the base of the thermocline in the eastern EEP (a possible consequence of higher global pCO_2 warming high latitudes and transporting water through an oceanic tunnel) would produce zonal differences in SST akin to the observed SST gradient reduction recorded in the alkenone data presented here (Brierley et al., 2009; Dekens et al., 2007; Fedorov et al., 2006; Ford et al., 2015; Gu & Philander, 1997; Lee &

Poulsen, 2005). Source waters for the Equatorial Undercurrent in the South Pacific and Southern Ocean likely experienced warmer SSTs during the Pliocene based on extratropical alkenone SST records and ocean general circulation models (Brierley et al., 2009). With warmer subsurface waters, upwelling would produce a less pronounced EEP cold tongue.

If our interpretation of strong east-west gradients in productivity in the warm Pliocene are correct, these observations raise the question of background changes in wind stress and subsurface nutrient content, factors that would exert primary control on productivity. The significant reduction in Pliocene C_{37} total and biogenic opal MARs from the eastern to western EEP (**Figure 5c-d**) suggests that E-W differences in zonal upwelling velocity, zonal winds, or vertical density profiles (which would have been weaker with warmer subsurface waters feeding the thermocline) influenced productivity during the Pliocene when weaker zonal SST gradients prevailed. Upwelling rates would depend on the wind stress at the ocean surface, and on the density structure of the shallow subsurface, as the work required for wind stress to upwell water will depend on the density gradient.

Easterly trade winds, which drive EEP upwelling today, may have been weaker in the Pliocene when pole-equator temperature gradients were reduced (Dowsett et al., 1996). Since ~3.6 Ma, changes in tropical wind fields may have fueled increased upwelling and productivity as Northern Hemisphere glaciation intensified (Steph et al., 2010). However, upper-ocean stratification in the EEP may have been diminished during the Pliocene relative to modern (Bartoli et al., 2011; Burls et al., 2017), so average wind speeds equal to or slower than modern could result in upwelling strong enough to support the productivity gradients observed here. The observation that the Pliocene zonal productivity gradient was as strong if not stronger than modern suggests that Pliocene upwelling was more effective than today at supporting highly

productive waters in the eastern EEP (**Figure 5**). Further analyses of thermocline depth proxies and model simulations of trade winds and vertical upwelling velocity are necessary to elucidate implied changes in upwelling velocity.

An alternative possibility is that a greater nutrient content of upwelled waters, in addition to an increase in upwelling velocity, could account for the larger productivity gradient across the Pliocene EEP. Differences in intermediate water nutrient sources during the Pliocene compared to modern (i.e., North Pacific Deep Water formation) may explain the strengthened tropical zonal productivity gradient (Ford et al., 2022). Additionally, the biogeochemistry of high latitude waters may have changed between the Pliocene and today, and as these nutrient-rich high latitude source waters joined subtropical gyre surface waters as the oceanic tunnel, they delivered nutrients to the EEP thermocline (Lee & Poulsen, 2005; Palter et al., 2011; Philander & Fedorov, 2003; Sarmiento et al., 2004). Specifically, higher nitrate and phosphate from SAMW may have been exported through the Pliocene tunnel, independent of changes in ocean circulation (Rafter et al., 2013; Toggweiler et al., 1991). North Pacific $\delta^{13}C$ records show a reversal in the meridional carbon isotope gradient during the mid-Pliocene, suggesting that North Pacific Deep Water formed in the warmer Pliocene and could account for the proposed older, more nutrient-rich water upwelling in the EEP (Ford et al., 2022). Incomplete nutrient utilization in North Pacific Deep Water formation regions could export excess nutrients to lower latitudes, thereby fueling highly productive but warmer eastern EEP waters during the Pliocene (Burls et al., 2017; Shankle et al., 2021). Air-sea disequilibrium of CO_2 also indicates that warm but nutrient-rich waters upwelled in the EEP because the higher "excess CO_2 indicates incomplete nutrient utilization in the Mio-Pliocene (Zhang et al., 2017). Studies tracking pH as a proxy for water nutrient content (where lower pH is associated with higher nutrient concentrations) attest that

more nutrient-rich water upwelled in the Pliocene EEP relative to modern, which would allow for a smaller volume of less stratified upwelled water to support greater productivity (Shankle et al., 2021), potentially counteracting the influence of unchanged or even reduced easterly wind strength during the warmer Pliocene.

Despite the possibility that upwelled water nutrient content could influence the productivity gradient detected in the Pliocene EEP, a subsurface tilt of the nutricline and thermocline must have persisted to account for the continued zonal variations in upwelling that produce much stronger biogenic opal and alkenone concentration MARs in the eastern EEP than in the west (Etourneau et al., 2013). The prevalence of biogenic opal in the eastern EEP records presented here indicate that silicate concentrations were sufficiently high to support diatom blooms that diluted the carbonate record (**Figure 5c**); attributing the source of EEP silicate to either the North Pacific or Southern Ocean would be constructive. Today, the North Pacific is Si-rich (Reynolds et al., 2006), which may imply that North Pacific waters supplied EEP upwelling during the Pliocene to a greater degree than they do in the present. The main sites of biogenic opal deposition have shifted around the global oceans over at least the past 15 Ma, and during the Mid to Late Pliocene, the EEP was a major opal sink (Cortese et al., 2004), which the bio-SiO_2 MARs reported here confirm.

4.2 Orbital-scale controls on SST and upwelling

The interpretation of the importance of bottom-up versus top-down controls on background EEP state also affect the interpretation of the orbital-scale variability observed in our SST and paleoproductivity time series. The similarity of the zonal SST gradient to the $\delta^{18}O$ record (Pearson correlation between Site U1338-846 SST gradient and $\delta^{18}O$ = 0.547) is a strong

indicator of a global, and likely high-latitude, control (**Figure 4**). The strong coherence between $\delta^{18}O$ and the zonal SST gradient between the western and eastern EEP sites provides quantitative support for this global control on EEP SST (**Figure 7e**). Moreover, there are orbital-scale variations in both *Florisphaera profunda* nannofossil MAR and C_{37} total at Site 846 in the eastern EEP through the early Pleistocene (Bolton, Lawrence, et al., 2010), which indicate that the variations in temperature and biogeochemical properties reported here may reflect fluctuations in thermocline depth on orbital time scales.

As obliquity forcing is negligible in the tropics (Lawrence et al., 2006; Lee & Poulsen, 2005; Z. Liu & Herbert, 2004), the significant spectral sensitivity to obliquity reported here (**Figure 7**) attests to processes associates with the high latitudes (Etourneau et al., 2013; Lee & Poulsen, 2005). The strong sensitivity to obliquity in the Pliocene eastern EEP SST suggests that the upwelling of high latitude-sourced waters, which may respond to changes in Earth's tilt, was enhanced relative to western and central EEP sites (**Figure 7**; Bolton et al., 2010). *F. profunda* phytoplankton abundance varies with obliquity in the eastern EEP during the Early Pleistocene as well, implying that bottom-up forcings originating in the Southern Ocean affect the EEP before the western Pacific (Bolton, Lawrence, et al., 2010). The M2 glacial interval at ~3.295 Ma is clearly detected as a cold excursion lasting ~20 kyr in both the benthic $\delta^{18}O$ records and the alkenone SST and C_{37} total records (**Figure 3**), and it is a particular example of how a global anomaly in $\delta^{18}O$ manifests locally in enhanced EEP SST and productivity gradients (**Figure 4**).

5. Conclusion

The SST and productivity data reported here support a relaxation of the coupling between physical (SST) and biogeochemical (productivity) gradients evident during modern El Niño

events (Dekens et al., 2007; Shankle et al., 2021). This decoupling may reflect significantly different tropical Pacific water properties than modern and also from the hypothesized "El Padre" permanent El Niño-like state of the Pliocene (Ford et al., 2015). Instead, source water of Pliocene EEP upwelling could have been located either farther toward the pole in the Southern Ocean (Ford et al., 2012, 2015; Shankle et al., 2021) or in the North Pacific (Ford et al., 2022) before being brought up to intermediate depths (1000 m) in the tropical Indo-Pacific and upwelled in the EEP.

A mix of two scenarios can explain the paradoxically reduced SST gradient and strong productivity gradient measured in the Pliocene EEP: warmer waters were upwelled at faster rates than modern, or upwelling strength was unchanged but more nutrient-rich warm waters were delivered to the surface. Either the biogeochemical properties and temperature, or the origin region of the warm subsurface source water in the Late Pliocene were different than the cold and nutrient-rich water upwelling in the EEP today (Ma et al., 2015). Ultimately, vigorous upwelling of possibly more nutrient-rich and warmer waters from the base of the thermocline can explain the observed changes in the Late Pliocene EEP records (Dekens et al., 2007). In either case, the reduced Pliocene EEP SST gradient should not be interpreted as a signal of reduced upwelling.

These changes observed in the EEP sediment record and proposed high latitude forcings have implications for future warming and the ability of the EEP to sequester atmospheric CO_2. The record presented here reflects an equilibrated system in the Late Pliocene, while the next 100 years of anthropogenically-induced climate change will see the system transitioning and not necessarily replicating the Pliocene. In an equilibrated regime, a warmer world could see changes in equatorial Pacific upwelling akin to the Pliocene reduced zonal SST gradient and ecological shift toward high siliceous productivity in the eastern EEP. These changes present

significant consequences for adjacent communities dependent on the economic and ecosystem services provided by the EEP (Anderson et al., 2017; Christensen et al., 2014; Gutiérrez et al., 2016; Iizumi et al., 2014).

Acknowledgments

This research used samples and/or data provided by the International Ocean Discovery Program (IODP). Funding for this research was provided by NSF grants 1545859 and 1459280 awarded to TDH. This work was supported by a Geological Society of America Graduate Student Research Grant, an Institute at Brown for Environment and Society Graduate Research, Training, and Travel Grant, and a NASA Rhode Island Space Grant to KMK. We thank Weimin Si for assisting with the Gaussian Process modeling code. We thank Patrick Rafter, Yige Zhang, and two anonymous reviewers for comments that improved the manuscript. The authors report no conflicts of interest.

Data availability statement

The alkenone temperature and productivity core top and downcore data, the X-ray flourescence accumulation rate and element ratio data, and the spectral power and coherency data used for this research are archived at PANGAEA® - Data Publisher for Earth & Environmental Science. For core top and downcore data, see Kimble et al. (2024a, b). For the Gaussian Process code, see http://github.com/SheffieldML/GPy.

Figures

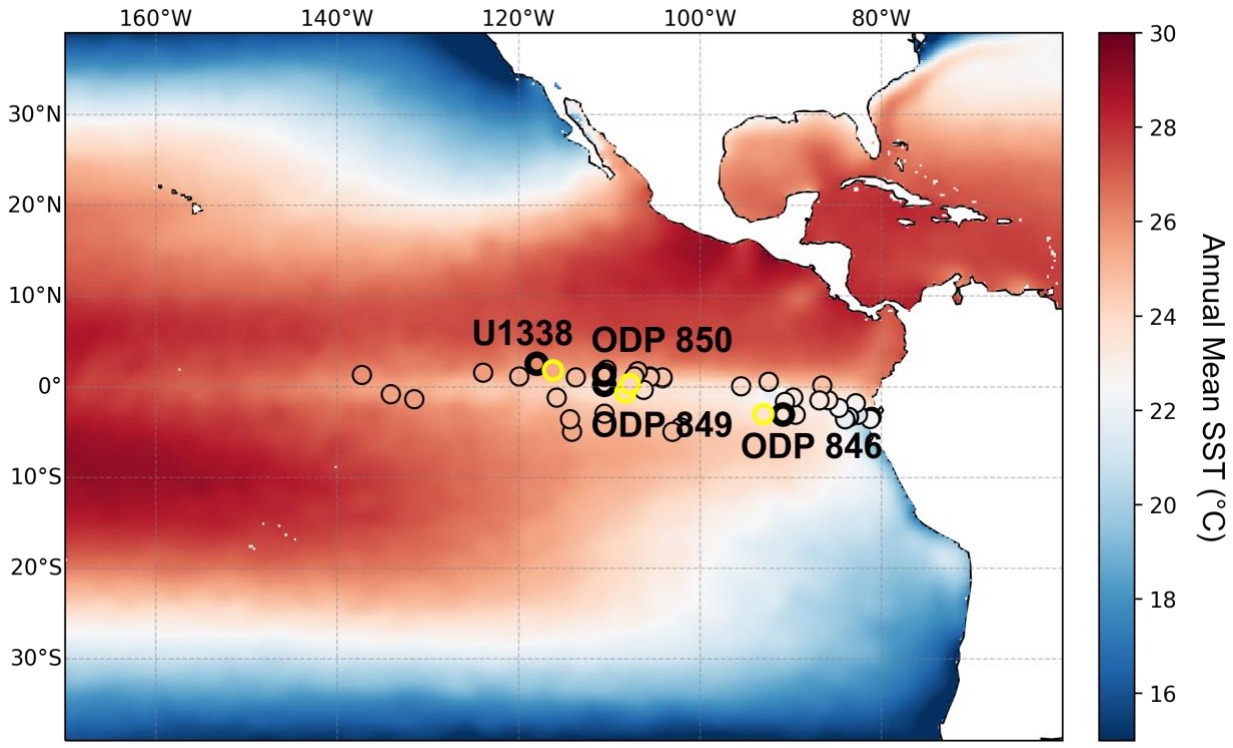

Figure 1. Locations of ODP Sites 846, 849, and 850 and IODP Site U1338 (bold black outlines) in the EEP, along with the paleo-locations of the four sites backtracked to 3 Ma (bold yellow outlines). The 44 core top sites are displayed with thin black outlines. Site locations are overlayed on modern annual mean SST from WOA18 (Boyer et al., 2018; Locarnini et al., 2019). The 3 Ma locations of Sites 846 and U1338 represent a modern zonal SST gradient of 1.8°C, while the meridional SST gradient between the 3 Ma locations of Sites 849 and 850 is 0.3°C.

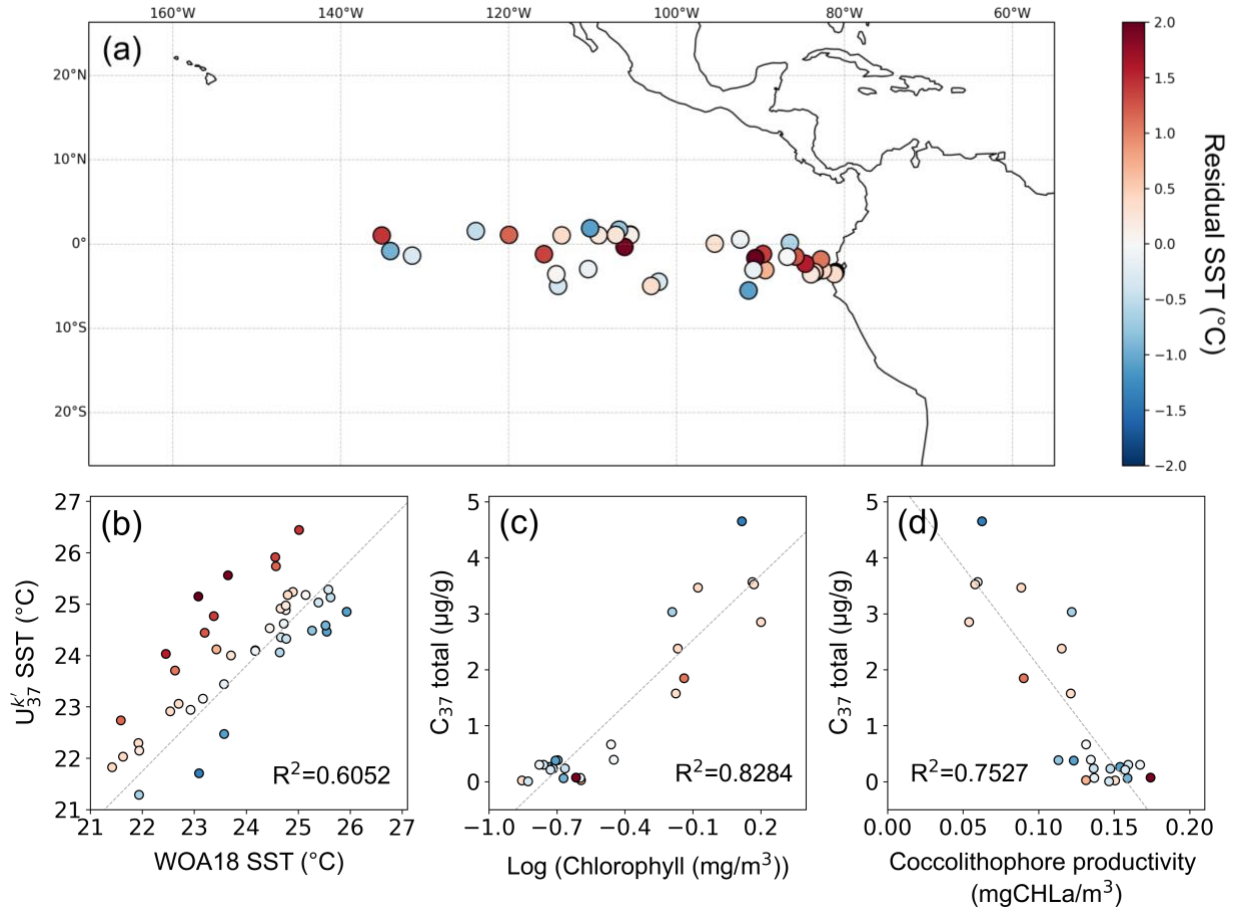

Figure 2. (a) Residual SST across the modern EEP, calculated as the difference between $U^{k'}_{37}$ SST (using the calibration of Prahl et al. [1988]) and WOA18 SST (Boyer et al., 2018; Locarnini et al., 2019). (b) Correlation between WOA18 SST and $U^{k'}_{37}$ SST, with slope of the linear trendline = 1.03. (c) Correlation between chlorophyll estimates from the MODIS satellite (NASA Goddard Space Flight Center, 2022) and core top C_{37} total concentration. (d) Core top coccolithophore productivity (measured in mg chlorophyll-*a* per m^3, from Losa et al. [2017]) compared to C_{37} total concentrations also suggests that C_{37} total does not reflect total coccolithophore community production.

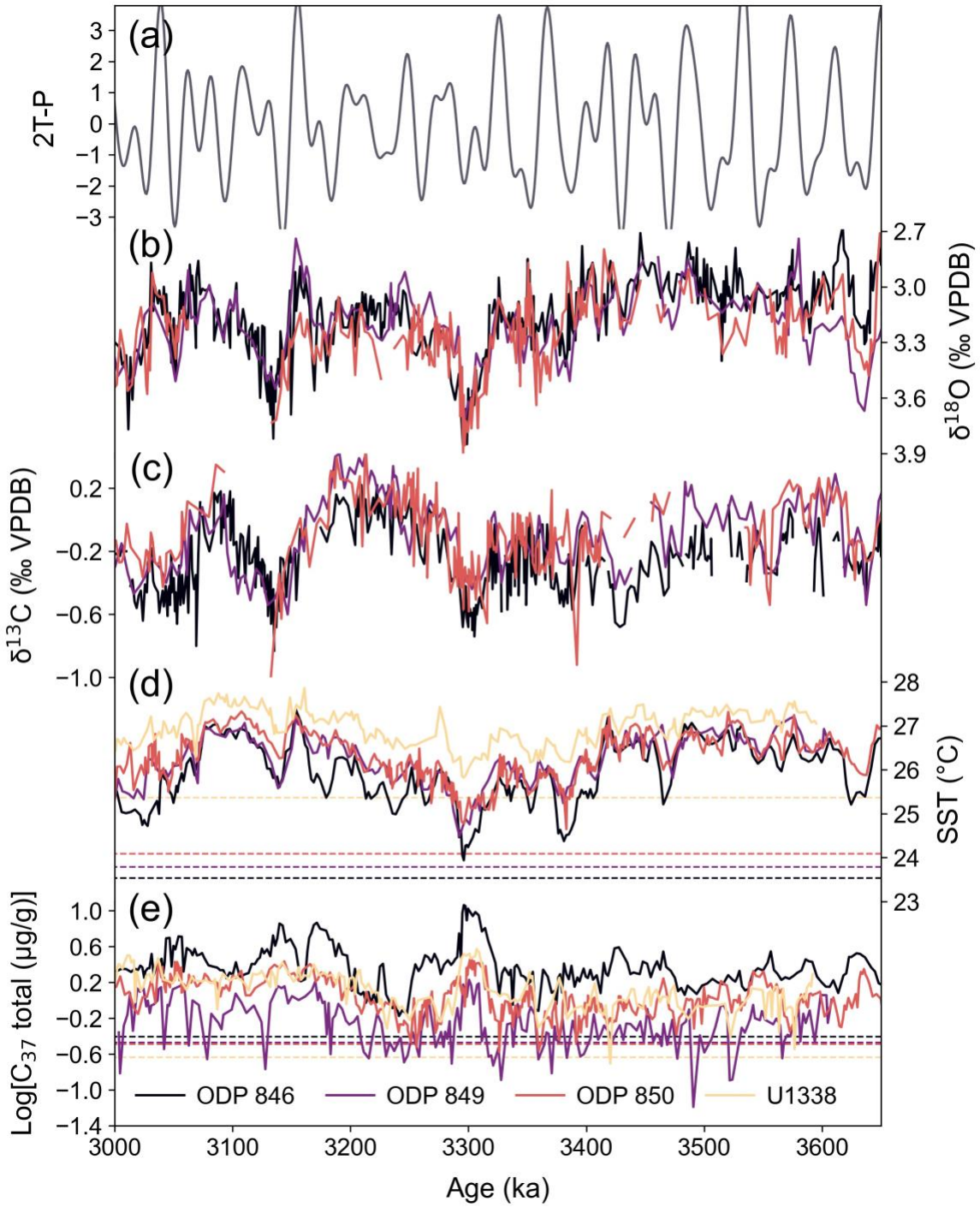

Figure 3. Time series of SST and productivity proxies from ODP Sites 846, 849, and 850 and IODP Site U1338 in the EEP from 3.0-3.6 Ma. (a) Orbital time series template displaying 2 × obliquity normalized - precession normalized (2T-P), (b) benthic $\delta^{18}O$, (c) benthic $\delta^{13}C$, (d) $U^{k'}_{37}$ SST (using the calibration of Müller et al. [1998]) with dashed lines representing modern SST derived from WOA18 observations (Boyer et al., 2018; Locarnini et al., 2019) at the backtracked site locations from 3 Ma, and (e) Log[C_{37} total concentration] with dashed lines representing modern Log[C_{37} total] estimated from core top samples corresponding to the 3 Ma paleo-locations of each site.

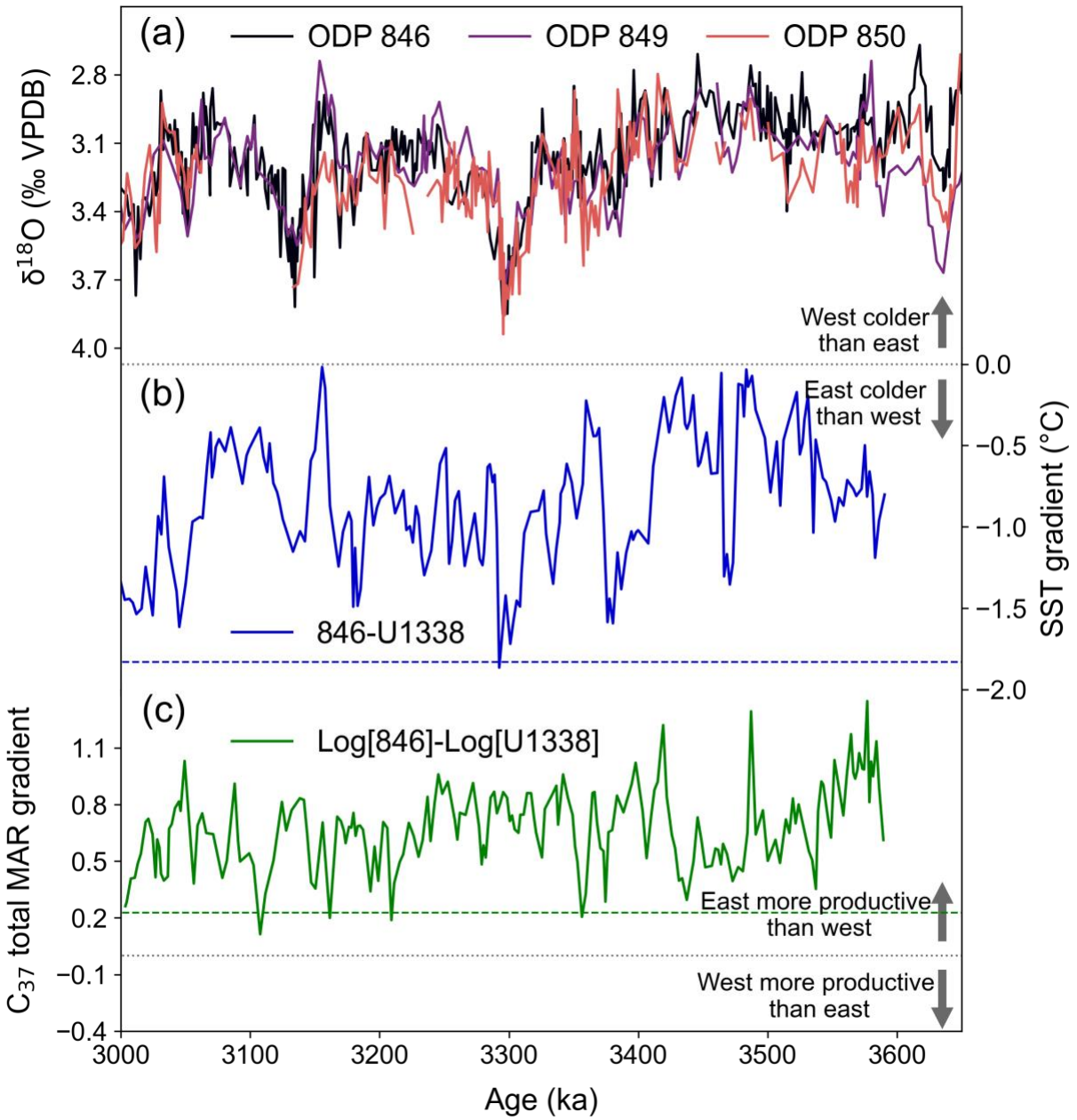

Figure 4. Time series of (a) benthic $\delta^{18}O$, (b) SST gradient between Sites U1338 and 846 and (c) Log[C_{37} total MAR] gradient between Sites 846 and U1338, with the blue and green dashed lines representing the modern SST and Log[C_{37} total] gradients, respectively, using the 3 Ma paleo-locations of Sites 846 and U1338. The gray dotted lines represent 0, or no gradient. Positive values in (b) reflect a cooler western EEP relative to the eastern EEP, and positive values in (c) reflect a more productive eastern EEP relative to the western EEP.

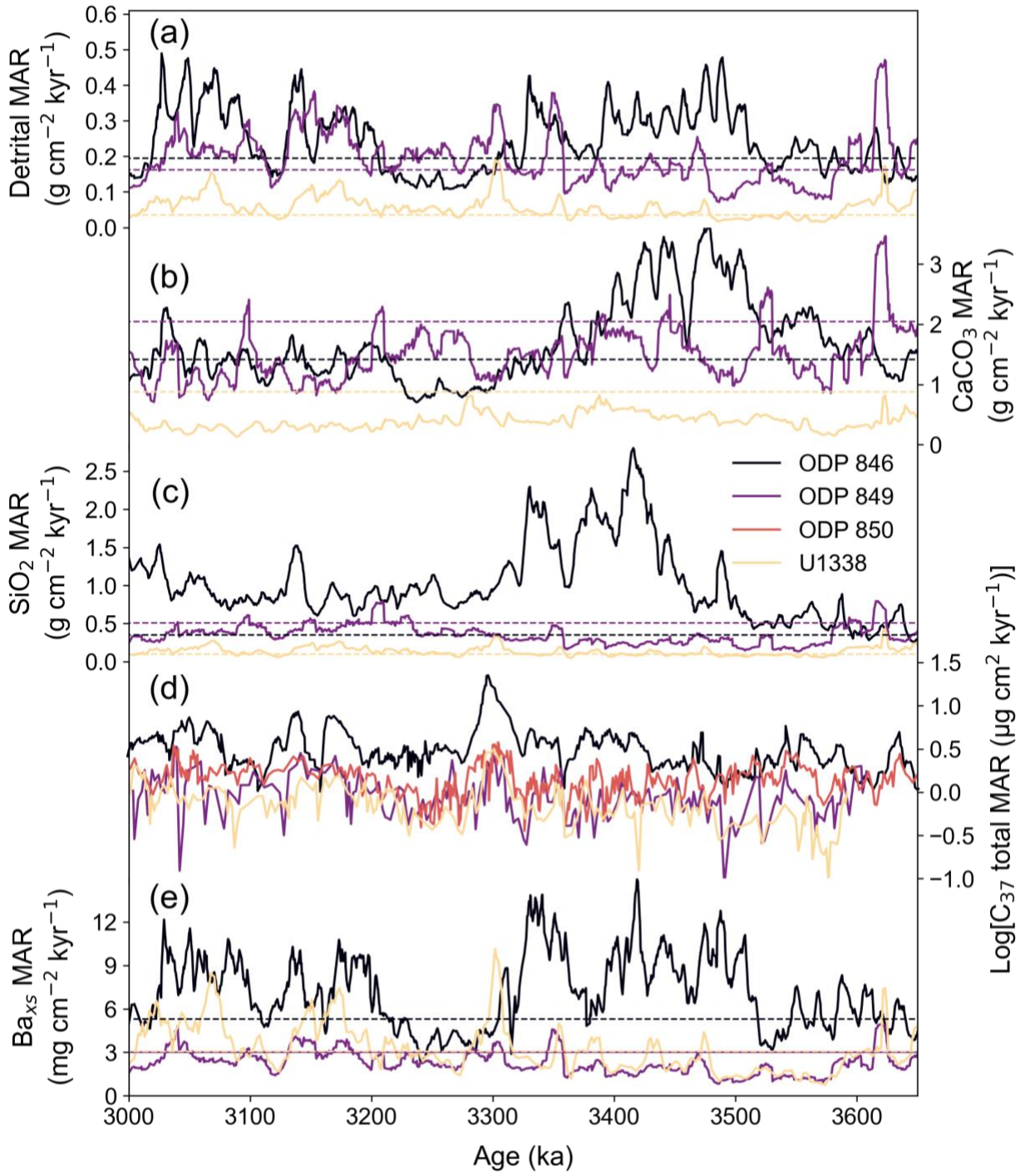

Figure 5. Time series of (a) detrital MAR, (b) $CaCO_3$ MAR, (c) bio-SiO_2 MAR, (d) Log[C_{37} total MAR], and (e) Ba_{xs} MAR with dashed lines representing modern MAR values from ODP Sites 846 and 849, and IODP Site U1338. Note that the Ba_{xs} MARs from Sites 849 and U1338 are calculated from 10kV XRF scans, which are less reliable than the 50 kV scans of Site 846.

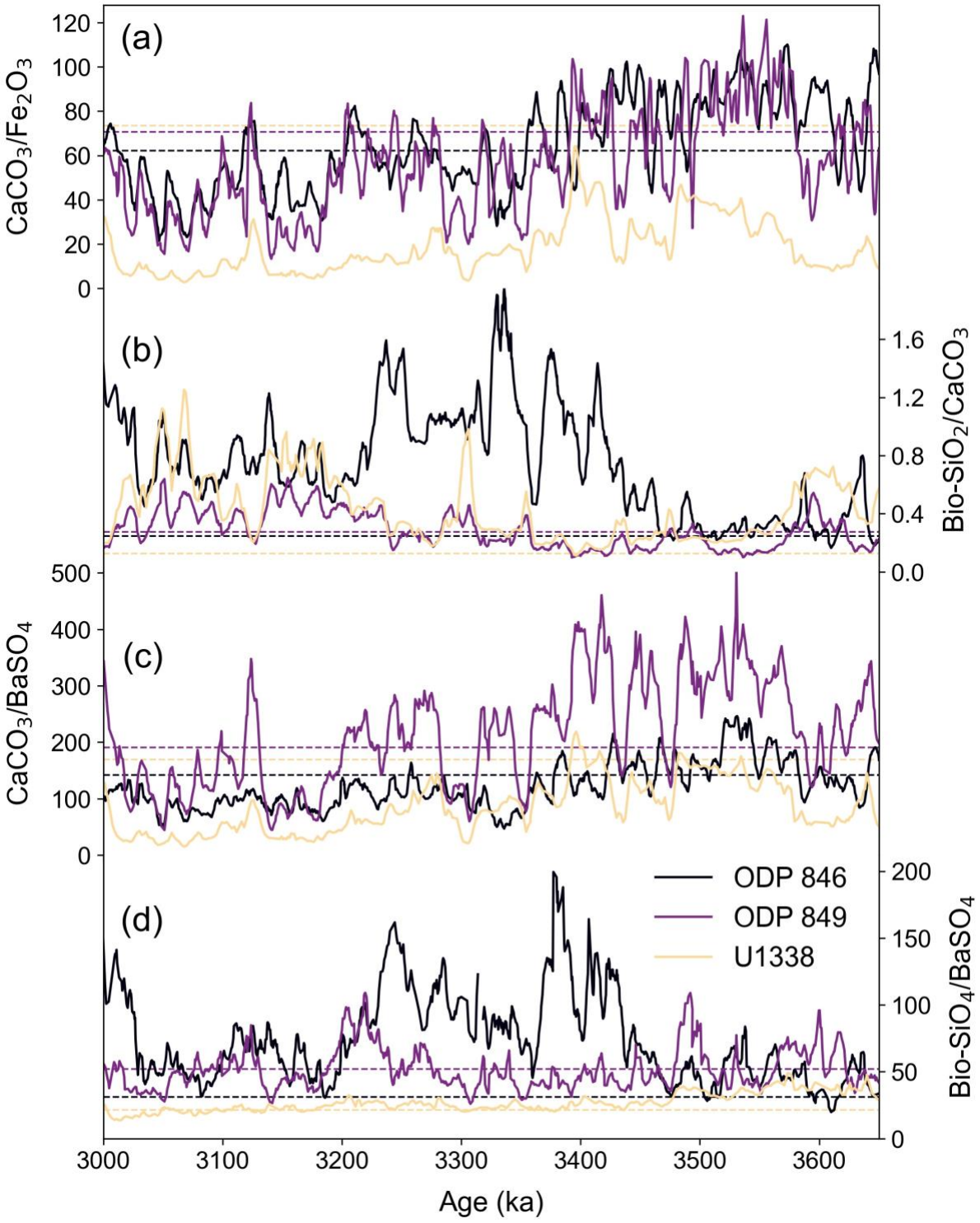

Figure 6. Time series of (a) $CaCO_3/Fe_2O_3$ ratios, (b) bio-$SiO_2/CaCO_3$ ratios, (c) $CaCO_3/BaSO_4$ ratios, and (d) bio-$SiO_2/BaSO_4$ ratios with dashed lines representing modern ratio values from ODP Sites 846 and 849, and IODP Site U1338.

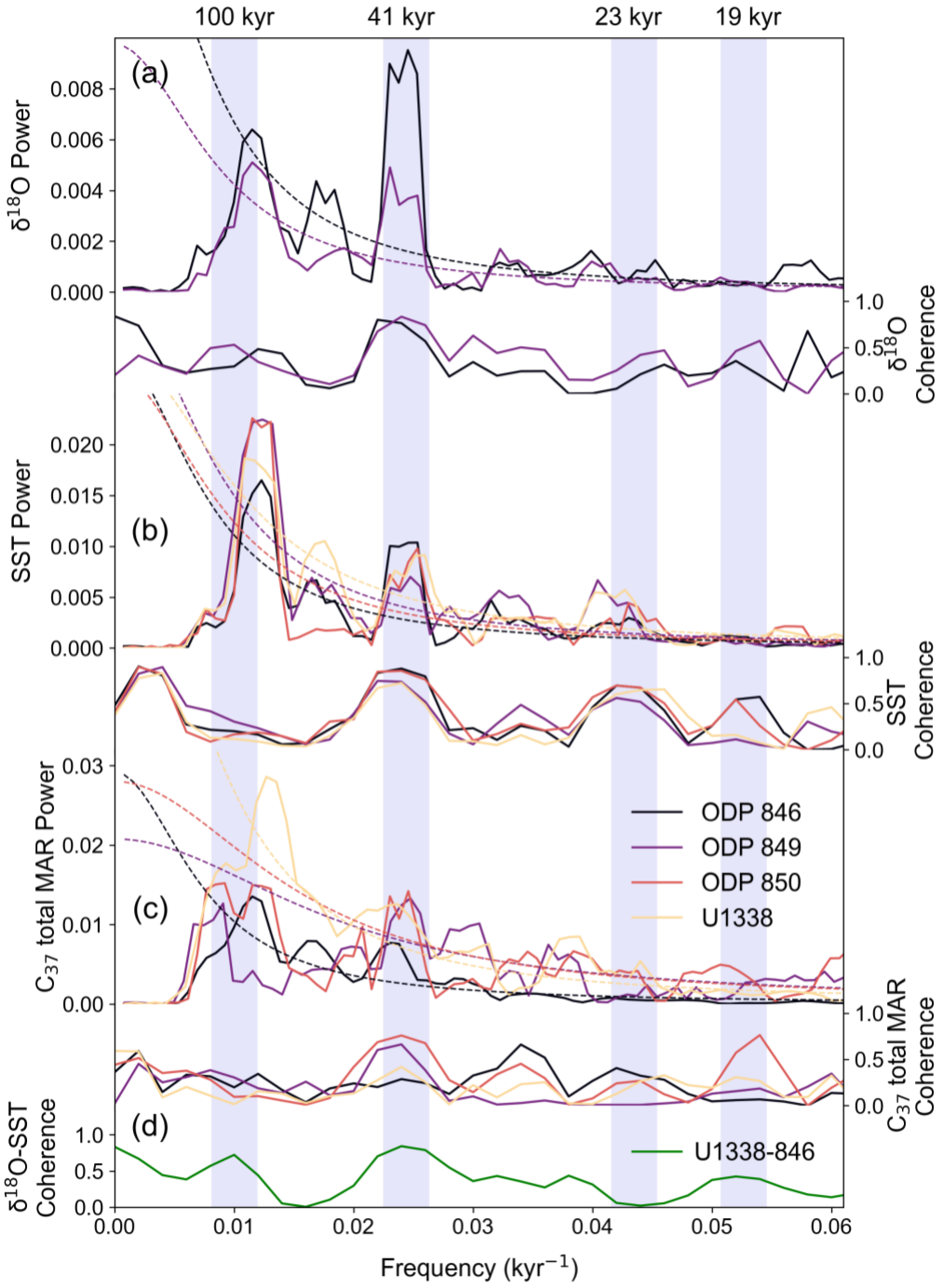

Figure 7. Spectral power and coherence relative to ETP of (a) benthic $\delta^{18}O$, (b) SST, and (c) C_{37} total MAR from ODP Sites 846, 849, 850, and IODP Site U1338, and (d) coherence of $\delta^{18}O$ relative to the SST gradient between U1338-846. Data are normalized, detrended, and linearly interpolated to an age scale with equal <3 kyr time steps prior to bandpass filtering between 10-130 kyr to remove high and low frequencies outside the range of orbital frequencies discussed here. The multitaper method Fourier transform is used to analyze spectral power (Meyers et al., 2021). The ARAND time-series analysis software was used to calculate coherency (Howell et al., 2006).

References

Anderson, R. F., Sachs, J. P., Fleisher, M. Q., Allen, K. A., Yu, J., Koutavas, A., & Jaccard, S. L. (2019). Deep-Sea Oxygen Depletion and Ocean Carbon Sequestration During the Last Ice Age. *Global Biogeochemical Cycles*, *33*(3), 301–317. https://doi.org/10.1029/2018GB006049

Anderson, W., Seager, R., Baethgen, W., & Cane, M. (2017). Crop production variability in North and South America forced by life-cycles of the El Niño Southern Oscillation. *Agricultural and Forest Meteorology*, *239*, 151–165. https://doi.org/10.1016/j.agrformet.2017.03.008

Bartoli, G., Hönisch, B., & Zeebe, R. E. (2011). Atmospheric CO2 decline during the Pliocene intensification of Northern Hemisphere glaciations. *Paleoceanography*, *26*(4). https://doi.org/10.1029/2010PA002055

Behrenfeld, M. J., Bale, A. J., Kolber, Z. S., Aiken, J., & Falkowski, P. G. (1996). Confirmation of iron limitation of phytoplankton photosynthesis in the equatorial Pacific Ocean. *Nature*, *383*(6600), Article 6600. https://doi.org/10.1038/383508a0

Bolton, C. T., Lawrence, K. T., Gibbs, S. J., Wilson, P. A., Cleaveland, L. C., & Herbert, T. D. (2010). Glacial–interglacial productivity changes recorded by alkenones and microfossils in late Pliocene eastern equatorial Pacific and Atlantic upwelling zones. *Earth and Planetary Science Letters*, *295*(3–4), 401–411. https://doi.org/10.1016/j.epsl.2010.04.014

Bostock, H. C., Opdyke, B. N., & Williams, M. J. M. (2010). Characterising the intermediate depth waters of the Pacific Ocean using δ13C and other geochemical tracers. *Deep Sea Research Part I: Oceanographic Research Papers*, *57*(7), 847–859. https://doi.org/10.1016/j.dsr.2010.04.005

Boyer, T. P., García, H. E., Locarnini, R. A., Zweng, M. M., Mishonov, A. V., Reagan, J. R., Weathers, K. A., Baranova, O. K., Paver, C. R., Seidov, D., & Smolyar, I. V. (2018). *World Ocean Atlas 2018. Temperature* [Dataset]. NOAA National Centers for Environmental Information. https://www.ncei.noaa.gov/archive/accession/NCEI-WOA18

Brierley, C. M., Fedorov, A. V., Liu, Z., Herbert, T. D., Lawrence, K. T., & LaRiviere, J. P. (2009). Greatly Expanded Tropical Warm Pool and Weakened Hadley Circulation in the Early Pliocene. *Science*, *323*(5922), 1714–1718. https://doi.org/10.1126/science.1167625

Burls, N. J., & Fedorov, A. V. (2014). Simulating Pliocene warmth and a permanent El Niño-like state: The role of cloud albedo. *Paleoceanography*, *29*(10), 893–910. https://doi.org/10.1002/2014PA002644

Burls, N. J., Fedorov, A. V., Sigman, D. M., Jaccard, S. L., Tiedemann, R., & Haug, G. H. (2017). Active Pacific meridional overturning circulation (PMOC) during the warm Pliocene. *Science Advances*, *3*(9), e1700156. https://doi.org/10.1126/sciadv.1700156

Christensen, V., de la Puente, S., Sueiro, J. C., Steenbeek, J., & Majluf, P. (2014). Valuing seafood: The Peruvian fisheries sector. *Marine Policy*, *44*, 302–311. https://doi.org/10.1016/j.marpol.2013.09.022

Conte, M. H., Sicre, M.-A., Rühlemann, C., Weber, J. C., Schulte, S., Schulz-Bull, D., & Blanz, T. (2006). Global temperature calibration of the alkenone unsaturation index (UK′37) in surface waters and comparison with surface sediments. *Geochemistry, Geophysics, Geosystems*, *7*(2). https://doi.org/10.1029/2005GC001054

Cortese, G., Gersonde, R., Hillenbrand, C.-D., & Kuhn, G. (2004). Opal sedimentation shifts in the World Ocean over the last 15 Myr. *Earth and Planetary Science Letters*, *224*(3), 509–527. https://doi.org/10.1016/j.epsl.2004.05.035

de la Vega, E., Chalk, T. B., Wilson, P. A., Bysani, R. P., & Foster, G. L. (2020). Atmospheric CO 2 during the Mid-Piacenzian Warm Period and the M2 glaciation. *Scientific Reports*, *10*(1), Article 1. https://doi.org/10.1038/s41598-020-67154-8

Dekens, P. S., Ravelo, A. C., & McCarthy, M. D. (2007). Warm upwelling regions in the Pliocene warm period. *Paleoceanography*, *22*(3). https://doi.org/10.1029/2006PA001394

Delcroix, T. (1998). Observed surface oceanic and atmospheric variability in the tropical Pacific at seasonal and ENSO timescales: A tentative overview. *Journal of Geophysical Research: Oceans*, *103*(C9), 18611–18633. https://doi.org/10.1029/98JC00814

Diz, P., Hernández-Almeida, I., Bernárdez, P., Pérez-Arlucea, M., & Hall, I. R. (2018). Ocean and atmosphere teleconnections modulate east tropical Pacific productivity at late to middle Pleistocene terminations. *Earth and Planetary Science Letters*, *493*, 82–91. https://doi.org/10.1016/j.epsl.2018.04.024

Dowsett, H., Barron, J., & Poore, R. (1996). Middle Pliocene sea surface temperatures: A global reconstruction. *Marine Micropaleontology*, *27*, 13–25. https://doi.org/10.1016/0377-8398(95)00050-X

Dowsett, H. J. (2007). The PRISM palaeoclimate reconstruction. In M. Williams (Ed.), *Deep-time perspective on climate change: Marrying the signal from computer models and biological proxies*. Geological Society of London.

Dugdale, R. C., & Goering, J. J. (1967). Uptake of New and Regenerated Forms of Nitrogen in Primary Productivity1. *Limnology and Oceanography*, *12*(2), 196–206. https://doi.org/10.4319/lo.1967.12.2.0196

Dymond, J., Suess, E., & Lyle, M. (1992). Barium in Deep-Sea Sediment: A Geochemical Proxy for Paleoproductivity. *Paleoceanography*, *7*(2), 163–181. https://doi.org/10.1029/92PA00181

Etourneau, J., Robinson, R. S., Martinez, P., & Schneider, R. (2013). Equatorial Pacific peak in biological production regulated by nutrient and upwelling during the late Pliocene/early Pleistocene cooling. *Biogeosciences*, *10*(8), 5663–5670. https://doi.org/10.5194/bg-10-5663-2013

Fedorov, A. V., Brierley, C. M., Lawrence, K. T., Liu, Z., Dekens, P. S., & Ravelo, A. C. (2013). Patterns and mechanisms of early Pliocene warmth. *Nature*, *496*(7443), Article 7443. https://doi.org/10.1038/nature12003

Fedorov, A. V., Dekens, P. S., McCarthy, M., Ravelo, A. C., deMenocal, P. B., Barreiro, M., Pacanowski, R. C., & Philander, S. G. (2006). The Pliocene Paradox (Mechanisms for a Permanent El Niño). *Science*, *312*(5779), 1485–1489. https://doi.org/10.1126/science.1122666

Fiedler, P. C., Philbrick, V., & Chavez, F. P. (1991). Oceanic upwelling and productivity in the eastern tropical Pacific. *Limnology and Oceanography*, *36*(8), 1834–1850. https://doi.org/10.4319/lo.1991.36.8.1834

Ford, H. L., Burls, N. J., Jacobs, P., Jahn, A., Caballero-Gill, R. P., Hodell, D. A., & Fedorov, A. V. (2022). Sustained mid-Pliocene warmth led to deep water formation in the North Pacific. *Nature Geoscience*, 1–6. https://doi.org/10.1038/s41561-022-00978-3

Ford, H. L., Ravelo, A. C., Dekens, P. S., LaRiviere, J. P., & Wara, M. W. (2015). The evolution of the equatorial thermocline and the early Pliocene El Padre mean state. *Geophysical Research Letters*, *42*(12), 4878–4887. https://doi.org/10.1002/2015GL064215

Ford, H. L., Ravelo, A. C., & Hovan, S. (2012). A deep Eastern Equatorial Pacific thermocline during the early Pliocene warm period. *Earth and Planetary Science Letters*, *355–356*, 152–161. https://doi.org/10.1016/j.epsl.2012.08.027

Foster, G. L., Royer, D. L., & Lunt, D. J. (2017). Future climate forcing potentially without precedent in the last 420 million years. *Nature Communications*, *8*(1), Article 1. https://doi.org/10.1038/ncomms14845

Gebregiorgis, D., Giosan, L., Hathorne, E. C., Anand, P., Nilsson-Kerr, K., Plass, A., Lückge, A., Clemens, S. C., & Frank, M. (2020). What Can We Learn From X-Ray Fluorescence Core Scanning Data? A Paleomonsoon Case Study. *Geochemistry, Geophysics, Geosystems*, *21*(2). https://doi.org/10.1029/2019GC008414

Gu, D., & Philander, S. G. (1997). Interdecadal Climate Fluctuations That Depend on Exchanges Between the Tropics and Extratropics. *Science*, *275*(5301), 805–807. https://doi.org/10.1126/science.275.5301.805

Gutiérrez, D., Akester, M., & Naranjo, L. (2016). Productivity and Sustainable Management of the Humboldt Current Large Marine Ecosystem under climate change. *Environmental Development*, *17*, 126–144. https://doi.org/10.1016/j.envdev.2015.11.004

Heede, U. K., & Fedorov, A. V. (2021). Eastern equatorial Pacific warming delayed by aerosols and thermostat response to CO2 increase. *Nature Climate Change*, *11*(8), Article 8. https://doi.org/10.1038/s41558-021-01101-x

Herbert, T. D., Caballero-Gill, R., & Novak, J. B. (2021). A revised mid-Pliocene composite section centered on the M2 glacial event for ODP Site 846. *Climate of the Past*, *17*(3), 1385–1394. https://doi.org/10.5194/cp-17-1385-2021

Herbert, T. D., Lawrence, K. T., Tzanova, A., Peterson, L. C., Caballero-Gill, R., & Kelly, C. S. (2016). Late Miocene global cooling and the rise of modern ecosystems. *Nature Geoscience*, *9*(11), Article 11. https://doi.org/10.1038/ngeo2813

Herbert, T. D., & Mayer, L. A. (1991). Long Climatic Time Series from Sediment Physical Property Measurements. *SEPM Journal of Sedimentary Research*, *Vol. 61*. https://doi.org/10.1306/D4267843-2B26-11D7-8648000102C1865D

Howell, P., Pisias, N., Ballance, J., Baughman, J., & Ochs, L. (2006). *ARAND Time-Series Analysis Software* [Computer software]. Brown University.

Iizumi, T., Luo, J.-J., Challinor, A. J., Sakurai, G., Yokozawa, M., Sakuma, H., Brown, M. E., & Yamagata, T. (2014). Impacts of El Niño Southern Oscillation on the global yields of major crops. *Nature Communications*, *5*(1), 3712. https://doi.org/10.1038/ncomms4712

Jacobel, A. W., Anderson, R. F., Jaccard, S. L., McManus, J. F., Pavia, F. J., & Winckler, G. (2020). Deep Pacific storage of respired carbon during the last ice age: Perspectives from bottom water oxygen reconstructions. *Quaternary Science Reviews*, *230*, 106065. https://doi.org/10.1016/j.quascirev.2019.106065

Jia, F., & Wu, L. (2013). A Study of Response of the Equatorial Pacific SST to Doubled-CO2 Forcing in the Coupled CAM–1.5-Layer Reduced-Gravity Ocean Model. *Journal of Physical Oceanography*, *43*(7), 1288–1300. https://doi.org/10.1175/JPO-D-12-0144.1

Kessler, W. S. (2006). The circulation of the eastern tropical Pacific: A review. *Progress in Oceanography*, *69*(2), 181–217. https://doi.org/10.1016/j.pocean.2006.03.009

Kienast, M., MacIntyre, G., Dubois, N., Higginson, S., Normandeau, C., Chazen, C., & Herbert, T. D. (2012). Alkenone unsaturation in surface sediments from the eastern equatorial

Pacific: Implications for SST reconstructions. *Paleoceanography*, *27*(1). https://doi.org/10.1029/2011PA002254

Kimble, K., Herbert, T. D., & Jones, C. (2024). Core top alkenone sea surface temperature and productivity data compared to modern observations in the eastern equatorial Pacific [Dataset]. *PANGAEA*. 10.1594/PANGAEA.963335

Kimble, K., Herbert, T. D., & Jones, C. (2024). Pliocene alkenone sea surface temperature and productivity gradients at eastern equatorial Pacific ODP Sites 138-846, 849, and 850 and IODP Site 321-U1338 [Dataset]. *PANGAEA*. 10.1594/PANGAEA.962716

Ko, T. W., Lee, K. E., Bae, S. W., & Lee, S. (2018). Spatial and temporal distribution of C37 alkenones in suspended materials in the northern East China Sea. *Palaeogeography, Palaeoclimatology, Palaeoecology*, *493*, 102–110. https://doi.org/10.1016/j.palaeo.2018.01.004

Koning, E., Epping, E., & Raaphorst, W. V. (2002). *Determining Biogenic Silica in Marine Samples by Tracking Silicate and Aluminium Concentrations in Alkaline Leaching Solutions*. 32.

Lavín, M. F., Fiedler, P. C., Amador, J. A., Ballance, L. T., Färber-Lorda, J., & Mestas-Nuñez, A. M. (2006). A review of eastern tropical Pacific oceanography: Summary. *Progress in Oceanography*, *69*(2), 391–398. https://doi.org/10.1016/j.pocean.2006.03.005

Lawrence, K. T., Liu, Z., & Herbert, T. D. (2006). Evolution of the Eastern Tropical Pacific Through Plio-Pleistocene Glaciation. *Science*, *312*(5770), 79–83. https://doi.org/10.1126/science.1120395

Lee, S.-Y., & Poulsen, C. J. (2005). Tropical Pacific climate response to obliquity forcing in the Pleistocene: TROPICAL PACIFIC RESPONSE TO OBLIQUITY FORCING. *Paleoceanography*, *20*(4), n/a-n/a. https://doi.org/10.1029/2005PA001161

Lehmann, N., Granger, J., Kienast, M., Brown, K. S., Rafter, P. A., Martínez-Méndez, G., & Mohtadi, M. (2018). Isotopic Evidence for the Evolution of Subsurface Nitrate in the Western Equatorial Pacific. *Journal of Geophysical Research: Oceans*, *123*(3), 1684–1707. https://doi.org/10.1002/2017JC013527

Li, Y.-H. (2000). *A Compendium of Geochemistry: From Solar Nebula to the Human Brain*. Princeton University Press.

Lisiecki, L. E., & Lisiecki, P. A. (2002). Application of dynamic programming to the correlation of paleoclimate records. *Paleoceanography*, *17*(4), 1-1-1–12. https://doi.org/10.1029/2001PA000733

Lisiecki, L. E., & Raymo, M. E. (2005). A Pliocene-Pleistocene stack of 57 globally distributed benthic δ^{18}O records: PLIOCENE-PLEISTOCENE BENTHIC STACK. *Paleoceanography*, *20*(1), n/a-n/a. https://doi.org/10.1029/2004PA001071

Liu, J., Tian, J., Liu, Z., Herbert, T. D., Fedorov, A. V., & Lyle, M. (2019). Eastern equatorial Pacific cold tongue evolution since the late Miocene linked to extratropical climate. *Science Advances*, *5*(4), eaau6060. https://doi.org/10.1126/sciadv.aau6060

Liu, Z., & Herbert, T. D. (2004). High-latitude influence on the eastern equatorial Pacific climate in the early Pleistocene epoch. *Nature*, *427*(6976), Article 6976. https://doi.org/10.1038/nature02338

Liu, Z., & Yang, H. (2003). Extratropical control of tropical climate, the atmospheric bridge and oceanic tunnel. *Geophysical Research Letters*, *30*(5). https://doi.org/10.1029/2002GL016492

Locarnini, M., Mishonov, A., Baranova, O., Boyer, T., Zweng, M., Garcia, H., Reagan, J., Seidov, D., Weathers, K., Paver, C., & Smolyar, I. (2019). World Ocean Atlas 2018, Volume 1: Temperature. *A. Mishonov Technical Ed.*, *NOAA Atlas NESDIS 81*, 52 pp.

Losa, S. N., Soppa, M. A., Dinter, T., Wolanin, A., Brewin, R. J. W., Bricaud, A., Oelker, J., Peeken, I., Gentili, B., Rozanov, V., & Bracher, A. (2017). Synergistic Exploitation of Hyper- and Multi-Spectral Precursor Sentinel Measurements to Determine Phytoplankton Functional Types (SynSenPFT). *Frontiers in Marine Science*, *4*, 203. https://doi.org/10.3389/fmars.2017.00203

Lu, P., McCreary, J. P., & Klinger, B. A. (1998). Meridional Circulation Cells and the Source Waters of the Pacific Equatorial Undercurrent. *Journal of Physical Oceanography*, *28*(1), 62–84. https://doi.org/10.1175/1520-0485(1998)028<0062:MCCATS>2.0.CO;2

Lyle, M., Drury, A. J., Tian, J., Wilkens, R., & Westerhold, T. (2019). Late Miocene to Holocene high-resolution eastern equatorial Pacific carbonate records: Stratigraphy linked by dissolution and paleoproductivity. *Climate of the Past*, *15*, 1715–1739.

Lyle, M., Lyle, A. O., Gorgas, T., Holbourn, A., Westerhold, T., Hathorne, E., Kimoto, K., & Yamamoto, S. (2012). Data report: Raw and normalized elemental data along the Site U1338 splice from X-ray flourescence scanning. *Proceedings of the IODP*, *320/321*. https://doi.org/10.2204/iodp.proc.320321.203.2012

Ma, Z., Ravelo, A. C., Liu, Z., Zhou, L., & Paytan, A. (2015). Export production fluctuations in the eastern equatorial Pacific during the Pliocene-Pleistocene: Reconstruction using

barite accumulation rates. *Paleoceanography*, *30*(11), 1455–1469. https://doi.org/10.1002/2015PA002860

McClymont, E. L., Ford, H. L., Ho, S. L., Tindall, J. C., Haywood, A. M., Alonso-Garcia, M., Bailey, I., Berke, M. A., Littler, K., Patterson, M. O., Petrick, B., Peterse, F., Ravelo, A. C., Risebrobakken, B., De Schepper, S., Swann, G. E. A., Thirumalai, K., Tierney, J. E., van der Weijst, C., … Zhang, Z. (2020). Lessons from a high-CO_2 world: An ocean view from ~ 3 million years ago. *Climate of the Past*, *16*(4), 1599–1615. https://doi.org/10.5194/cp-16-1599-2020

Meyers, S., Malinverno, A., Hinnov, L., Zeeden, C., Liu, H., & Moron, V. (2021). *astrochron: A Computational Tool for Astrochronology*. 144.

Mix, A. C., Pisias, N. G., Rugh, W., Wilson, J., Morey, A., & Hagelberg, T. K. (1995). Benthic foraminifer stable isotope record from Site 849 (0-5 Ma): Local and global climate changes. *Proceedings of the Ocean Drilling Program, Scientific Results*, *138*, 371–412.

Müller, P. J., Kirst, G., Ruhland, G., von Storch, I., & Rosell-Melé, A. (1998). Calibration of the alkenone paleotemperature index U37K′ based on core-tops from the eastern South Atlantic and the global ocean (60°N-60°S). *Geochimica et Cosmochimica Acta*, *62*(10), 1757–1772. https://doi.org/10.1016/S0016-7037(98)00097-0

NASA Goddard Space Flight Center, Ocean Ecology Laboratory, Ocean Biology Processing Group. (2022). *Moderate-resolution Imaging Spectroradiometer (MODIS) Aqua Chlorophyll Data* [dataset]. NASA OB.DAAC. https://doi.org/10.5067/AQUA/MODIS/L3B/CHL/2022

O'Brien, C. L., Foster, G. L., Martínez-Botí, M. A., Abell, R., Rae, J. W. B., & Pancost, R. D. (2014). High sea surface temperatures in tropical warm pools during the Pliocene. *Nature Geoscience*, *7*(8), 606–611. https://doi.org/10.1038/ngeo2194

Palter, J. B., Lozier, M. S., Sarmiento, J. L., & Williams, R. G. (2011). The supply of excess phosphate across the Gulf Stream and the maintenance of subtropical nitrogen fixation. *Global Biogeochemical Cycles*, *25*(4). https://doi.org/10.1029/2010GB003955

Philander, S. G., & Fedorov, A. V. (2003). Role of tropics in changing the response to Milankovich forcing some three million years ago: TROPICS AND GLACIAL CYCLES. *Paleoceanography*, *18*(2), n/a-n/a. https://doi.org/10.1029/2002PA000837

Pisias, N. G., Mayer, L. A., Janecek, T. R., Palmer-Julson, A., & van Andel, T. H. (Eds.). (1995). *Proceedings of the Ocean Drilling Program, 138 Scientific Results* (Vol. 138). Ocean Drilling Program. https://doi.org/10.2973/odp.proc.sr.138.1995

Prahl, F. G., Muehlhausen, L. A., & Zahnle, D. L. (1988). Further evaluation of long-chain alkenones as indicators of paleoceanographic conditions. *Geochimica et Cosmochimica Acta*, *52*, 2303–2310. https://doi.org/10.1016/0016-7037(88)90132-9

Rafter, P. A., DiFiore, P. J., & Sigman, D. M. (2013). Coupled nitrate nitrogen and oxygen isotopes and organic matter remineralization in the Southern and Pacific Oceans. *Journal of Geophysical Research: Oceans*, *118*(10), 4781–4794. https://doi.org/10.1002/jgrc.20316

Rafter, P. A., & Sigman, D. M. (2016). Spatial distribution and temporal variation of nitrate nitrogen and oxygen isotopes in the upper equatorial Pacific Ocean. *Limnology and Oceanography*, *61*(1), 14–31. https://doi.org/10.1002/lno.10152

Raja, M., & Rosell-Melé, A. (2021). Appraisal of sedimentary alkenones for the quantitative reconstruction of phytoplankton biomass. *Proceedings of the National Academy of Sciences*, *118*(2). https://doi.org/10.1073/pnas.2014787118

Rasmussen, C. E., & Williams, C. K. (2006). *Gaussian processes for machine learning* (Vol. 1, p. 159). MIT press.

Ravelo, A. C., Andreasen, D. H., Lyle, M., Olivarez Lyle, A., & Wara, M. W. (2004). Regional climate shifts caused by gradual global cooling in the Pliocene epoch. *Nature*, *429*(6989), 263–267. https://doi.org/10.1038/nature02567

Ravelo, A. C., Dekens, P., & McCarthy, M. (2006). Evidence for El Niño—Like conditions during the Pliocene. *Gsa Today*, *16*. https://doi.org/10.1130/1052-5173(2006)016<4:EFENLC>2.0.CO;2

Ravelo, A. C., Lawrence, K. T., Fedorov, A., & Ford, H. L. (2014). Comment on "A 12-million-year temperature history of the tropical Pacific Ocean." *Science*, *346*(6216), 1467.1-1467. https://doi.org/10.1126/science.1257618

Reynolds, B. C., Frank, M., & Halliday, A. N. (2006). Silicon isotope fractionation during nutrient utilization in the North Pacific. *Earth and Planetary Science Letters*, *244*(1), 431–443. https://doi.org/10.1016/j.epsl.2006.02.002

Robinson, R. S., Jones, C. A., Kelly, R. P., Rafter, P., Etourneau, J., & Martinez, P. (2019). A Cool, Nutrient-Enriched Eastern Equatorial Pacific During the Mid-Pleistocene Transition. *Geophysical Research Letters*, *46*(4), 2187–2195. https://doi.org/10.1029/2018GL081315

Rostek, F., Bard, E., Beaufort, L., Sonzogni, C., & Ganssen, G. (1997). Sea surface temperature and productivity records for the past 240 kyr in the Arabian Sea. *Deep Sea Research Part*

II: Topical Studies in Oceanography, *44*(6–7), 1461–1480. https://doi.org/10.1016/S0967-0645(97)00008-8

Rousselle, G., Beltran, C., Sicre, M.-A., Raffi, I., & De Rafélis, M. (2013). Changes in sea-surface conditions in the Equatorial Pacific during the middle Miocene–Pliocene as inferred from coccolith geochemistry. *Earth and Planetary Science Letters*, *361*, 412–421. https://doi.org/10.1016/j.epsl.2012.11.003

Sarmiento, J. L., Gruber, N., Brzezinski, M. A., & Dunne, J. P. (2004). High-latitude controls of thermocline nutrients and low latitude biological productivity. *Nature*, *427*(6969), Article 6969. https://doi.org/10.1038/nature02127

Scheinost, A. C. (2005). Metal oxides. In *Encyclopedia of Soils in the Environment* (pp. 428–438). Elsevier Academic Press.

Shankle, M. G., Burls, N. J., Fedorov, A. V., Thomas, M. D., Liu, W., Penman, D. E., Ford, H. L., Jacobs, P. H., Planavsky, N. J., & Hull, P. M. (2021). Pliocene decoupling of equatorial Pacific temperature and pH gradients. *Nature*, *598*(7881), 457–461. https://doi.org/10.1038/s41586-021-03884-7

Steph, S., Tiedemann, R., Prange, M., Groeneveld, J., Schulz, M., Timmermann, A., Nürnberg, D., Rühlemann, C., Saukel, C., & Haug, G. H. (2010). Early Pliocene increase in thermohaline overturning: A precondition for the development of the modern equatorial Pacific cold tongue. *Paleoceanography*, *25*(2). https://doi.org/10.1029/2008PA001645

Takahashi, T., Sutherland, S. C., Wanninkhof, R., Sweeney, C., Feely, R. A., Chipman, D. W., Hales, B., Friederich, G., Chavez, F., Sabine, C., Watson, A., Bakker, D. C. E., Schuster, U., Metzl, N., Yoshikawa-Inoue, H., Ishii, M., Midorikawa, T., Nojiri, Y., Körtzinger, A., … de Baar, H. J. W. (2009). Climatological mean and decadal change in surface ocean

pCO2, and net sea–air CO2 flux over the global oceans. *Deep Sea Research Part II: Topical Studies in Oceanography*, *56*(8), 554–577. https://doi.org/10.1016/j.dsr2.2008.12.009

Tierney, J. E., & Tingley, M. P. (2018). BAYSPLINE: A New Calibration for the Alkenone Paleothermometer. *Paleoceanography and Paleoclimatology*, *33*(3), 281–301. https://doi.org/10.1002/2017PA003201

Toggweiler, J. R., & Carson, S. (1995). What are upwelling systems contributing to the ocean's carbon and nutrient budgets? *Environmental Sciences Research Report ES*, *18*, 337–360. https://doi.org/10.1016/s0304-4203(96)00087-4

Toggweiler, J. R., Dixon, K., & Broecker, W. S. (1991). The Peru upwelling and the ventilation of the south Pacific thermocline. *Journal of Geophysical Research: Oceans*, *96*(C11), 20467–20497. https://doi.org/10.1029/91JC02063

Toggweiler, J. R., & Sarmiento, J. L. (1985). Glacial to Interglacial Changes in Atmospheric Carbon Dioxide: The Critical Role of Ocean Surface Water in High Latitudes. In *The Carbon Cycle and Atmospheric CO2: Natural Variations Archean to Present* (pp. 163–184). American Geophysical Union (AGU). https://doi.org/10.1029/GM032p0163

Villanueva, J., Flores, J. A., & Grimalt, J. O. (2002). A detailed comparison of the Uk′37 and coccolith records over the past 290 kyears: Implications to the alkenone paleotemperature method. *Organic Geochemistry*, *33*(8), 897–905. https://doi.org/10.1016/S0146-6380(02)00067-0

Volkman, J. K., Barrerr, S. M., Blackburn, S. I., & Sikes, E. L. (1995). Alkenones in Gephyrocapsa oceanica: Implications for studies of paleoclimate. *Geochimica et Cosmochimica Acta*, *59*(3), 513–520. https://doi.org/10.1016/0016-7037(95)00325-T

Volkman, J. K., Barrett, S. M., Blackburn, S. I., Mansour, M. P., Sikes, E. L., & Gelin, F. (1998). Microalgal biomarkers: A review of recent research developments. *Organic Geochemistry*, *29*(5), 1163–1179. https://doi.org/10.1016/S0146-6380(98)00062-X

Wang, C., Deser, C., Yu, J.-Y., DiNezio, P., & Clement, A. (2017). El Niño and Southern Oscillation (ENSO): A Review. In P. W. Glynn, D. P. Manzello, & I. C. Enochs (Eds.), *Coral Reefs of the Eastern Tropical Pacific: Persistence and Loss in a Dynamic Environment* (pp. 85–106). Springer Netherlands. https://doi.org/10.1007/978-94-017-7499-4_4

Wara, M. W., Ravelo, A. C., & Delaney, M. L. (2005). Permanent El Nino-Like Conditions During the Pliocene Warm Period. *Science*, *309*(5735), 758–761. https://doi.org/10.1126/science.1112596

Zhang, Y. G., Pagani, M., Henderiks, J., & Ren, H. (2017). A long history of equatorial deep-water upwelling in the Pacific Ocean. *Earth and Planetary Science Letters*, *467*, 1–9. https://doi.org/10.1016/j.epsl.2017.03.016

Zhang, Y., Pagani, M., & Liu, Z. (2014). A 12-Million-Year Temperature History of the Tropical Pacific Ocean. *Science*, *344*(6179), 84–87. https://doi.org/10.1126/science.1246172

Supporting information

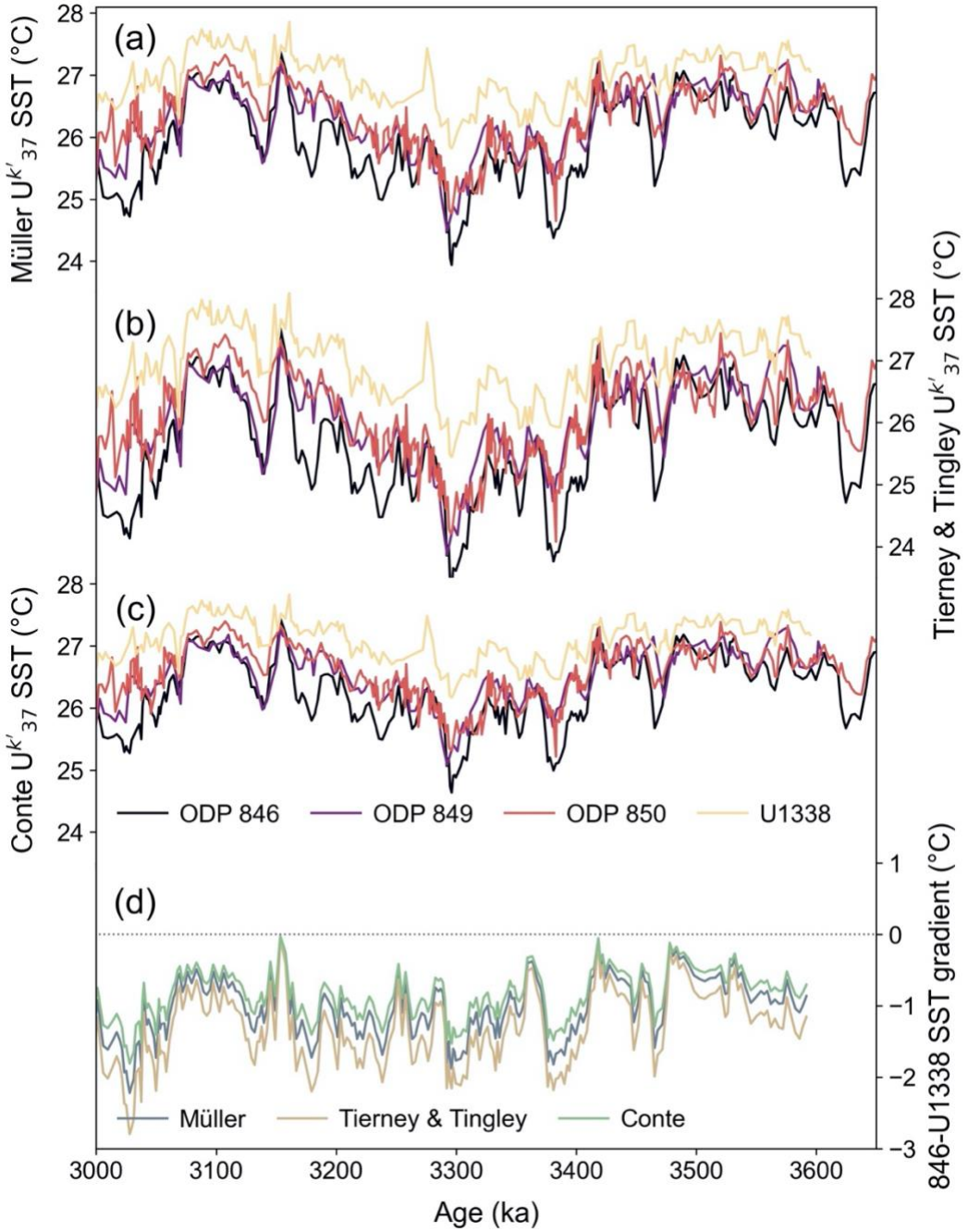

Figure S1. Three linear and non-linear $U^{k'}_{37}$ SST calibrations applied to Sites 846, 849, 850, and U1338 to assess how much the zonal gradient between sites changes depending on the calibration method. The calibrations compared here are from (a) Müller et al. (1998), (b) Tierney & Tingley (2018), and (c) Conte et al. (2006). Note that the zonal SST gradient appears similar (the western Site U1338 is warmer than the central and eastern Sites 850, 849, and 846, which plot on top of one another) no matter the calibration. The east-west SST gradient between Sites 846 and U1338 (d) calculated using the three calibrations shows negligible differences between the calibrations.

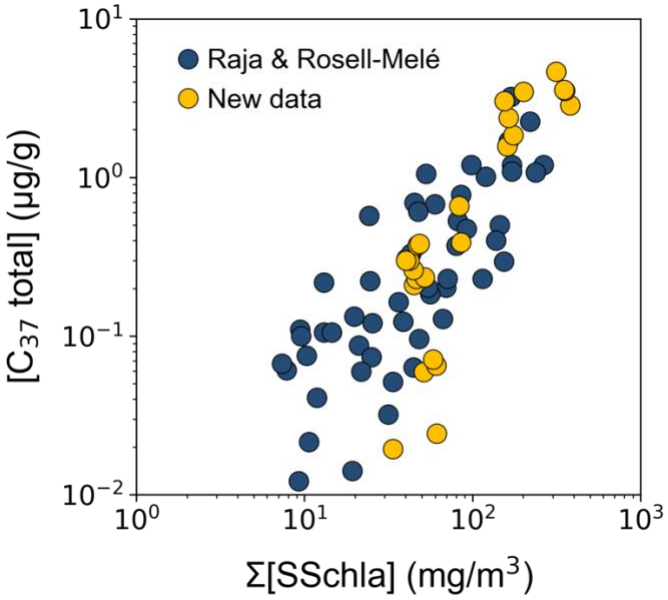

Figure S2. Correlation between C_{37} total and chlorophyll concentration. Yellow markers are the data reported in this study, plotted on top of the global tropical compilation from Raja & Rosell-Melé (2021), suggesting that C_{37} total is a reliable proxy for net primary productivity.

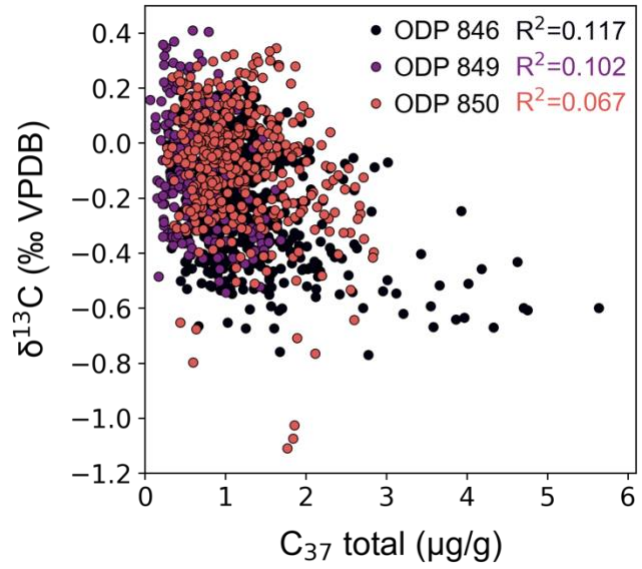

Figure S3. Relationship between $\delta^{13}C$ and C_{37} total from 3.0-3.6 Ma at ODP Sites 846, 849, and 850. Although complicated, the main $\delta^{13}C$ signal on glacial-interglacial time scales comes from changes in dissolved inorganic carbon (DIC). Greater respired carbon and lower oxygen results in higher DIC and more depleted $\delta^{13}C$ values. Even though there might be correlation without causation (e.g., high DIC at depth and high productivity at the surface, which are not directly connected to one another), the weak correlations between C_{37} total and $\delta^{13}C$ at each site imply that oxygen had little effect on the C_{37} total signal.

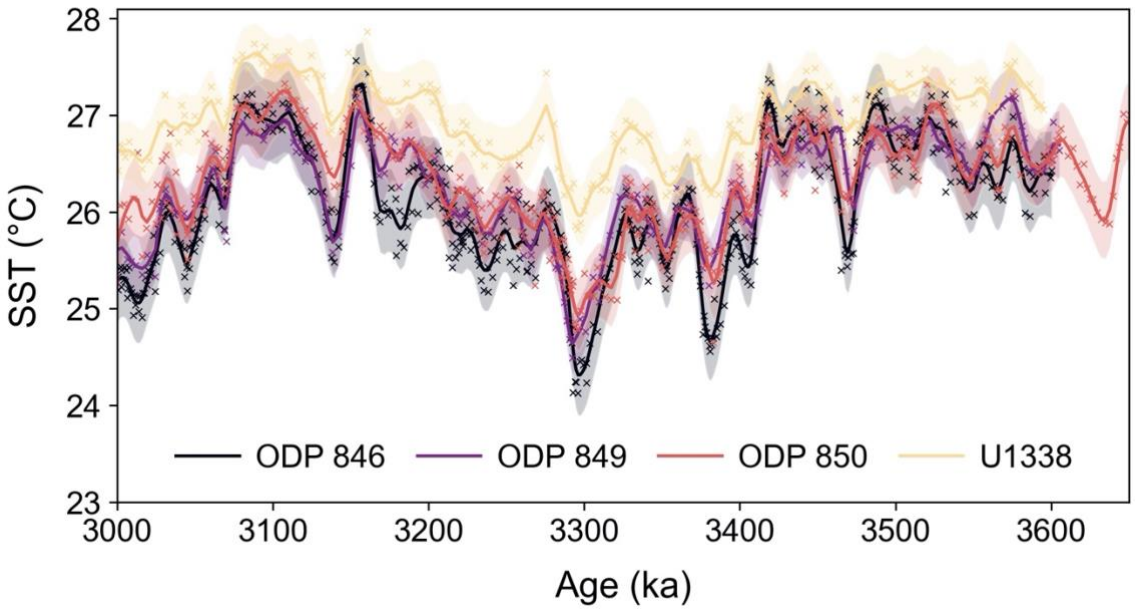

Figure S4. Error estimates of the Pliocene alkenone SST reconstructions from Sites 846, 849, 850, and U1338. A Gaussian Process model with Matérn32 and radial basis function kernels (Rasmussen & Williams, 2006) was applied to each SST record to produce a predicted mean SST (thick lines) and predicted upper and lower 95% confidence intervals (shading). Individual SST measurements are represented as crosses. The Gaussian Process model estimates the likelihood of a value at a given position, given the values at adjacent points. The kernel (in this case, the sum of Matérn32 and radial basis function kernels) defines the length and weighting function of the covariance matrix, which returns the most likely value. See the Open Research source for the Gaussian Process code.

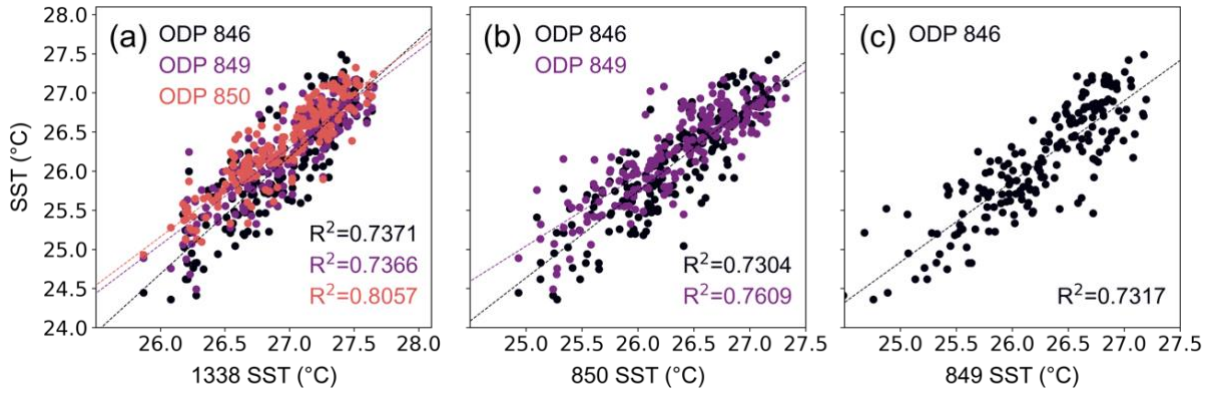

Figure S5. Correlations between alkenone $U^{k'}_{37}$ SST at (a-c) Sites 846, 849, 850, and U1338 for 3.0-3.6 Ma show strong SST agreement between sites, indicating temperatures vary across the EEP transect in concert.

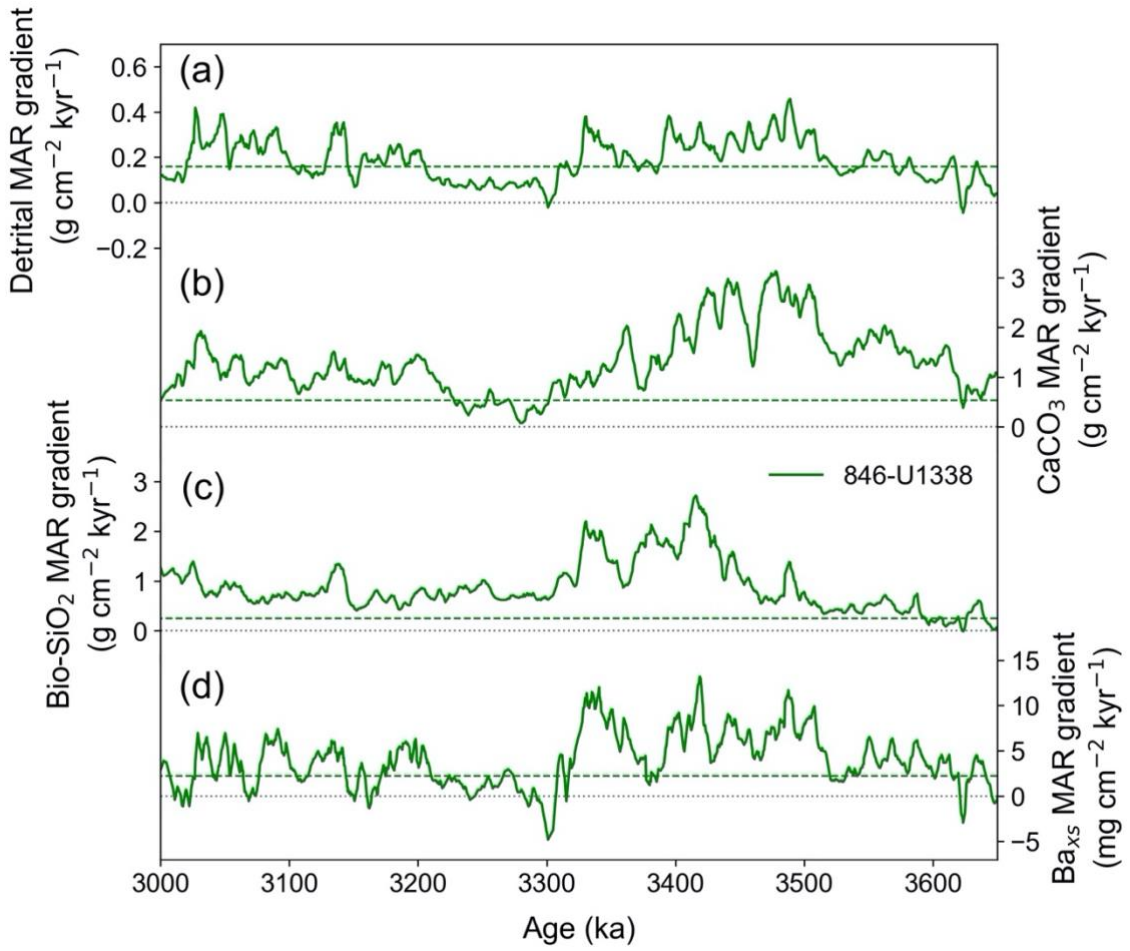

Figure S6. XRF MAR gradients between Sites 846 and U1338 for (a) detrital MAR, (b) $CaCO_3$ MAR, (c) bio-SiO_2 MAR, and (d) Ba_{xs} MAR, shown with the modern gradients between the sites (dashed lines). The gray dotted lines represent 0, or no gradient. Note that the Ba_{xs} MARs from Site U1338 are calculated from 10 kV XRF scans, which are less reliable than the 50 kV scans of Site 846.

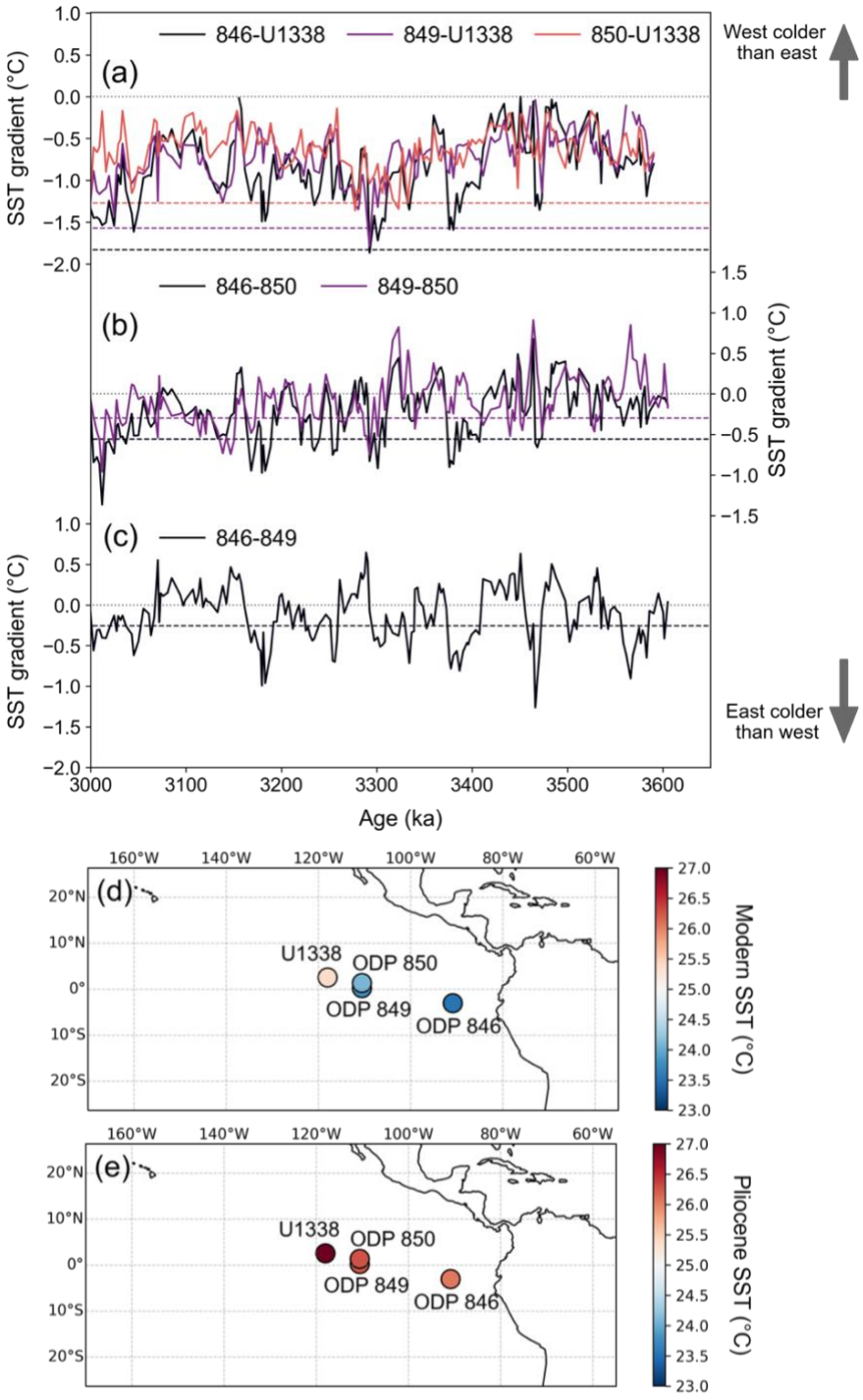

Figure S7. SST gradients between (a-c) Sites 846, 849, 850, and U1338 during the Pliocene, shown with the modern SST gradients between the sites (dashed lines). The gray dotted lines represent 0, or no gradient. Maps of (d) modern and (e) Pliocene average SSTs at each downcore site indicate that the boundary between warmer westerns and cooler eastern SSTs at ~115°W persisted during the Pliocene, despite the weaker overall zonal SST gradient.

References

Conte, M. H., Sicre, M.-A., Rühlemann, C., Weber, J. C., Schulte, S., Schulz-Bull, D., & Blanz, T. (2006). Global temperature calibration of the alkenone unsaturation index (UK′37) in surface waters and comparison with surface sediments. *Geochemistry, Geophysics, Geosystems*, *7*(2). https://doi.org/10.1029/2005GC001054

Müller, P. J., Kirst, G., Ruhland, G., von Storch, I., & Rosell-Melé, A. (1998). Calibration of the alkenone paleotemperature index U37K′ based on core-tops from the eastern South Atlantic and the global ocean (60°N-60°S). *Geochimica et Cosmochimica Acta*, *62*(10), 1757–1772. https://doi.org/10.1016/S0016-7037(98)00097-0

Raja, M., & Rosell-Melé, A. (2021). Appraisal of sedimentary alkenones for the quantitative reconstruction of phytoplankton biomass. *Proceedings of the National Academy of Sciences*, *118*(2). https://doi.org/10.1073/pnas.2014787118

Rasmussen, C. E., & Williams, C. K. (2006). *Gaussian processes for machine learning* (Vol. 1, p. 159). MIT press.

Tierney, J. E., & Tingley, M. P. (2018). BAYSPLINE: A New Calibration for the Alkenone Paleothermometer. *Paleoceanography and Paleoclimatology*, *33*(3), 281–301. https://doi.org/10.1002/2017PA003201

CHAPTER 3

High latitude oceanic tunnel controls of eastern equatorial Pacific surface temperature and productivity over the past 3.6 Myr

K. M. Kimble[1] and T. D. Herbert[1]

[1]Department of Earth, Environmental, and Planetary Sciences, Brown University, Providence, Rhode Island, 02912, USA.

Key Points:

- The modern tight coupling between ocean temperature and productivity gradients in the eastern equatorial Pacific was weaker during the Pliocene.
- Modern east-west temperature gradients developed during the mid-Pleistocene, but stronger than modern productivity gradients persisted through 400 ka.
- The strengthening of temperature gradients largely reflects the upwelling of progressively cooler but less nutrient-rich waters sourced from high latitudes.

Abstract

Robust modern gradients in sea surface temperature (SST) and biological primary productivity across the eastern equatorial Pacific Ocean (EEP) between 80° and 140° W derive from vigorous upwelling of cold and nutrient-rich intermediate waters. However, during the mid-Pliocene warm period (3.0-3.3 Ma), the zonal SST gradient was reduced to <0.5°C but the productivity gradient remained as strong if not stronger than modern. We consider the oceanographic mechanisms and external climate forcings responsible for the evolution of the Pliocene decoupling between SST and productivity to the modern tight SST-productivity coupling. We synthesize existing records and present new reconstructions of alkenone biomarker SST and productivity from four EEP sites spanning an east-west transect along the equator. In contrast to the increasing SST gradient development throughout the Plio-Pleistocene, alkenone mass accumulation rates indicate that the surface productivity gradient was stronger during the Late Pliocene compared to modern. The observations are best explained by dominance of the oceanic tunnel over surface forcings: SST changes dominantly reflect the cooling of high latitude water masses toward the present while productivity proxies suggest these waters became less nutrient-rich.

Plain language summary

The modern eastern tropical Pacific Ocean is cold and highly biologically productive because nutrients important to organisms at the base of the marine food web are brought from the colder deeper ocean to the sunlit zone. Therefore, cold waters found at the eastern margin of the equatorial Pacific are more productive than the central and western regions. However, during a globally warmer period three million years ago, warm waters in the eastern tropical Pacific

supported higher productivity than in the recent past. We reconstructed the surface temperature and productivity from four sites in the eastern Pacific over the last three million years to assess how the temperature and productivity relationship evolved to the modern state. We proposed that changes in ocean temperature and nutrient conditions at the high latitude origination of water emerging in the tropical Pacific influenced the evolving relationship between temperature and productivity as opposed to regional factors such as wind-driven upwelling of deeper water. These connections between the poles and the tropics are important to consider as the oceans warm in the coming decades.

1. Introduction

Ocean temperature and biological primary productivity are often closely linked to one another in upwelling zones, where colder subsurface water replete with nutrients outcrops at the surface (Lyle et al., 1992). The eastern equatorial Pacific (EEP) Ocean cold tongue upwelling zone contains high concentrations of nitrate and phosphate, but is limited in the micronutrient iron, which is thought to reduce the capacity to support surface productivity and results in incomplete nutrient utilization (Brzezinski et al., 2011; Costa et al., 2016). Dissolved marine CO_2 can freely exchange with the atmosphere because primary producers do not fully consume nutrients in the surface ocean, which links changes in atmospheric CO_2 to biological pump efficiency (Farrell et al., 1995). Stronger upwelling velocity in the eastern relative to the western EEP results in colder and more productive waters in the east, which yields gradients in the degree to which the EEP influences the carbon cycle.

Walker circulation and El Niño-Southern Oscillation (ENSO) cycles govern east-west patterns in sea surface temperature (SST) and marine biological productivity in the modern EEP

(Wang et al., 2017). These cycles accentuate the strong negative relationship between SST and productivity: during El Niño years, reduced east-west wind stress diminishes upwelling velocity in the EEP, resulting in warmer than average water and reduced surface productivity (Delcroix, 1998).

There are two possible mechanisms that influence EEP SST and productivity relationships on ENSO and orbital timescales. First, a top-down forcing like atmospheric CO_2 concentrations would affect the eastern and western EEP equally, so if decreasing pCO_2 during the Plio-Pleistocene was responsible for cooling EEP SSTs, then the region should experience uniform cooling (Bolton, Gibbs, et al., 2010; Burton et al., 2024). Additional top-down forcings, such as local wind fields (Amador et al., 2006), cloud feedbacks (Burls & Fedorov, 2014), and orbital forcing (specifically, precession; Clement et al., 2004), contribute to the ENSO-style SST and productivity relationship.

The second mechanism encompasses bottom-up forcings like oceanic tunnels, which transport water from the southern and northern high latitudes to the EEP through the thermocline, allow the EEP subsurface to respond at decadal and longer timescales to extratropical temperature changes (Gu & Philander, 1997; Lee & Poulsen, 2005; Z. Liu & Yang, 2003). Progressive high latitude cooling over the Plio-Pleistocene would first materialize as cooler SSTs in the eastern EEP upwelling core, then progress to cooling in the central and western EEP (Lu et al., 1998). Excess nutrients in high latitude waters may be subducted and transported through oceanic tunnels and upwell in the EEP to fuel primary productivity in the iron-limited regime (Burls et al., 2017; Sarmiento et al., 2004; Shankle et al., 2021; Toggweiler et al., 1991). Subantarctic Mode Water and Antarctic Intermediate Water, both of which are major components of Equatorial Pacific Intermediate Water, are sourced from the southern high

latitudes and reach the EEP surface through oceanic tunnels (Bostock et al., 2010; Toggweiler et al., 1991). Changes in high latitude temperature and nutrient content are transferred to the EEP through these high-low latitude connections (Burls et al., 2017; Lee & Poulsen, 2005; Philander & Fedorov, 2003).

Thermocline temperature, depth, and tilt are also crucial subsurface controls on nutrient delivery and surface temperature in the EEP across the Plio-Pleistocene. Ford et al. (2015) identified cooling, shoaling, and steepening of the equatorial Pacific thermocline as responsible for the cooling of the eastern EEP beginning in the mid-Pliocene. Further cooling of the rest of the EEP throughout the Pleistocene was attributed to cooling and shoaling of the thermocline (Ford et al., 2015).

The development of the modern EEP cold tongue and the high latitude and/or global forcings responsible for the evolution of EEP temperature and productivity relationships are not well understood. Although EEP waters were warmer than modern during the mid-Pliocene warm period (3.0-3.3 Ma), zonal productivity gradients were as strong if not stronger than modern (Kimble et al., 2024), suggesting that a weaker correlation between SST and productivity persisted in the Pliocene EEP (**Figure 1**). The modern tight coupling between SST and productivity may have developed at some point between the Pliocene and the present. This work assesses the timing and mechanisms of SST and productivity gradient evolution in the EEP over the last 3.6 Ma.

Here, we address two questions: (1) What was the timing of the Plio-Pleistocene SST and productivity gradient development? (2) What mechanisms were responsible for the development of modern temperature and productivity gradients across the EEP? We present new alkenone biomarker SST and productivity reconstructions from four cores from the International Ocean

Discovery Program and its previous iterations spanning an east-west transect across the EEP. We reconstruct zonal gradients in SST and the accumulation of alkenone biomarker concentrations to investigate the role of upwelling in the evolution of these EEP gradients over the Plio-Pleistocene relative to modern conditions derived from core top measurements and instrumental observations.

2. Setting and methods

Four EEP marine sediment core sites collected by the International Ocean Discovery Program (IODP) and its previous iterations were used to reconstruct SST and productivity. IODP Site U1338 (2°30.47'N, 117°58.18'W, 4,200 mbsl), ODP Sites 849 (0°10.98'N, 110°31.18'W, 3,837 mbsl), 846 (3° 5.70'S, 90°49.08'W, 3,296 mbsl), and 1239 (0°40.32'S, 82° 4.86, 1,414 mbsl). The sites are arranged in a transect along the equator (**Figure 2**), with eastern sites (Sites 1239 and 846) receiving a greater proportion of cooler upwelled Equatorial Undercurrent water than western sites (Sites 849 and U1338). The paleo-locations of each site were backtracked to 3 Ma, and modern temperatures at these backtracked locations, derived from the World Ocean Atlas 2018 (Boyer et al., 2018; Locarnini et al., 2019), were used to estimate Pliocene SST anomalies relative to modern SST at the paleo-location.

Sedimentation rates at all four sites were relatively stable over the Plio-Pleistocene, ranging from 1.3 cm/kyr at Site U1338, 2.6 cm/kyr at Site 849, 4.3 cm/kyr at Site 846, to 8.4 cm/kyr at Site 1239, averaged over the last 3.6 Ma. There were few intervals of increased sedimentation rate, with only Site 1239 displaying much variability (~17 cm/kyr at ~1.8 Ma, ~14 cm/kyr at ~2.0 Ma, and ~16 cm/kyr from 2.9-3.1 Ma). Sediment composition estimated from X-ray fluorescence (XRF) elemental intensities indicate that less than 10% of the sediment was

inorganic detrital material over the entire the Pliocene to modern interval. The major sediment component (>70% at Sites U1338 and 849 and >50% at Site 846) was carbonate. Biogenic silica made up ~15% of the sediment at Sites U1338 and 849 and >30% at Site 846 (Kimble et al., 2024; Lyle et al., 2019).

The downcore SST estimates were derived from the widely used $U^{k'}_{37}$ index, which is a SST proxy calculated from the degree of unsaturation of alkenones, organic molecules synthesized by one lineage of coccolithophore phytoplankton. SSTs are reported using the Müller et al. (1998) global core-top calibration. Kimble et al. (2024) showed negligible differences between other non-linear alkenone-SST calibrations (Tierney & Tingley, 2018) and the Müller et al. (1998) calibration.

Relative marine surface productivity was estimated using the concentration of C_{37} alkenones (C_{37} total), which is positively correlated to modern primary productivity and surface chlorophyll concentration (Kimble et al., 2024; Raja & Rosell-Melé, 2021; Volkman et al., 1995). C_{37} total mass accumulation rates (MAR) were estimated for each time step to normalize the different sedimentation rates at each site. C_{37} total MARs (μg/cm^2/kyr) were calculated as the C_{37} total mass (μg/g) × dry bulk density (g/cm^3) × linear sedimentation rate (cm/kyr) for each time step. MARs are displayed on a log scale to account for differences in alkenone concentration and sedimentation rates between eastern and western EEP sites. Sediment samples were prepared for alkenone SST and C_{37} total analyses and measured on an Agilent Technologies gas chromatograph-flame ionization detector according to Herbert et al. (2021).

Four time intervals were selected for SST and productivity reconstruction because the zonal SST gradients between the EEP and western Pacific warm pool exhibited significant change according to Wara et al. (2005): a Pliocene interval (3.0-3.6 Ma), a Plio-Pleistocene

interval (2.4-2.8 Ma), a mid-Pleistocene interval (1.4-1.7 Ma), and a Late Pleistocene interval (350-650 ka). The existing Site 846 SST and productivity records are continuous from modern to 3.6 Ma (Herbert et al., 2021; Lawrence et al., 2006, 2020), while the Site 1239 records extend only to 3.1 Ma (Etourneau et al., 2010; Shaari et al., 2013). The Site 849 records span three intervals, 0.3 to 1.7 (new data generated at Brown University and McClymont & Rosell-Melé, 2005), 2.4 to 2.8 (new data), and 3.0 to 3.6 Ma (Kimble et al., 2024). Due to a consistent laboratory offset between the McClymont & Rosell-Melé (2005) data and newly generated SST data, 0.74°C was subtracted from the McClymont & Rosell-Melé (2005) Site 849 data spanning 650-1380 ka. The remaining Site U1338 SST and productivity data were generated at Brown University including the previously published interval from 3.0-3.6 Ma (Kimble et al., 2024).

A slightly modified version of the age-depth tuning of Lisiecki and Raymo (2005) was used to assign ages to the Site 846 data, updated with the revised composite section of Herbert et al. (2021) spanning the M2 glacial interval. The Match program (Lisiecki & Lisiecki, 2002) was used to align SST data from Sites U1338, 849, and 1239 to the age-depth model of Site 846, using XRF data from Sites 846, 849, and U1338 as secondary alignment records.

Evolutive power spectral analyses using the Thomson multitaper method (Thomson, 1982) were conducted on SST and productivity data to assess changes in the dominance of different orbital frequencies over the Plio-Pleistocene (Meyers et al., 2021). Data were detrended and linearly interpolated to 3-kyr timesteps prior to analysis.

Error estimates for reconstructed SST and C_{37} total MAR values were calculated using a Gaussian Process model (Rasmussen & Williams, 2006). The Gaussian Process model estimates the likelihood of a value at a given position, given the values at adjacent points. The kernel (in this case, the sum of Matérn32 and radial basis function kernels) defines the length and

weighting function of the covariance matrix, which returns the most likely value (see the data availability statement for the Gaussian Process code). The adaptively smoothed time series are much less sensitive to analytical or proxy noise than raw values and hence used to estimate gradients between sites. SST gradients between sites were calculated by Gaussian Process resampling of the higher-resolution data to the age points of the lower-resolution data.

3. Results

3.1 SST evolution

The modern average >2°C SST gradient between 82° and 118°W (Sites 1239 and U1338, respectively) diminished to <0.9°C during the mid-Pliocene (3.0-3.6 Ma; **Figures 3, 4**). By the Plio-Pleistocene transition (2.4-2.8 Ma), the average SST gradient between Sites 846 and U1338 increased to ~1.5°C. By the mid-Pleistocene (1.4-1.7 Ma), SSTs in the eastern EEP cooled to nearly modern temperatures (24.0°C at Site 846) but western and central EEP SSTs were still warmer than modern, resulting in a ~1.8°C ΔSST between Sites 846 and U1338. Cooling SSTs across the transect yielded the modern ΔSST gradient of >2°C by the Late Pleistocene ~650 ka (**Figure 4**).

SST variability was clearly present on glacial-interglacial timescales. Eastern EEP SST gradients intensified during glacial intervals beginning at the ~2.7 Ma glaciation, increasing the zonal ΔSST to 3°C between Sites 846 and U1338 during glacials but retaining the Pliocene weakened gradient of <0.9°C during interglacials. By the Late Pleistocene (350-650 ka) eastern EEP (Site 846) SSTs frequently cooled below modern and only warmed to modern temperatures during interglacial periods (**Figure 3**). SSTs at Site 1239, located a couple degrees north of the heart of modern cold tongue upwelling, very closely track Site U1338 SSTs, also located just

north of the cold tongue, despite the two sites' positions on opposite ends of the equatorial transect (**Figure 3**), arguing for a coherent evolution of temperatures at the margins of the cold tongue. Thus, we assume that SSTs at the western EEP Site U1338 would behave similarly to the more continuous Site 1239 SST record, so that SST estimates at Site 1239 augment data gaps at Site U1338.

The spatial evolution of EEP temperature reconstructions are consistent with amplified cooling in the heart of the modern cold tongue which first appeared during glacial intervals at Site 846 and persisted through long term Plio-Pleistocene cooling. The western and central Pacific did not begin to cool as soon as the EEP, nor did the western and central Pacific experience as dramatic Plio-Pleistocene cooling as the EEP (Lawrence et al., 2006).

3.2 Productivity evolution

Eastern EEP (Sites 846 and 1239) C_{37} total MAR was higher throughout the Plio-Pleistocene relative to modern (**Figure 3**). However, C_{37} total MAR of the western and central EEP (Sites U1338 and 849) decreased from the Pliocene through the Late Pleistocene and the modern gradient established as late as the Holocene, resulting in a stronger Pliocene C_{37} total MAR gradient (7.1 μg cm^{-2} kyr^{-1}) between Sites U1338 and 846 (**Figure 4**) compared to the weaker modern gradient (0.9 μg cm^{-2} kyr^{-1}). X-ray fluorescence (XRF) elemental data and mass accumulation rates of biogenic SiO_2 (calculated according to Kimble et al., 2024) support the Plio-Pleistocene C_{37} total MAR patterns as Pliocene bio-SiO_2 in the eastern EEP was greater than modern, suggesting that both C_{37} total and bio-SiO_2 productivity during the Plio-Pleistocene was heightened relative to today (**Figure S1**).

Glacial-interglacial variability was present in the surface productivity records as well, with stronger zonal productivity gradients generally accompanying glacial intervals. By the beginning of the Pleistocene (2.6 Ma) the zonal gradient in C_{37} total MAR was ~9 μg cm^{-2} kyr^{-1} (still an order of magnitude greater than the modern 0.9 μg cm^{-2} kyr^{-1} gradient) during interglacials and increased to the more typical average Pleistocene values of ~20 μg cm^{-2} kyr^{-1} during glacials. The zonal productivity gradient contrast increased throughout Pleistocene cooling, but eventually had to weaken to reach Holocene values. The disparate timing of SST and productivity gradient evolution implies that the eastern EEP productivity developed quite differently from SST.

3.3 Spectral sensitivity to high latitude forcings

Evolutive power spectral analyses assessed at the 90% confidence interval indicate that SSTs at all four EEP sites were significantly tuned to 41-kyr obliquity cycles during the Pliocene and through the Plio-Pleistocene transition (**Figure 5a**). Although EEP SSTs were still sensitive to obliquity (especially in the eastern part of the transect) throughout the Pleistocene, 100-kyr eccentricity paced SSTs at all sites by the Late Pleistocene. Site 846 $\delta^{18}O$ and SST show strong coherence in the eccentricity and obliquity bands, especially as both records share significant 41-kyr components from the Pliocene through the mid-Pleistocene (**Figure 5b**). The coherence between eastern EEP SST spectra and the more globally attuned $\delta^{18}O$ suggests persistent connections between high latitudes and equatorial temperatures.

By the Plio-Pleistocene transition C_{37} total MAR-estimated productivity at both the two eastern EEP sites (Sites 846 and 1239) was responsive to 41-kyr periodicity (**Figure 5c**). By the mid-Pleistocene (1.4-1.7 Ma), productivity at the western and central sites (Sites U1338 and 849) were paced by obliquity as well. The abundance of eastern EEP *Florisphaera profunda*, a nannofossil that inhabits the lower photic zone, exhibited 41-kyr periodicity and was anticorrelated with log[C_{37} total MAR] during the Early Pleistocene (Bolton, Gibbs, et al., 2010). Nutricline depth, as recorded by *F. profunda* abundance, fluctuated with obliquity such that the nutricline shoaled during glacials (**Figure S2**). High latitude physical and biogeochemical changes may have been transmitted through oceanic tunnels to reach the eastern EEP before the western EEP.

4. Discussion

4.1 Top-down vs. bottom-up controls on SST and productivity gradients

Both top-down forcings like the regional effects of atmospheric CO_2 concentrations and bottom-up forcings like subsurface oceanic tunnels governed the relationship between EEP SST and productivity gradients over the last 3.6 Ma. However, the forcings' spatial patterns took different shapes, and therefore gave insights into which processes dominated the trends we document here.

The Plio-Pleistocene decrease in pCO_2 would influence SST at all sites equally (Burton et al., 2024; Heede & Fedorov, 2021; Jia & Wu, 2013; Lee & Poulsen, 2005), which is not apparent in the SST records presented here because the eastern EEP (Site 846) cooled before (and more intensely than) the central and western sites (Sites 849 and U1338; **Figure 3**). During the globally warmer Pliocene, high latitude waters warmed significantly and weakened pole-tropics

SST gradients, producing smaller zonal SST gradients by warming the eastern EEP where the high latitude water upwelled (Dekens et al., 2007; Fedorov et al., 2006, 2015). As atmospheric CO_2 concentrations decreased over the Pleistocene, extratropical SST records depicted greater cooling relative to low latitudes (Brierley et al., 2009).

Top-down forcings exerted through other means may have influenced Plio-Pleistocene EEP SST and productivity. Changes to easterly wind strength and position would alter EEP upwelling velocity (Amador et al., 2006). Grain size evidence of decreasing eolian input to the EEP since the Pliocene reflects relatively wetter conditions, but trade wind strength has remained relatively constant since 3.0 Ma (Hovan, 1995). Reconstructed strong eastern EEP productivity implies vigorous upwelling persisted. The weakly stratified mixed layer of the Pliocene EEP would have required lower wind stress to result in the same amount of water upwelled as a higher wind stress under more stratified conditions. Therefore, weaker easterlies could have upwelled sufficient nutrients given the weaker density stratification of the Pliocene relative to the Pleistocene and modern. Orbital forcings influence EEP physical and biogeochemical patterns, but the strong Plio-Pleistocene obliquity pacing we report here would not be expected to dominate either SST or productivity in the tropics where precession is more influential (Clement et al., 2004). Finally, cloud albedo feedbacks are critical controls on meridional SST gradients between the tropical and extratropical Pacific, with changes to cloud albedo necessary to maintain Pliocene EEP warmth (Burls & Fedorov, 2014). However, neither the pCO_2 decrease, wind field changes, orbital forcings, nor cloud feedbacks alone cannot account for the reconstructed EEP productivity gradient evolution.

The bottom-up oceanic tunnel mechanism transported cooler waters from southern and northern high latitude sources to the base of the eastern EEP thermocline (Gu & Philander, 1997;

Lee & Poulsen, 2005; Z. Liu & Yang, 2003). Progressive high latitude cooling over the Plio-Pleistocene would first materialize as cooler SSTs in the eastern EEP upwelling core, then advance to cooling in the central and western EEP (Lu et al., 1998), resulting in a steepening, cooling, and shoaling thermocline (Ford et al., 2015). "Pre-formed" nutrients in high latitude waters may have been subducted and transported through oceanic tunnels and upwelled in the EEP, fueling primary productivity in the iron-limited regime (Burls et al., 2017; Shankle et al., 2021). High-low latitude connections are apparent in the strong spectral response to 41-kyr obliquity cycles from the SST records, especially in the eastern EEP, which strengthened at the Plio-Pleistocene transition (**Figure 5**). The evolution of the zonal EEP SST gradient synchronous with benthic $\delta^{18}O$ also points to high latitude or global forcings transmitted through the oceanic tunnel (Fedorov et al., 2013) rather than tropical insolation forcing, which was opposite SST gradient changes on glacial-interglacial timescales (**Figure 4**).

Previous work pointed to around or prior to (Dekens et al., 2007) the initiation of Northern Hemisphere glaciation near the Plio-Pleistocene boundary, or to ~1.7 Ma prior to the Mid-Pleistocene Transition (Ravelo et al., 2006; Wara et al., 2005) as potential stages when the zonal SST gradient intensified between the eastern and western Pacific. The EEP alkenone SST records reported here indicate strengthened zonal SST gradients during glacial intervals beginning as early as ~2.7 Ma, but there is evidence for continued cold tongue evolution fed by cool waters of the oceanic tunnel through the mid to Late Pleistocene (Lawrence et al., 2006). Ravelo et al. (2006) suggest Walker circulation strengthened at ~1.7 Ma when planktic foraminiferal oxygen isotope from sites at either side of the equatorial Pacific approached the modern zonal SST gradient of 5°C. A modern cross-Pacific SST gradient achieved by ~1.7 Ma

does not necessarily oppose continued development of the EEP zonal SST and productivity gradients into the Late Pleistocene, especially when evaluated on glacial-interglacial timescales.

4.2 High latitude influences on EEP upwelling through oceanic tunneling

The timing of the evolving zonal SST gradient, which reached the modern gradient as early as the Plio-Pleistocene boundary, and the productivity gradient, which was stronger than modern until at least the Late Pleistocene (**Figure 4**), suggests that physical and biogeochemical properties of the EEP evolved separately. The Site 1239 SST and productivity records indicate that warmer temperatures (relative to those of Site 846) can support strong productivity (relative to Site 846). Despite the weakened Pliocene SST gradient, subsurface tilting (Etourneau et al., 2013) and shoaling (Jakob et al., 2021) of both the thermocline and nutricline would be necessary to maintain vigorous upwelling of nutrients to the EEP surface.

However, the Pliocene decoupling of SST from productivity remains to be explained. Either source waters contained higher nutrient concentrations that eventually outcropped in the EEP, or upwelling velocity was greater during the Pliocene relative to modern to explain a warmer but highly productive Pliocene EEP (Bartoli et al., 2011; Burls et al., 2017; H. Dowsett et al., 1996; Ford et al., 2022). The recoupling between SST and productivity that is observed between the Pliocene and modern may have occurred due to a breakdown of one or both of the two listed mechanisms: (1) high latitude waters went from warm to cool and from containing high to low nutrient concentrations from the Pliocene to modern, and/or (2) high latitude waters went from warm to cool and EEP upwelling velocity went from stronger to weaker from the Pliocene to modern.

Possible changes in the source water locations between the Southern Ocean and the North Pacific may have been responsible for the continuous cooling of EEP SSTs concurrent with strengthening productivity gradients. Comparable cooling would have occurred at southern and northern high latitudes, but different nutrient concentrations were associated with the water sources (Sarmiento et al., 2004), so the disconnect between SST and productivity may be attributed to progressively lower nutrient concentrations from different source waters fueling eastern EEP productivity over the Pleistocene (Ford et al., 2015, 2022; Shankle et al., 2021).

5. Conclusion

The alkenone SST and productivity data reported here indicate a strengthening of the zonal EEP SST gradient throughout the Plio-Pleistocene, in contrast to the surface productivity gradient, which was stronger during the Late Pliocene compared to modern. The evidence from productivity proxies is thus that the combination of wind-induced upwelling and subsurface nutrient content and/or utilization has not strengthened as the equatorial cold tongue intensified. Existing alkenone-based and Mg/Ca paleothermometer records show increasing zonal SST gradients between the western Pacific warm pool and the EEP over the Plio-Pleistocene (Dekens et al., 2007; Fedorov et al., 2006; Lawrence et al., 2006; Ravelo et al., 2006; Wara et al., 2005), supporting our reconstructions of eastern EEP cooling. Upwelling of nutrient-rich water occurred despite warmer-than-modern eastern EEP temperatures through the Plio-Pleistocene (Dekens et al., 2007). At the orbital scale, the dominant frequency of eastern EEP SST and $\delta^{18}O$ cycles was 41-kyr until Late Pleistocene 100-kyr cycles prevailed. High-latitude forcings influenced tropical upwelling during the Plio-Pleistocene because the EEP's polar water sources cooled but remained nutrient-rich throughout the 41-kyr world, keeping SST and productivity decoupled

through the Late Pleistocene. These results suggest a reexamination of the "permanent El Niño-like" or "El Padre" idea, given that productivity gradients appeared to have evolved independently from SST gradients over the last 3.6 Myr. Neither the intensification of Northern Hemisphere glaciation near the Plio-Pleistocene transition nor ~1.7 Ma Walker circulation strengthening appeared to interrupt the continuously increasing SST gradients and decreasing productivity gradients across the EEP.

Acknowledgments

This research used samples and data provided by the International Ocean Discovery Program (IODP). Funding for this research was provided by NSF grants 1930651 and 1459280 awarded to TDH. The authors report no conflicts of interest.

Data availability statement

All SST and productivity data generated for this research will be archived at PANGAEA® - Data Publisher for Earth & Environmental Science. For the Gaussian Process code, see http://github.com/SheffieldML/GPy.

Figures

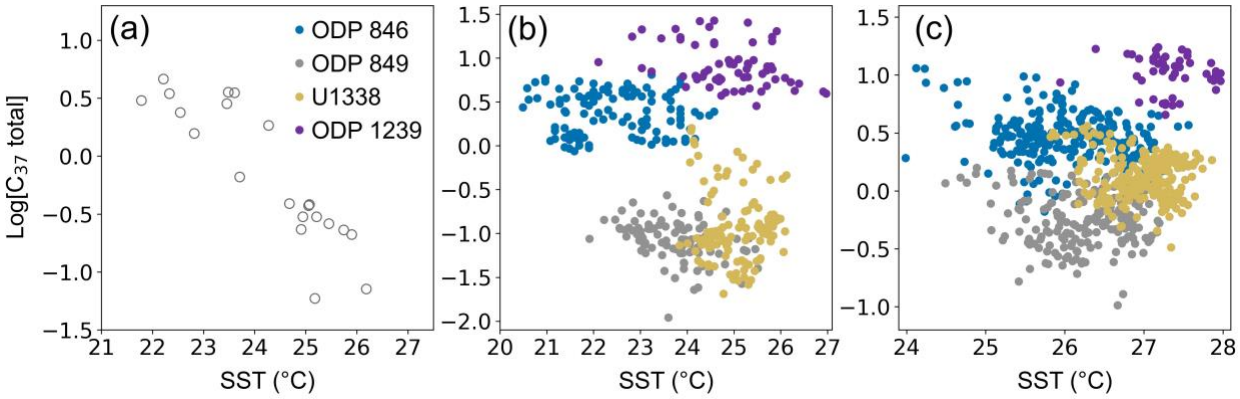

Figure 1. Correlations between SST and log[C_{37} total] from the four sites during (a) the Holocene, (b) the Late Pleistocene (350-650 ka), and (c) the Pliocene (3.0-3.6 Ma). The modern tight coupling between SST and productivity evolved from much weaker relationships in the Pliocene and through the Late Pleistocene.

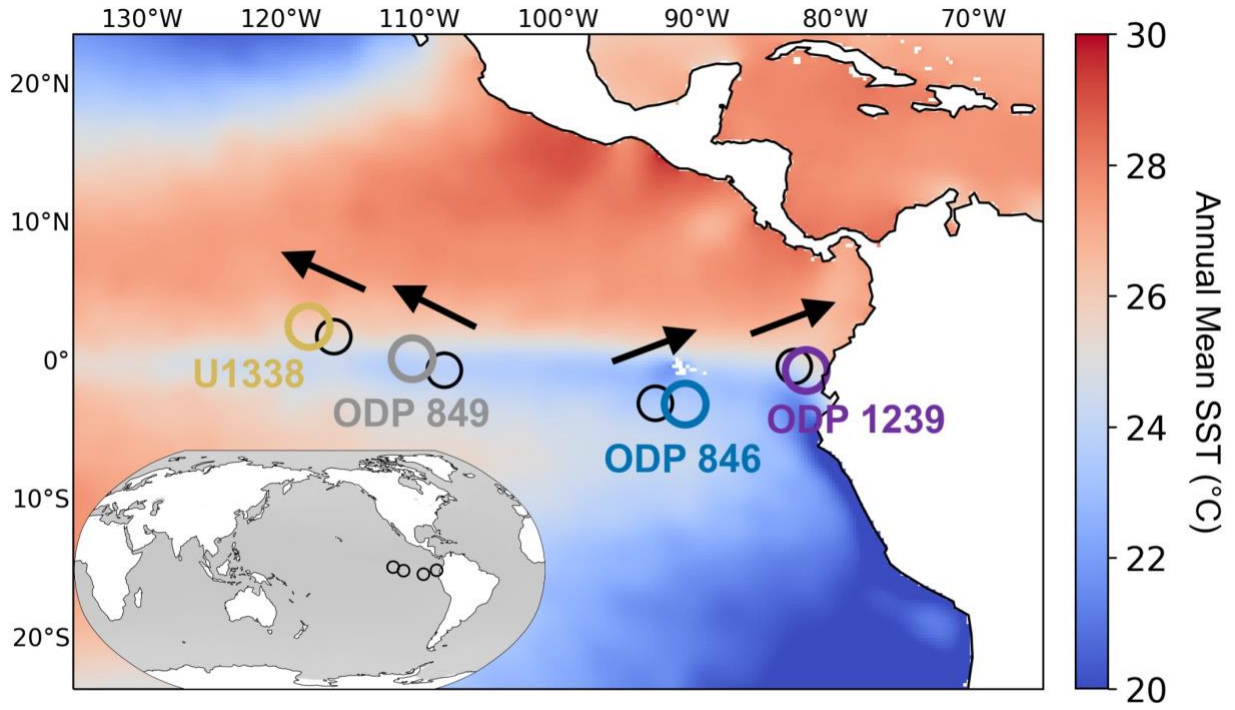

Figure 2. Locations of IODP Site U1338 and ODP Sites 849, 846, and 1239 (colorful circles) in the EEP overlayed on modern annual mean SST from World Ocean Atlas 2018 (Boyer et al., 2018; Locarnini et al., 2019). The paleo-locations of each site backtracked to 3 Ma are displayed as black circles with arrows showing the direction of site migration. The inset map shows the modern position of the four sites with respect to the Pacific Ocean.

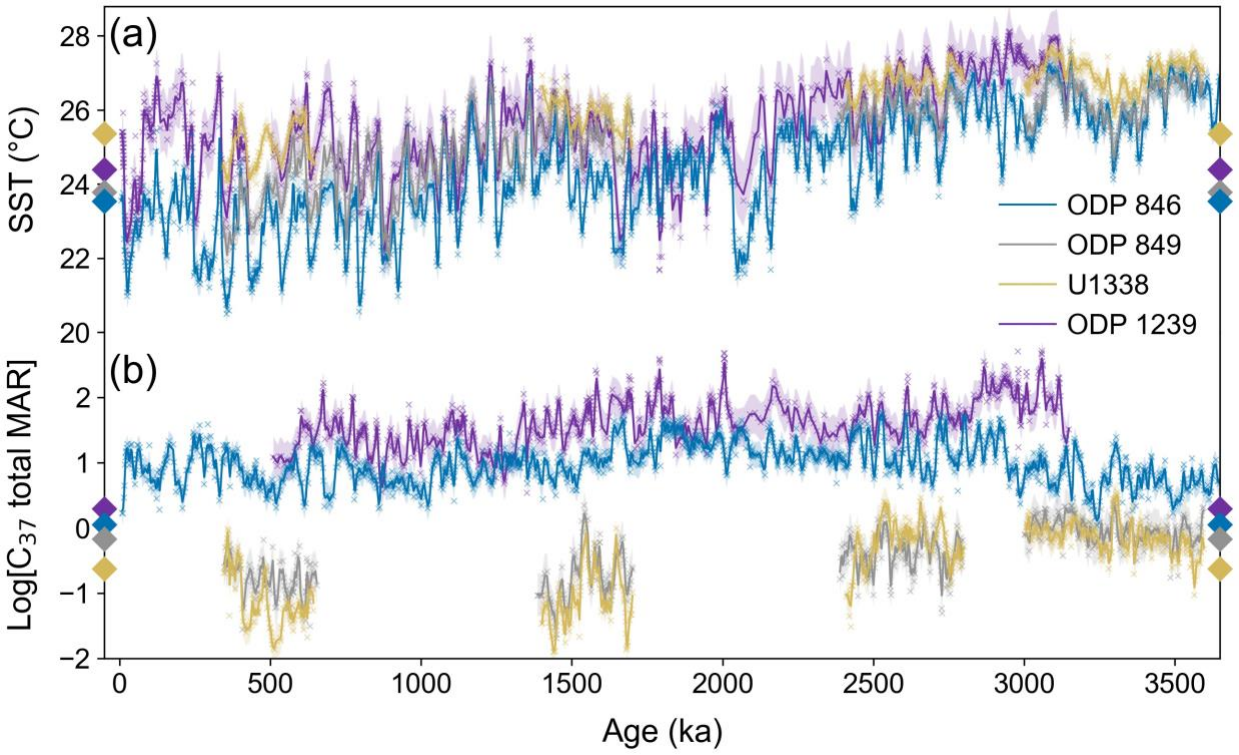

Figure 3. Time series of SST and productivity from four IODP and ODP sites over the last 3.6 Ma. (a) $U^{k'}_{37}$ SST (using the calibration of (Müller et al., 1998) with bold crosses representing modern SST derived from WOA18 observations (Boyer et al., 2018; Locarnini et al., 2019) at the backtracked site locations from 3 Ma, and (b) Log[C_{37} total MAR] with diamonds representing modern Log[C_{37} total MAR] estimated from core top samples corresponding to the 3 Ma paleo-locations of each site. Note that there is no Site 1239 C_{37} total record from ~500 ka to modern. Error estimates on SST and Log[C_{37} total MAR] were calculated using a Gaussian Process model with Matérn32 and radial basis function kernels (Rasmussen & Williams, 2006). Predicted mean values (thick lines), predicted upper and lower 95% confidence intervals (shading), and original values (small crosses).

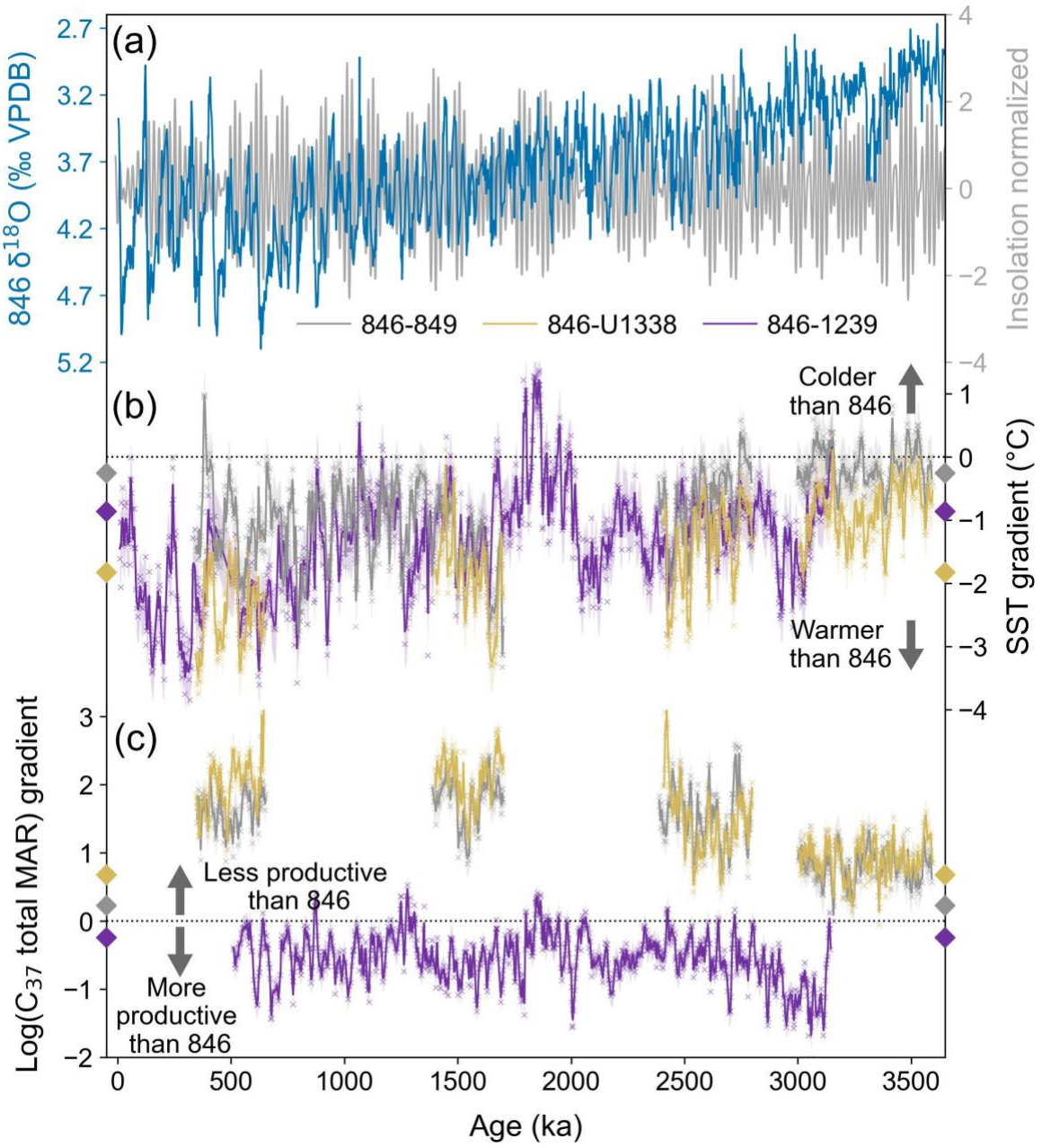

Figure 4. Time series of (a) benthic $\delta^{18}O$ from Site 846 (blue) and June 21st insolation at 0° (gray), (b) SST gradients between Sites 846 and 1239, 849, and U1338, and (c) Log[C_{37} total MAR] gradients between Sites 846 and 849 and U1338. Diamonds represent the modern SST and Log[C_{37} total] gradients, using the 3 Ma paleo-locations of all sites. The gray dotted lines represent 0, or no gradient. Positive values in (b) reflect a cooler western EEP relative to the eastern EEP, and positive values in (c) reflect a more productive eastern EEP relative to the western EEP. Results of Gaussian Process models with Matérn32 and radial basis function kernels (Rasmussen & Williams, 2006) are represented as predicted mean values (thick lines), predicted upper and lower 95% confidence intervals (shading), and original values (small crosses).

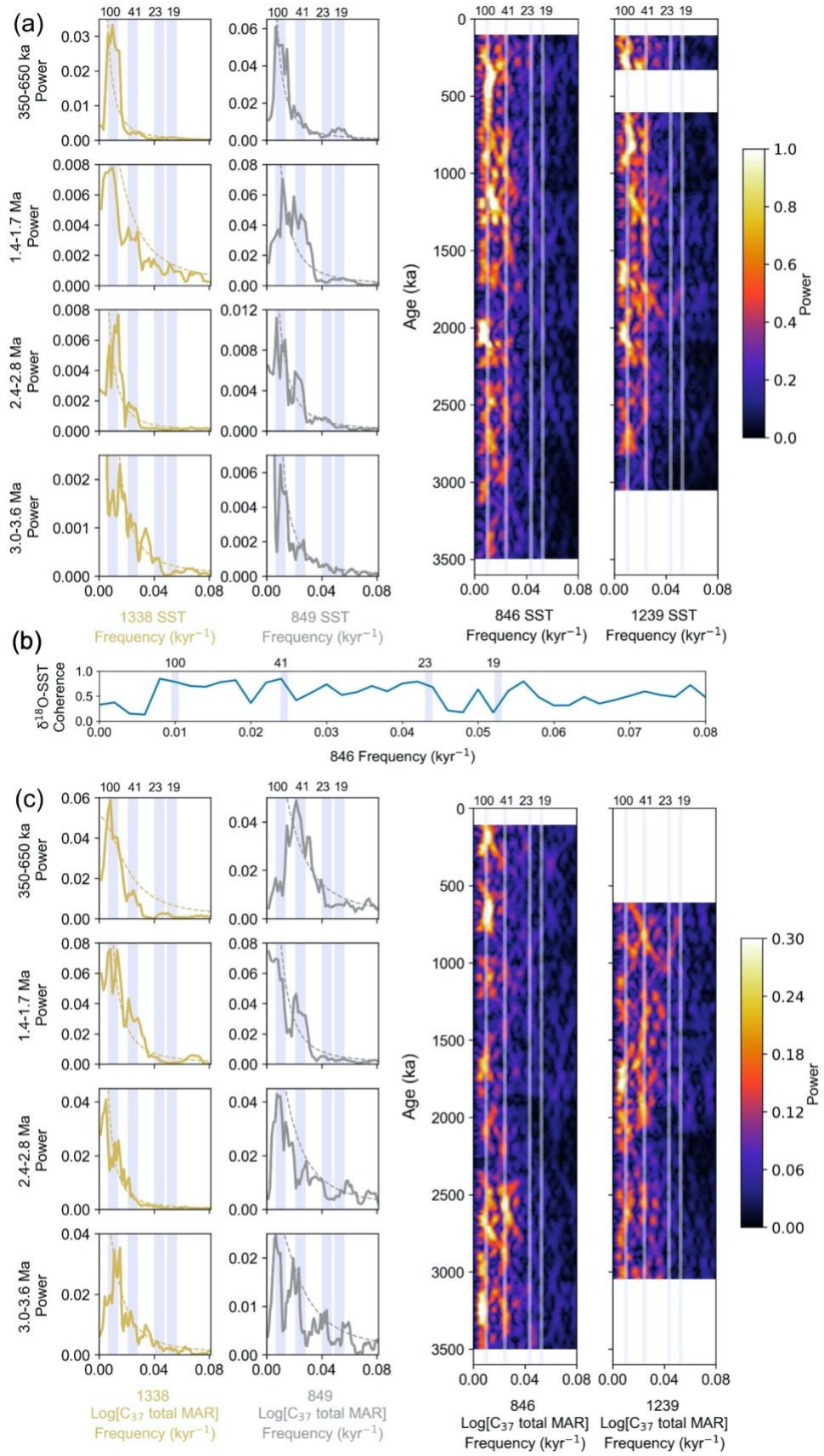
(a)
100 41 23 19
350-650 ka Power
1.4-1.7 Ma Power
2.4-2.8 Ma Power
3.0-3.6 Ma Power
Age (ka)
Power
1338 SST Frequency (kyr^{-1})
849 SST Frequency (kyr^{-1})
846 SST Frequency (kyr^{-1})
1239 SST Frequency (kyr^{-1})
(b)
δ^{18}O-SST Coherence
846 Frequency (kyr^{-1})
(c)
1338 Log[C_{37} total MAR] Frequency (kyr^{-1})
849 Log[C_{37} total MAR] Frequency (kyr^{-1})
846 Log[C_{37} total MAR] Frequency (kyr^{-1})
1239 Log[C_{37} total MAR] Frequency (kyr^{-1})

Figure 5. (a) Evolutive power spectra of SST and (c) log[C_{37} total MAR] at Sites U1338, 849, 846, and 1239 showing the changing influence of eccentricity, obliquity, and precession in each record spanning the Pliocene to modern. (b) Coherence between $\delta^{18}O$ and SST at Site 846 throughout the 3.6-myr record shows strong coherence at orbital frequencies. Lavender bands represent orbital cycles at 100-kyr, 41-kyr, 23-kyr, and 19-kyr frequencies. Power spectra are displayed for each time window at Sites 849 and U1338 instead of evolutive spectra due to the discontinuous nature of these records.

References

Amador, J. A., Alfaro, E. J., Lizano, O. G., & Magaña, V. O. (2006). Atmospheric forcing of the eastern tropical Pacific: A review. *Progress in Oceanography*, *69*(2), 101–142. https://doi.org/10.1016/j.pocean.2006.03.007

Bartoli, G., Hönisch, B., & Zeebe, R. E. (2011). Atmospheric CO2 decline during the Pliocene intensification of Northern Hemisphere glaciations. *Paleoceanography*, *26*(4). https://doi.org/10.1029/2010PA002055

Bolton, C. T., Gibbs, S. J., & Wilson, P. A. (2010). Evolution of nutricline dynamics in the equatorial Pacific during the late Pliocene. *Paleoceanography*, *25*(1). https://doi.org/10.1029/2009PA001821

Bostock, H. C., Opdyke, B. N., & Williams, M. J. M. (2010). Characterising the intermediate depth waters of the Pacific Ocean using δ13C and other geochemical tracers. *Deep Sea Research Part I: Oceanographic Research Papers*, *57*(7), 847–859. https://doi.org/10.1016/j.dsr.2010.04.005

Boyer, T. P., García, H. E., Locarnini, R. A., Zweng, M. M., Mishonov, A. V., Reagan, J. R., Weathers, K. A., Baranova, O. K., Paver, C. R., Seidov, D., & Smolyar, I. V. (2018). *World Ocean Atlas 2018. Temperature* [Dataset]. NOAA National Centers for Environmental Information. https://www.ncei.noaa.gov/archive/accession/NCEI-WOA18

Brierley, C. M., Fedorov, A. V., Liu, Z., Herbert, T. D., Lawrence, K. T., & LaRiviere, J. P. (2009). Greatly Expanded Tropical Warm Pool and Weakened Hadley Circulation in the Early Pliocene. *Science*, *323*(5922), 1714–1718. https://doi.org/10.1126/science.1167625

Brzezinski, M. A., Baines, S. B., Balch, W. M., Beucher, C. P., Chai, F., Dugdale, R. C., Krause, J. W., Landry, M. R., Marchi, A., Measures, C. I., Nelson, D. M., Parker, A. E., Poulton,

A. J., Selph, K. E., Strutton, P. G., Taylor, A. G., & Twining, B. S. (2011). Co-limitation of diatoms by iron and silicic acid in the equatorial Pacific. *Deep Sea Research Part II: Topical Studies in Oceanography*, *58*(3), 493–511. https://doi.org/10.1016/j.dsr2.2010.08.005

Burls, N. J., & Fedorov, A. V. (2014). Simulating Pliocene warmth and a permanent El Niño-like state: The role of cloud albedo. *Paleoceanography*, *29*(10), 893–910. https://doi.org/10.1002/2014PA002644

Burls, N. J., Fedorov, A. V., Sigman, D. M., Jaccard, S. L., Tiedemann, R., & Haug, G. H. (2017). Active Pacific meridional overturning circulation (PMOC) during the warm Pliocene. *Science Advances*, *3*(9), e1700156. https://doi.org/10.1126/sciadv.1700156

Burton, L. E., Haywood, A. M., Tindall, J. C., Dolan, A. M., Hill, D. J., McClymont, E. L., Ho, S. L., & Ford, H. L. (2024). The role of atmospheric CO_2 in controlling sea surface temperature change during the Pliocene. *Climate of the Past*, *20*(5), 1177–1194. https://doi.org/10.5194/cp-20-1177-2024

Clement, A. C., Hall, A., & Broccoli, A. J. (2004). The importance of precessional signals in the tropical climate. *Climate Dynamics*, *22*(4), 327–341. https://doi.org/10.1007/s00382-003-0375-8

Costa, K. M., McManus, J. F., Anderson, R. F., Ren, H., Sigman, D. M., Winckler, G., Fleisher, M. Q., Marcantonio, F., & Ravelo, A. C. (2016). No iron fertilization in the equatorial Pacific Ocean during the last ice age. *Nature*, *529*(7587), 519–522. https://doi.org/10.1038/nature16453

Dekens, P. S., Ravelo, A. C., & McCarthy, M. D. (2007). Warm upwelling regions in the Pliocene warm period. *Paleoceanography*, *22*(3). https://doi.org/10.1029/2006PA001394

Delcroix, T. (1998). Observed surface oceanic and atmospheric variability in the tropical Pacific at seasonal and ENSO timescales: A tentative overview. *Journal of Geophysical Research: Oceans*, *103*(C9), 18611–18633. https://doi.org/10.1029/98JC00814

Dowsett, H., Barron, J., & Poore, R. (1996). Middle Pliocene sea surface temperatures: A global reconstruction. *Marine Micropaleontology*, *27*, 13–25. https://doi.org/10.1016/0377-8398(95)00050-X

Etourneau, J., Robinson, R. S., Martinez, P., & Schneider, R. (2013). Equatorial Pacific peak in biological production regulated by nutrient and upwelling during the late Pliocene/early Pleistocene cooling. *Biogeosciences*, *10*(8), 5663–5670. https://doi.org/10.5194/bg-10-5663-2013

Etourneau, J., Schneider, R., Blanz, T., & Martinez, P. (2010). Intensification of the Walker and Hadley atmospheric circulations during the Pliocene–Pleistocene climate transition. *Earth and Planetary Science Letters*, *297*(1–2), 103–110. https://doi.org/10.1016/j.epsl.2010.06.010

Farrell, J. W., Pedersen, T. F., Calvert, S. E., & Nielsen, B. (1995). Glacial-interglacial changes in nutrient utilization in the equatorial Pacific Ocean. *Letters to Nature*, *377*, 514–517.

Fedorov, A. V., Brierley, C. M., Lawrence, K. T., Liu, Z., Dekens, P. S., & Ravelo, A. C. (2013). Patterns and mechanisms of early Pliocene warmth. *Nature*, *496*(7443), Article 7443. https://doi.org/10.1038/nature12003

Fedorov, A. V., Burls, N. J., Lawrence, K. T., & Peterson, L. C. (2015). Tightly linked zonal and meridional sea surface temperature gradients over the past five million years. *Nature Geoscience*, *8*(12), Article 12. https://doi.org/10.1038/ngeo2577

Fedorov, A. V., Dekens, P. S., McCarthy, M., Ravelo, A. C., deMenocal, P. B., Barreiro, M., Pacanowski, R. C., & Philander, S. G. (2006). The Pliocene Paradox (Mechanisms for a Permanent El Niño). *Science*, *312*(5779), 1485–1489. https://doi.org/10.1126/science.1122666

Ford, H. L., Burls, N. J., Jacobs, P., Jahn, A., Caballero-Gill, R. P., Hodell, D. A., & Fedorov, A. V. (2022). Sustained mid-Pliocene warmth led to deep water formation in the North Pacific. *Nature Geoscience*, 1–6. https://doi.org/10.1038/s41561-022-00978-3

Ford, H. L., Ravelo, A. C., Dekens, P. S., LaRiviere, J. P., & Wara, M. W. (2015). The evolution of the equatorial thermocline and the early Pliocene El Padre mean state. *Geophysical Research Letters*, *42*(12), 4878–4887. https://doi.org/10.1002/2015GL064215

Gu, D., & Philander, S. G. (1997). Interdecadal Climate Fluctuations That Depend on Exchanges Between the Tropics and Extratropics. *Science*, *275*(5301), 805–807. https://doi.org/10.1126/science.275.5301.805

Heede, U. K., & Fedorov, A. V. (2021). Eastern equatorial Pacific warming delayed by aerosols and thermostat response to CO2 increase. *Nature Climate Change*, *11*(8), Article 8. https://doi.org/10.1038/s41558-021-01101-x

Herbert, T. D., Caballero-Gill, R., & Novak, J. B. (2021). A revised mid-Pliocene composite section centered on the M2 glacial event for ODP Site 846. *Climate of the Past*, *17*(3), 1385–1394. https://doi.org/10.5194/cp-17-1385-2021

Hovan, S. (1995). Late Cenozoic atmospheric circulation intensity and climatic history recorded by eolian deposition in the eastern equatorial Pacific Ocean, Leg 138. In N. G. Pisias, L. A. Mayer, T. R. Janecek, A. Palmer-Julson, & T. H. Van Andel (Eds.), *Proceedings of the Ocean Drilling Program, 138 Scientific Results* (Vol. 138). Ocean Drilling Program.

Jakob, K. A., Ho, S. L., Meckler, A. N., Pross, J., Fiebig, J., Keppler, F., & Friedrich, O. (2021). Stable Biological Production in the Eastern Equatorial Pacific Across the Plio-Pleistocene Transition (~3.35–2.0 Ma). *Paleoceanography and Paleoclimatology*, *36*(4), e2020PA003965. https://doi.org/10.1029/2020PA003965

Jia, F., & Wu, L. (2013). A Study of Response of the Equatorial Pacific SST to Doubled-CO2 Forcing in the Coupled CAM–1.5-Layer Reduced-Gravity Ocean Model. *Journal of Physical Oceanography*, *43*(7), 1288–1300. https://doi.org/10.1175/JPO-D-12-0144.1

Kimble, K. M., Herbert, T. D., & Jones, C. A. (2024). Pliocene Weakening of Gradients in Temperature but Not in Productivity in the Eastern Equatorial Pacific. *Paleoceanography and Paleoclimatology*, *39*(3), e2023PA004711. https://doi.org/10.1029/2023PA004711

Lawrence, K. T., Liu, Z., & Herbert, T. D. (2006). Evolution of the Eastern Tropical Pacific Through Plio-Pleistocene Glaciation. *Science*, *312*(5770), 79–83. https://doi.org/10.1126/science.1120395

Lawrence, K. T., Pearson, A., Castañeda, I. S., Ladlow, C., Peterson, L. C., & Lawrence, C. E. (2020). Comparison of Late Neogene U ^{k'} $_{37}$ and TEX $_{86}$ Paleotemperature Records from the Eastern Equatorial Pacific at Orbital Resolution. *Paleoceanography and Paleoclimatology*. https://doi.org/10.1029/2020PA003858

Lee, S.-Y., & Poulsen, C. J. (2005). Tropical Pacific climate response to obliquity forcing in the Pleistocene: TROPICAL PACIFIC RESPONSE TO OBLIQUITY FORCING. *Paleoceanography*, *20*(4), n/a-n/a. https://doi.org/10.1029/2005PA001161

Lisiecki, L. E., & Lisiecki, P. A. (2002). Application of dynamic programming to the correlation of paleoclimate records. *Paleoceanography*, *17*(4), 1-1-1–12. https://doi.org/10.1029/2001PA000733

Lisiecki, L. E., & Raymo, M. E. (2005). A Pliocene-Pleistocene stack of 57 globally distributed benthic δ ^{18} O records: PLIOCENE-PLEISTOCENE BENTHIC STACK. *Paleoceanography*, *20*(1), n/a-n/a. https://doi.org/10.1029/2004PA001071

Liu, Z., & Yang, H. (2003). Extratropical control of tropical climate, the atmospheric bridge and oceanic tunnel. *Geophysical Research Letters*, *30*(5). https://doi.org/10.1029/2002GL016492

Locarnini, M., Mishonov, A., Baranova, O., Boyer, T., Zweng, M., Garcia, H., Reagan, J., Seidov, D., Weathers, K., Paver, C., & Smolyar, I. (2019). World Ocean Atlas 2018, Volume 1: Temperature. *A. Mishonov Technical Ed.*, *NOAA Atlas NESDIS 81*, 52 pp.

Lu, P., McCreary, J. P., & Klinger, B. A. (1998). Meridional Circulation Cells and the Source Waters of the Pacific Equatorial Undercurrent. *Journal of Physical Oceanography*, *28*(1), 62–84. https://doi.org/10.1175/1520-0485(1998)028<0062:MCCATS>2.0.CO;2

Lyle, M., Drury, A. J., Tian, J., Wilkens, R., & Westerhold, T. (2019). Late Miocene to Holocene high-resolution eastern equatorial Pacific carbonate records: Stratigraphy linked by dissolution and paleoproductivity. *Climate of the Past*, *15*, 1715–1739.

Lyle, M. W., Prahl, F. G., & Sparrow, M. A. (1992). Upwelling and productivity changes inferred from a temperature record in the central equatorial Pacific. *Nature*, *355*(6363), 812–815. https://doi.org/10.1038/355812a0

McClymont, E. L., & Rosell-Melé, A. (2005). Links between the onset of modern Walker circulation and the mid-Pleistocene climate transition. *Geology*, *33*(5), 389–392. https://doi.org/10.1130/G21292.1

Meyers, S., Malinverno, A., Hinnov, L., Zeeden, C., Liu, H., & Moron, V. (2021). *astrochron: A Computational Tool for Astrochronology*. 144.

Müller, P. J., Kirst, G., Ruhland, G., von Storch, I., & Rosell-Melé, A. (1998). Calibration of the alkenone paleotemperature index U37K′ based on core-tops from the eastern South Atlantic and the global ocean (60°N-60°S). *Geochimica et Cosmochimica Acta*, *62*(10), 1757–1772. https://doi.org/10.1016/S0016-7037(98)00097-0

Philander, S. G., & Fedorov, A. V. (2003). Role of tropics in changing the response to Milankovich forcing some three million years ago: TROPICS AND GLACIAL CYCLES. *Paleoceanography*, *18*(2), n/a-n/a. https://doi.org/10.1029/2002PA000837

Raja, M., & Rosell-Melé, A. (2021). Appraisal of sedimentary alkenones for the quantitative reconstruction of phytoplankton biomass. *Proceedings of the National Academy of Sciences*, *118*(2). https://doi.org/10.1073/pnas.2014787118

Rasmussen, C. E., & Williams, C. K. (2006). *Gaussian processes for machine learning* (Vol. 1, p. 159). MIT press.

Ravelo, A. C., Dekens, P., & McCarthy, M. (2006). Evidence for El Niño—Like conditions during the Pliocene. *Gsa Today*, *16*. https://doi.org/10.1130/1052-5173(2006)016<4:EFENLC>2.0.CO;2

Sarmiento, J. L., Gruber, N., Brzezinski, M. A., & Dunne, J. P. (2004). High-latitude controls of thermocline nutrients and low latitude biological productivity. *Nature*, *427*(6969), Article 6969. https://doi.org/10.1038/nature02127

Shaari, H. B., Yamamoto, M., & Irino, T. (2013). Enhanced upwelling in the eastern equatorial Pacific at the last five glacial terminations. *Palaeogeography, Palaeoclimatology, Palaeoecology*, *386*, 8–15. https://doi.org/10.1016/j.palaeo.2013.03.022

Shankle, M. G., Burls, N. J., Fedorov, A. V., Thomas, M. D., Liu, W., Penman, D. E., Ford, H. L., Jacobs, P. H., Planavsky, N. J., & Hull, P. M. (2021). Pliocene decoupling of

equatorial Pacific temperature and pH gradients. *Nature*, *598*(7881), 457–461. https://doi.org/10.1038/s41586-021-03884-7

Thomson, D. J. (1982). Spectrum estimation and harmonic analysis. *Proceedings of the IEEE*, *70*(9), 1055–1096. Proceedings of the IEEE. https://doi.org/10.1109/PROC.1982.12433

Tierney, J. E., & Tingley, M. P. (2018). BAYSPLINE: A New Calibration for the Alkenone Paleothermometer. *Paleoceanography and Paleoclimatology*, *33*(3), 281–301. https://doi.org/10.1002/2017PA003201

Toggweiler, J. R., Dixon, K., & Broecker, W. S. (1991). The Peru upwelling and the ventilation of the south Pacific thermocline. *Journal of Geophysical Research: Oceans*, *96*(C11), 20467–20497. https://doi.org/10.1029/91JC02063

Volkman, J. K., Barrerr, S. M., Blackburn, S. I., & Sikes, E. L. (1995). Alkenones in Gephyrocapsa oceanica: Implications for studies of paleoclimate. *Geochimica et Cosmochimica Acta*, *59*(3), 513–520. https://doi.org/10.1016/0016-7037(95)00325-T

Wang, C., Deser, C., Yu, J.-Y., DiNezio, P., & Clement, A. (2017). El Niño and Southern Oscillation (ENSO): A Review. In P. W. Glynn, D. P. Manzello, & I. C. Enochs (Eds.), *Coral Reefs of the Eastern Tropical Pacific: Persistence and Loss in a Dynamic Environment* (pp. 85–106). Springer Netherlands. https://doi.org/10.1007/978-94-017-7499-4_4

Wara, M. W., Ravelo, A. C., & Delaney, M. L. (2005). Permanent El Nino-Like Conditions During the Pliocene Warm Period. *Science*, *309*(5735), 758–761. https://doi.org/10.1126/science.1112596

Supporting information

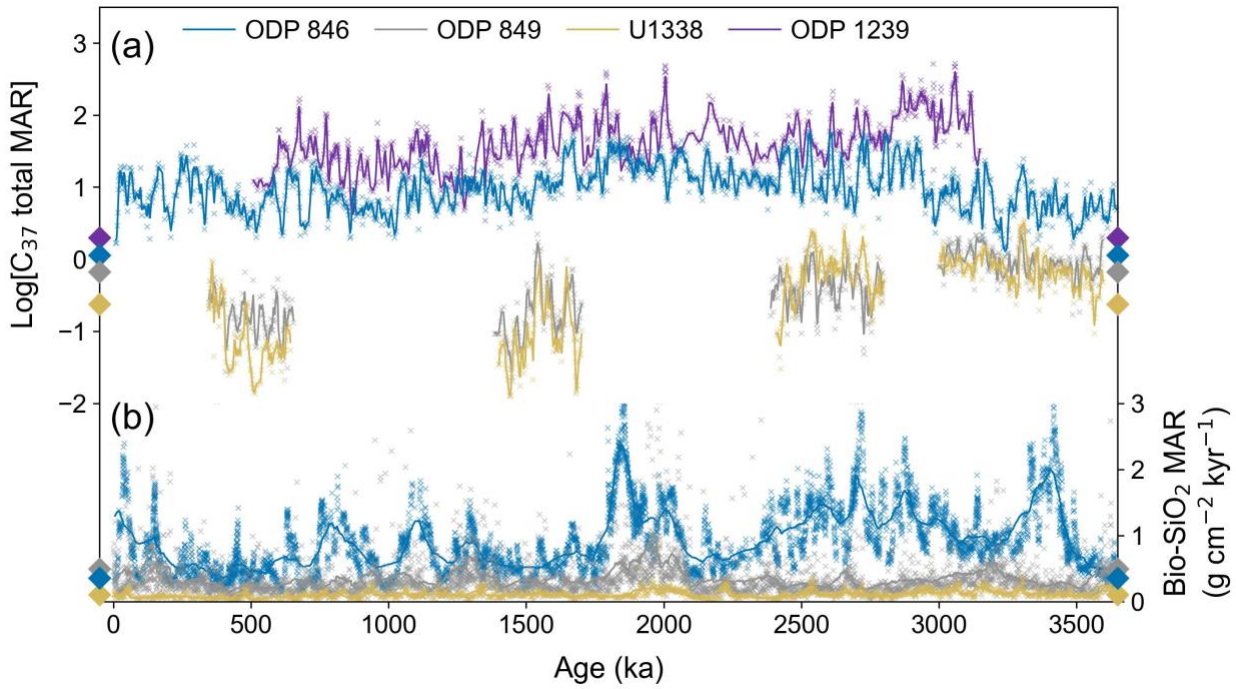

Figure S1. (a) Log[C_{37} total mass accumulation rates] at Sites 1239, 846, 849, and U1338 with diamonds representing modern log[C_{37} total MAR] estimated from core top samples corresponding to the 3 Ma paleo-locations of each site. Predicted mean values (thick lines) were calculated using a Gaussian Process model with Matérn32 and radial basis function kernels (Rasmussen & Williams, 2006). Original values are small crosses. (b) Bio-SiO_2 MAR at Sites 846, 849, and U1338 with diamonds representing modern bio-SiO_2 estimated from X-ray fluorescence scan data. Thick lines are 30-kyr smoothed data and original values are small crosses.

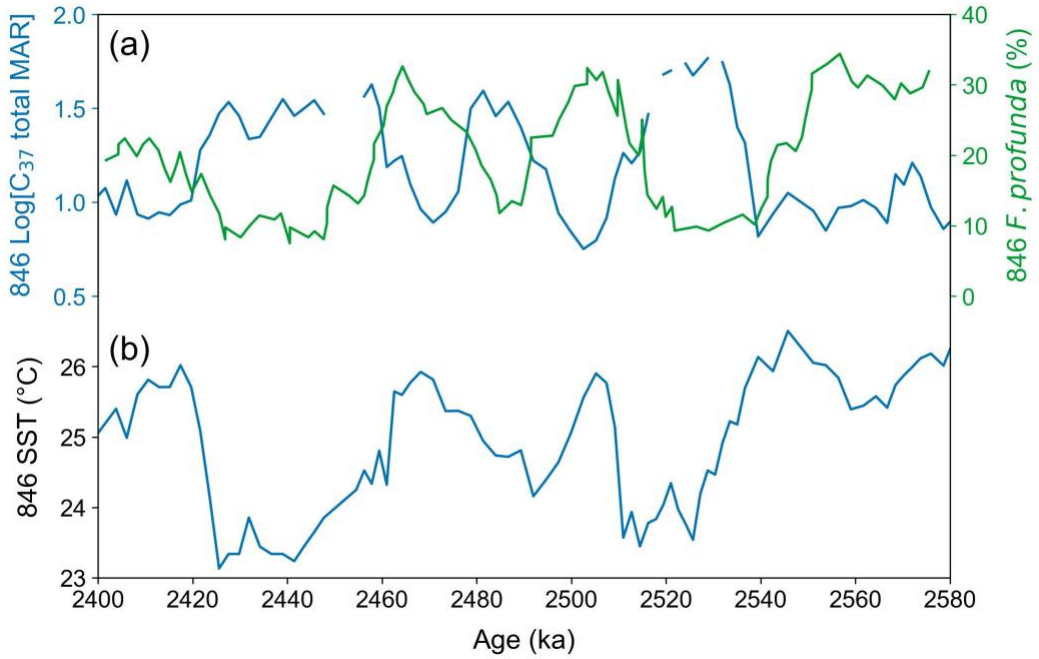

Figure S2. (a) Log[C_{37} total MAR] overlayed on the abundance of the lower photic zone nannofossil *Florisphaera profunda* at Site 846 (Bolton, Gibbs, et al., 2010), showing clear anticorrelation between the two records paced by 41-kyr cycles during an early Pleistocene interval. High surface productivity was correlated with low *F. profunda* abundance and a shoaled nutricline. (b) Alkenone SST from Site 846 indicates that glacial intervals were marked by a shoaled nutricline and high surface productivity.

References

Bolton, C. T., Gibbs, S. J., & Wilson, P. A. (2010). Evolution of nutricline dynamics in the equatorial Pacific during the late Pliocene. *Paleoceanography*, *25*(1). https://doi.org/10.1029/2009PA001821

Rasmussen, C. E., & Williams, C. K. (2006). *Gaussian processes for machine learning* (Vol. 1, p. 159). MIT press.

CHAPTER 4

Thermocline steepening and shoaling in the eastern equatorial Pacific since 3.5 Ma

K. M. Kimble[1] and T. D. Herbert[1]

[1]Department of Earth, Environmental, and Planetary Sciences, Brown University, Providence, Rhode Island, 02912, USA.

Key Points:

- New planktic foraminiferal stable isotope evidence indicates the eastern equatorial Pacific thermocline cooled and shoaled at the end of the Pliocene, initiating a protracted evolution toward modern temperature gradients that only arrived during the Late Pleistocene 100-kyr world.
- Progressively cooler and less nutrient-rich waters from high latitude source regions were conveyed through the ventilated thermocline to the equatorial Pacific, forcing low-latitude temperature and productivity changes through bottom-up mechanisms.
- High-low latitude connections persisted over the last 3.5 Myr, driving possible thermocline steepening and shoaling coincident with nutricline deepening over the Plio-Pleistocene, suggesting decoupled temperature and productivity extended into the Late Pleistocene.

Abstract

The Pliocene permanent El Niño-like mean state of the eastern equatorial Pacific Ocean (EEP) was defined by reduced east-west sea surface temperature (SST) gradients due to a deeper and warmer thermocline and weaker atmospheric Walker circulation. Over the last 3.5 Myr, the EEP thermocline shoaled and zonal SST gradients increased to reach modern conditions, where cool and nutrient-rich intermediate waters sourced from high latitude formation regions upwell in the tropics. Although the EEP surface temperature gradient evolution is constrained spatially and temporally, the relatively unknown development of zonal nutrient gradients would provide insight into the evolving relationship between temperature and biological productivity. Paired surface and subsurface reconstructions of temperature and nutrient availability guide novel interpretations of EEP thermocline and nutricline evolution forced by high latitude physical and biogeochemical changes over the Plio-Pleistocene. Here we present zonal and vertical transects of planktic foraminiferal stable oxygen and carbon isotopes from two cores in the EEP for the Pliocene (3.2-3.5 Ma), Plio-Pleistocene (2.5-2.8 Ma), mid-Pleistocene (1.5-1.7 Ma), and Late Pleistocene (0.4-0.6 Ma). We assess high-low latitude connections and forcings of the EEP thermocline and nutricline using windows of orbitally resolved, paired surface- and thermocline-dwelling foraminiferal stable isotopic data collected along the east-west axis of the modern EEP cold tongue. We report signs of incipient Northern Hemisphere glaciation beginning at ~2.72 Ma outcropping as cooling eastern EEP subsurface waters. These new planktic isotope records are consistent with previous reports of warmer Pliocene water supporting strong productivity, and we find evidence that subsurface nutrient availability weakened since 3.5 Ma. Plio-Pleistocene cooling of high latitude waters was transferred to the EEP subsurface through oceanic tunnels, which cooled and shoaled the thermocline, while diminishing nutrient availability may have

deepened the nutricline over the last 3.5 Myr. The temperature and nutrient gradient evolutions reported here may be attributed to changing temperature and nutrient properties of the oceanic tunnel waters, perhaps as a consequence of shifting source locations from the nutrient-replete Pliocene North Pacific to the modern Southern Ocean.

Plain language summary

Three million years ago, both surface and subsurface waters in the eastern tropical Pacific Ocean were warmer than they are today. The temperature contrast between the eastern and western part of the region was small and but there was still high biological activity of phytoplankton, marine organisms at the base of the food web. These past average conditions gradually evolved to the modern scenario where cold polar water travels through the deep ocean to emerge in the eastern tropical Pacific surface, bringing nutrients and oxygen to fuel strong biological productivity. We used geochemical signals trapped in the shells of fossilized marine plankton that live in the ocean surface and subsurface to address how eastern tropical Pacific temperature and nutrients changed over the last three million years. We found that as global climate and polar waters cooled over the last three million years, progressively cooler but less nutrient-rich water traveled from polar formation regions through the deep ocean and emerged in the subsurface tropical Pacific, which resulted in cooling and decreasing nutrient content. The three-million-year-old relationship between water temperature and nutrient availability is contrary to modern conditions, demonstrating the importance of looking to the fossil record to address future changes in the tropical Pacific Ocean.

1. Introduction

The tropical Pacific Ocean regulates global climate over long time scales by transporting heat poleward, while cold and nutrient-rich water sourced from high southern and northern latitudes emerges in the eastern equatorial Pacific (EEP) through upwelling (Cane, 1998). High latitude surface water is subducted and transported to the EEP thermocline through oceanic tunnels, thereby linking physical (temperature) and biogeochemical (primary productivity) changes in high latitudes to those in low latitudes (Liu & Yang, 2003). These high-low latitude connections make the EEP an ideal area to address how the intensification of Northern Hemisphere glaciation over the Plio-Pleistocene boundary influenced tropical ocean temperature and marine primary productivity (Lawrence et al., 2006) because the imprint of high latitude cooling emerges in equatorial upwelling zones like the EEP. Furthermore, the Plio-Pleistocene evolution of thermal and nutrient properties of the EEP may become relevant as global climate equilibrates to anthropogenic climate change. As the high latitude sources of tropical upwelled waters warm in the coming decades, high-low latitude connections that distribute heat throughout the planet are compromised (Cai et al., 2021; Wang et al., 2017).

The modern east-west sea surface temperature (SST) gradient is tightly coupled to thermocline depth (Wara et al., 2005), both of which dictate surface primary productivity (Pennington et al., 2006) in the EEP. Easterly trade winds drive surface water westward across the tropical Pacific, creating asymmetrical upwelling, temperature, and biological productivity patterns. A shallow thermocline and strong upwelling bring cold water temperatures and high nutrient concentrations to the EEP surface, while the deep western Pacific thermocline is associated with warm surface temperatures and reduced surface productivity. High surface air pressure over the EEP and low pressure over the western Pacific strengthens the trade winds and

enhances zonal SST and thermocline depth asymmetry, which is a diagnostic feature of strong atmospheric Walker circulation (Cane, 1986). When Walker circulation severely weakens on 2-7-year time scales during El Niño events, the tropical Pacific zonal SST and productivity gradients decrease, largely because the thermocline becomes deeper and less steep in the EEP, diminishing upwelling strength and nutrient delivery to warmer surface waters (Cane, 2005).

Several characteristics of the Pliocene (5.3-2.6 Ma) tropical Pacific resembled modern El Niño events, namely, warmer EEP SSTs relative to today, a reduced zonal SST gradient, and a deeper EEP thermocline (Wara et al., 2005). The Pliocene permanent El Niño state assumes a fundamental restructuring of the tropical Pacific thermocline, with a deeper, less tilted, and warmer thermocline necessary to explain subsurface temperature records (Ford et al., 2015) and SST patterns reconstructed across the equatorial Pacific (Wara et al., 2005). Several independent lines of evidence support a Pliocene reduction in the zonal SST gradient, including foraminiferal assemblage studies (Chaisson, 1995), foraminiferal magnesium to calcium ratios (Rickaby & Halloran, 2005; Wara et al., 2005), geochemical analyses using alkenones (Ravelo et al., 2006), and model simulations (Haywood et al., 2007; Scroxton et al., 2011). As high latitude waters cooled between the Pliocene and the present, Fedorov et al. (2006) have postulated that extratropical heat loss increased, causing the EEP thermocline to shoal, became more steeply tilted, and cool relative to ~3 Ma. Upwelling strength may have increased with the shoaled and steepened thermocline, based on a South Atlantic example of cooling SST concurrent with increasing upwelling species abundance (Marlow et al., 2000). High latitude cooling prior to and during the intensification of Northern Hemisphere glaciation and the development of permanent Northern Hemisphere ice sheets would have transported cooler water to the base of the EEP thermocline (Dekens et al., 2007; Fedorov et al., 2006), sparking the transition from the proposed

Pliocene permanent El Niño state of a deeper, warmer, flatter EEP thermocline to the modern shallow, cool, and tilted structure (Ford et al., 2015).

Contrary to the El Niño-like characteristics of the Pliocene EEP thermocline, the nutricline was likely still slightly tilted to allow strong eastern EEP productivity, and nutrient content of waters upwelled in the EEP may have decreased from relatively high concentrations in the Pliocene to lower modern concentrations (Kimble et al., 2024). It is unclear whether EEP nutricline shoaling and steepening accompanied Plio-Pleistocene cooling (Shaari et al., 2014), but the nutrient concentration of upwelled waters likely decreased to reflect the observed pattern of stronger than modern Pliocene eastern EEP productivity relative to the western EEP. Surface records indicate a decoupling of EEP temperature and productivity as warm Pliocene SSTs still supported high productivity through the upwelling of nutrient-rich water or through stronger than modern upwelling (Dekens et al., 2007; Kimble et al., 2024).

However, coupled thermocline-nutricline evolution in the EEP remains unconstrained during the intensification of Northern Hemisphere glaciation and throughout the Plio-Pleistocene. Specifically, questions remain about the degree to which colder water and nutrients were transmitted from high latitude source regions through oceanic tunnels to the EEP subsurface (Ford et al., 2022). Here we present new orbitally resolved planktic foraminiferal stable isotope data from two sites in the EEP over four time intervals of roughly ~250 kyr which span the last 3.5 Myr. The position of the two sites in an east-west transect along the EEP allows us to examine fluctuations in thermocline and nutricline depth, tilt steepness, and intensity that a single site alone would be unable to capture. Temperature properties are monitored by a combination of alkenone paleothermometry and planktic foraminiferal oxygen isotope offsets between surface and thermocline-dwelling species, while nutricline properties are tracked using a

combination of carbon stable isotopic analyses and paleoproductivity indices. The contrast between surface and subsurface oxygen isotope values measured on the same samples eliminates global ice volume fluctuations and focuses on local temperature or salinity effects (Ravelo et al., 2006).

2. Methods

2.1 Site location and chronology

The two cores used in this study were collected by the International Ocean Discovery Program (IODP) and its previous iterations. IODP Site U1338 (2°30.47'N, 117°58.18'W, 4,200 m water depth) was collected in spring 2009, and ODP Site 846 (3°5.70'S, 90°49.08'W, 3,296 m water depth) was collected in spring 1991. The sites are positioned at the eastern and western bounds of the EEP cold tongue (**Figure 1**), with cool and nutrient-rich Equatorial Undercurrent and Equatorial Pacific Intermediate Water (sourced from southern high latitude Subantarctic Mode Water and Antarctic Intermediate Water) bathing the eastern Site 846 to a greater degree than the western Site U1338 (Bostock et al., 2010; Toggweiler et al., 1991).

The age-depth tuning reported in Chapter 3 was used to assign ages to the Site 846 data, which is based on slightly modified versions of the age-depth tuning of Lisiecki and Raymo (2005) and updated with the revised composite section of Herbert et al. (2021) for the M2 glacial interval. The Match program (Lisiecki & Lisiecki, 2002) was used to align SST data from Site

U1338 to the age-depth model of Site 846, adjusted with secondary alignment records from Sites 846 and U1338 X-ray fluorescence elemental data.

2.2 Analytical methods and data acquisition

Foraminiferal stable oxygen ($\delta^{18}O$) and carbon ($\delta^{13}C$) isotope analyses were conducted on 291 samples from Site 846 and 264 samples from Site U1338 spanning four time intervals over the last 3.5 Myr: Pliocene (3.22-3.46 Ma), Plio-Pleistocene (2.50-2.78 Ma), mid-Pleistocene (1.50-1.72 Ma), and Late Pleistocene (0.42-0.63 Ma). Two planktic species were analyzed per sample: *Trilobatus sacculifer* (without sac), a surface-dwelling foraminifer that lives in the upper ~50 m of the mixed layer (Ravelo & Fairbanks, 1992; Spero et al., 2003), and *Neogloboquadrina dutertrei*, a middle to deep thermocline-dwelling species associated with the chlorophyll maximum and that lives at ~60-150 m water depth (Fairbanks et al., 1982; Spero et al., 2003).

Sample preparation consisted of wet-sieving to >150 μm, drying at 40°C, and picking 20-30 individual *T. sacculifer* and *N. dutertrei* in the dry-sieved 250-355 μm fraction. A sample size of ~30 individual planktic foraminifera has been shown to produce consistent stable isotope results (Thirumalai et al., 2013). The specimens were cleaned prior to analysis by sonicating for ~30 s in 200 μL ethanol and pipetting off excess carbonate, then crushing the specimens to homogenize the samples prior to removing roughly half the sample for analysis. Samples in ethanol dried overnight at room temperature.

Isotope ratio mass spectrometry (IRMS) analyses were conducted on a MAT253+ coupled to a Kiel IV Carbonate Device at Brown University. Results are reported relative to ‰

VPDB with uncertainties of ±0.02‰ for $\delta^{13}C$ and ±0.06‰ for $\delta^{18}O$ of in-house Carrara standard (n=81, 1σ) and ±0.03‰ for $\delta^{13}C$ and ±0.08‰ for $\delta^{18}O$ of in-house BYM standard (n=53, 1σ).

Site 846 alkenone SST and productivity mass accumulation rate (MAR) data are from Herbert et al. (2021) and Lawrence et al. (2006, 2020). SST and productivity MAR data from Site U1338 are from Kimble et al. (2024) and Chapter 3. The alkenone $U^{k'}_{37}$ index reliably estimates SST based on the number of double bonds and type of ketone group in alkenone molecules (Herbert, 2014), while the alkenone C_{37} total value indicates the abundance of alkenone molecules in sediment, which positively correlates with surface chlorophyll and primary productivity (Kimble et al., 2024; Raja & Rosell-Melé, 2021).

We took alkenone SST as an approximation of mean annual SST, which allowed us to scale surface-dwelling *T. sacculifer* $\delta^{18}O$ to temperature and vertical isotope gradients using the Bemis et al. (1998) high light equation:

$$\delta^{18}\mathbf{O}_{\mathbf{expected\ planktic}} = \delta^{18}\mathbf{O}_{\mathbf{seawater}} + \frac{\mathbf{14.9 - SST}}{\mathbf{4.8}}$$

We used modern estimates of EEP $\delta^{18}O_{seawater}$ = 0.3‰, and we assumed that both alkenone producers and surface-dwelling *T. sacculifer* lived in the mixed layer throughout our record. After accounting for the temperature effect with the independent alkenone proxy, residual *T. sacculifer* $\delta^{18}O$ variability can be attributed to global ice volume change (Shackleton, 1987) and local $\delta^{18}O_{seawater}$ variability. Assuming the *T. sacculifer* $\delta^{18}O$ and alkenone producers lived in the surface mixed layer, we can roughly approximate subsurface temperatures using the difference between *T. sacculifer* and *N. dutertrei* $\delta^{18}O$ ($\Delta\delta^{18}O$) and the relationship between the change in temperature (ΔT) and vertical $\Delta\delta^{18}O$, where $\Delta\delta^{18}O$ of 1.0‰ is equivalent to ΔT of ~4.5°C. We converted the vertical $\Delta\delta^{18}O$ for each sample to ΔT and subtracted from the

alkenone SST records at Sites 846 and U1338 to produce rough subsurface temperature estimates, a close enough approximation if SST and subsurface temperatures are relatively tightly coupled.

A Gaussian Process model using the sum of Matérn32 and radial basis function kernels (Rasmussen & Williams, 2006) was applied to more robustly constrain trends and gradients in the face of analytical noise (see the data availability section for the Gaussian Process code).

Spectral analyses using the Thomson multitaper method (Thomson, 1982) were conducted on the $\delta^{18}O$ and $\delta^{13}C$ data from each time interval to assess the dominance of different orbital frequencies at each site (Meyers et al., 2021). Data were detrended and linearly interpolated to 3-kyr timesteps prior to analysis.

3. Results

3.1 Planktic $\delta^{18}O$ and SST

Planktic foraminiferal $\delta^{18}O$ records a combination of local ocean temperature and global ice volume, with more depleted $\delta^{18}O$ coinciding with warmer intervals and more enriched $\delta^{18}O$ corresponding to colder intervals (Spero et al., 2003). The core top zonal gradient in planktic $\delta^{18}O$ between ~110° and ~90°W is ~0.4‰ at the surface and ~0.6‰ at a depth of 100 m, and vertical $\delta^{18}O$ gradients between the inferred depth habitats of *T. sacculifer* and *N. dutertrei* are ~1.4‰ at Site 846 and ~1.6‰ at Site U1338 (**Figure 2**). More depleted *T. sacculifer* and *N. dutertrei* $\delta^{18}O$ values were recorded in eastern core tops relative to the west, despite the modern ~2°C temperature contrast between 110° and 90°W at the surface and at depth (**Figures 1, 2**). The depleted planktic $\delta^{18}O$ values may be attributed to strong modern upwelling of isotopically depleted $\delta^{18}O_{seawater}$ in the eastern part of the EEP because Sub-Antarctic Mode Water formation

regions in the Southern Ocean have $\delta^{18}O_{seawater}$ values that are >0.5‰ lighter than those of the modern EEP (Bigg & Rohling, 2000; Schmidt, 1999; Schmidt et al., 1999).

The sufficient magnitude of modern zonal and vertical $\delta^{18}O$ gradients justifies their reconstruction through the Plio-Pleistocene because they exceed the expected error of isotopic analyses. Over the four time windows, both surface and subsurface temperatures cooled toward modern based on progressively heavier *T. sacculifer* and *N. dutertrei* $\delta^{18}O$ values (**Figure 3**). Cooling recorded in alkenone SSTs from both sites agrees with reconstructed surface planktic $\delta^{18}O$, with Plio-Pleistocene cooling at Site 846 in the east appearing earlier and more intensely than at the western Site U1338. Zonal *T. sacculifer* and *N. dutertrei* $\delta^{18}O$ gradients were consistently offset through ~2.5 Ma, but during the mid- and Late Pleistocene *T. sacculifer* $\delta^{18}O$ values at both sites converged while *N. dutertrei* $\delta^{18}O$ retained a stronger zonal gradient (**Figure 3b**). Progressively greater proportions of more depleted Sub-Antarctic Mode Water $\delta^{18}O_{seawater}$ may have upwelled in the EEP beginning in the mid-Pleistocene, affecting the eastern site to a greater degree than the west and making Site 846 *T. sacculifer* $\delta^{18}O$ values appear more depleted than the alkenone SST records suggest.

The difference in $\delta^{18}O$ between surface-dwelling *T. sacculifer* and subsurface-dwelling *N. dutertrei* ($\Delta\delta^{18}O$) tracked the combination of the difference in temperature between the surface and ~100 m water depth (ΔT), and isotopic gradients correlated to the vertical salinity gradient of the EEP. Lakhani et al. (2024) reported relatively strong correlations (R=0.76) between the observed modern thermocline depth and core top $\Delta\delta^{18}O$ across 20 sites in the tropical Pacific. The vertical $\Delta\delta^{18}O$ gradients at both sites were comparable during the Pliocene through early Pleistocene (average $\Delta\delta^{18}O$ of ~0.8 ‰ equates to ΔT of ~3.6°C). A similar $\Delta\delta^{18}O$

at the eastern and western site, combined with a reduced alkenone SST zonal gradient relative to the Late Pleistocene, implied that the EEP thermocline was not steeply tilted through 2.5 Ma because both surface and subsurface temperatures were comparable in the eastern and western parts of the transect (**Figure 3c**). However, by the mid-Pleistocene (~1.7 Ma) and through the Late Pleistocene (~400 ka), the vertical $\Delta\delta^{18}O$ gradient was larger in the east (average $\Delta\delta^{18}O$ of ~1.2 ‰, ΔT of ~5.4°C) than in the west (average $\Delta\delta^{18}O$ of ~0.9 ‰, ΔT of ~4.1°). The thermocline was more steeply tilted to produce a greater contrast between the surface and subsurface temperatures in the east due to more cold water upwelling in the east relative to the west.

On orbital time scales, eastern Site 846 *T. sacculifer* $\delta^{18}O$ and alkenone SST (both representative of surface temperatures) cooled to reach *N. dutertrei* $\delta^{18}O$ values of western Site U1338 (which reflected subsurface temperatures) beginning ~2.7 Ma, a pattern that was repeated during every major glacial event recorded in these time intervals. During glacials, cold water upwelled in the east to a much greater degree than in the west, extending the western subsurface isotherm in a steepened slope to the eastern surface (**Figure 3b**). Specifically, the late Pliocene-early Pleistocene glacials at ~2.72, ~2.68, ~2.64, ~2.61, ~2.57, and ~2.53 Ma mark times when Site U1338 *N. dutertrei* $\delta^{18}O$ values matched those of Site 846 *T. sacculifer*, suggesting that western subsurface temperatures apparently outcropped at the eastern surface.

Independently estimated alkenone SST records provide useful constraints surface temperature because *T. sacculifer* $\delta^{18}O$ values reflect global ice volume and local salinity conditions in addition to temperature. The *T. sacculifer* $\delta^{18}O$ records were corrected for the temperature effect by subtracting alkenone SST estimates of expected foraminiferal carbonate $\delta^{18}O$ from *T. sacculifer* $\delta^{18}O$. The smaller the residual between *T. sacculifer* $\delta^{18}O$ and SST-

estimated $\delta^{18}O$, the greater role temperature played in accounting for planktic $\delta^{18}O$. In the Pliocene, local temperature accounted for slightly more $\delta^{18}O$ variability at the western site relative to the east (**Figure 3e**). By the Late Pleistocene all but ~0.6‰ of planktic $\delta^{18}O$ could be attributed to SST change while the residual at the western site was closer to ~1.5‰, suggesting ice volume changes were more important in the Late Pleistocene western EEP while SST changes controlled eastern EEP $\delta^{18}O$ (**Figure 3e**). Overall, much of *T. sacculifer* $\delta^{18}O$ variance comes from SST change, based on alkenone SST estimates.

3.2 Planktic $\delta^{13}C$ and productivity

Subsurface *N. dutertrei* $\delta^{13}C$ values were always more depleted than those of surface *T. sacculifer* because surface photosynthesis discriminates against ^{13}C, while respiration at depth reintroduces ^{12}C back into the water column (Spero et al., 2003). Available nutrients are also utilized during surface photosynthesis and remineralized at depth, so depleted $\delta^{13}C$ strongly correlates with higher nutrient concentrations and incomplete nutrient utilization of surface primary producers in modern sediments (**Figure S1**). Given these interpretations, the more depleted $\delta^{13}C$ values of *N. dutertrei* at both sites corresponded to greater local upwelling and higher nutrient availability at depth, while the more enriched *T. sacculifer* $\delta^{13}C$ values indicated diminished upwelling strength and lower nutrient availability at the surface (**Figure 4**). Surface $\delta^{13}C$ values at both sites remained enriched over the last 3.5 Myr, but subsurface upwelling strength (as recorded by *N. dutertrei* $\delta^{13}C$) was greater during the Pliocene and decreased over the Pleistocene to a similar degree at both sites (**Figure 4**). By the Late Pleistocene (~400 ka), subsurface $\delta^{13}C$ had become nearly as enriched as surface values, coincident with stronger

vertical $\delta^{18}O$ gradients that point to colder water upwelling occurring across the EEP, but especially in the east (**Figure 3**).

The vertical gradient in $\delta^{13}C$ between surface-dwelling *T. sacculifer* and thermocline-dwelling *N. dutertrei* ($\Delta\delta^{13}C$) reflected a combination of the upwelled source water $\delta^{13}C$ and surface nutrient uptake associated with photosynthesis. Vertical $\Delta\delta^{13}C$ gradients evolved similarly at both sites, approaching no offset by the Late Pleistocene (**Figure 4c**). Unlike surface $\delta^{18}O$, which followed SST tightly at both sites, surface $\delta^{13}C$ weakly resembled surface productivity recorded by alkenone C_{37} total. High C_{37} total mass accumulation rates (MAR) are strongly correlated with high export productivity in modern sediments (Kimble et al., 2024; Raja & Rosell-Melé, 2021). In general, periods of depleted $\delta^{13}C$ coincided with increased C_{37} MAR or inferred primary productivity (**Figure S2**). As C_{37} total MAR and associated primary productivity decreased at the western site from the Pliocene to modern, western upwelling recorded by progressively enriched *N. dutertrei* $\delta^{13}C$ weakened as well (**Figure 4b)**. A combination of increased Pliocene upwelling strength and possibly greater nutrient concentrations allowed for higher western (and eastern) productivity in the Pliocene relative to the present.

Individual glacial events (notably at ~2.72, ~2.68, ~2.64, ~2.60 Ma, and throughout the mid- to Late Pleistocene) appear in the $\delta^{13}C$ records as more depleted eastern *T. sacculifer* excursions, coinciding with more enriched $\delta^{18}O$ events and cooler alkenone SSTs. During these Early Pleistocene glacials, vertical $\Delta\delta^{18}O$ and $\Delta\delta^{13}C$ gradients approached zero at the eastern site, largely because surface-dwelling *T. sacculifer* became more enriched in $\delta^{18}O$ and more depleted in $\delta^{13}C$, which suggested spans of enhanced upwelling and greater local nutrient availability coincident with glacial periods. By glacial intervals of the mid- and Late Pleistocene,

surface $\delta^{13}C$ still became more depleted while surface and subsurface $\delta^{18}O$ became more enriched at both sites, but subsurface $\delta^{13}C$ had become progressively more enriched, reflecting Pleistocene cooling and possible diminished nutrient concentrations of waters upwelling in the EEP (**Figures 3, 4**).

The nutricline may have been shallower during the Pliocene when the vertical $\Delta\delta^{13}C$ gradients at both sites were strong (**Figure 5**). A shoaled nutricline could account for greater Pliocene productivity relative to modern despite warmer EEP SSTs and a deeper thermocline during the Pliocene (Kimble et al., 2024). By the Late Pleistocene, the EEP thermocline had shoaled and steepened while the nutricline deepened relative to the Pliocene, suggesting that the thermocline and nutricline evolved independently.

3.3 $\delta^{18}O$ and $\delta^{13}C$ spectral power

Multitaper spectral analyses indicate that eastern subsurface $\delta^{18}O$ was more sensitive to obliquity and precession than the western surface or subsurface in the Pliocene and at the Plio-Pleistocene boundary (**Figure 6**). By the mid- to Late Pleistocene, eccentricity cycles paced $\delta^{18}O$ and $\delta^{13}C$ at both sites, signaling a shift from high latitude 41-kyr forcings affecting eastern EEP upwelling during the Pliocene to 100-kyr glacial-interglacial pacing after the mid-Pleistocene Transition.

4. Discussion

4.1 Controls on EEP thermocline and nutricline

EEP planktic $\delta^{18}O$ depended on local temperature of the surface or subsurface waters where the foraminifera lived, $\delta^{18}O_{seawater}$ of high latitude water from EEP upwelling source

regions, and global ice volume effects that influenced the global pool of ^{18}O and ^{16}O (Lea, 2003). Alkenone SST reflected top-down forcings like atmospheric CO_2 concentration that influenced surface water temperature where alkenone-producing organisms lived, as well as bottom-up forcings like the temperature of source water upwelling in the EEP delivered by oceanic tunnels (Bolton, Gibbs, et al., 2010). Planktic $\delta^{13}C$ values were related to nutrient concentrations both due to local tropical processes and high latitude conditions transferred to the EEP subsurface though upwelled waters. Strong local photosynthesis depleted nutrients and enriched planktic $\delta^{13}C$, while remineralization released nutrients back into the water column and respiration depleted $\delta^{13}C$ by adding ^{12}C at depth (Holden et al., 2013; Spero et al., 2003). High latitude source water could transmit ^{12}C and nutrient properties through the oceanic tunnel to the EEP subsurface (Liu & Yang, 2003). Upwelled water from older sources tended to be more nutrient-rich and isotopically depleted in $\delta^{13}C$ (Broecker et al., 1998). Air-sea gas exchange of CO_2 also affected the isotopic composition of planktic foraminiferal calcite (Gruber et al., 1999; Holden et al., 2013; J. Zhang & Quay, 1997) and could partly explain large glacial-interglacial $\delta^{13}C$ variability (Wolf-Gladrow et al., 1999).

4.2 Long-term cooling and decreasing nutrient availability

The Site 846 and U1338 SST records reflected surface cooling at both sites over the Plio-Pleistocene, but most significantly in the eastern EEP. The new *T. sacculifer* and *N. dutertrei* $\delta^{18}O$ data presented here showed cooling concurrent with alkenone SST change at both sites and in both the surface and subsurface over the same time windows. Progressive subsurface $\delta^{18}O$ enrichment at both sites reflected upwelling of cool high latitude waters, with eastern subsurface cooling especially noticeable during glacials (**Figure 3**). The eastern EEP vertical $\Delta\delta^{18}O$ gradient

increased more than in the west by the mid-Pleistocene, which likely pointed to a major thermocline cooling and tilt increase. The planktic $\delta^{13}C$ reconstructions indicated stable surface $\delta^{13}C$ at both sites but progressively more enriched subsurface $\delta^{13}C$ throughout the Pleistocene as the nutricline deepened and the subsurface nutrient inventory decreased (**Figure 4**). Depleted eastern EEP subsurface $\delta^{13}C$ excursions during glacials marked influxes of high latitude nutrients transmitted through the oceanic tunnel. The $\delta^{13}C$ values argued for a deepening nutricline over the last 3.5 Ma because the vertical $\Delta\delta^{13}C$ gradient shrank at both sites as the subsurface nutrient inventory decreased during the Pleistocene.

The combination of alkenone SST with surface and subsurface $\delta^{18}O$ presents the strongest available evidence for a major increase in EEP thermocline tilt coincident with high latitude source water cooling transmitted through the oceanic tunnel into the EEP subsurface during the Early Pleistocene. The EEP thermocline has evolved considerably since the Plio-Pleistocene, which poses a challenge to understanding how high latitude source waters changed.

Source regions for EEP waters in both northern and southern high latitudes cooled by at least 8°C (Brierley et al., 2009; Fedorov et al., 2015) prior to and during the intensification of Northern Hemisphere glaciation. Nutrient concentrations may have decreased either in source regions or due to shifting contributions of northern and southern high latitude waters (Ford et al., 2015, 2022; Shankle et al., 2021). These cooler and less nutrient-rich waters traveled through oceanic tunnels and emerged through the thermocline into the EEP surface, conveying physical (temperature) and biogeochemical (nutrient availability and productivity) characteristics to the upwelling location.

Increasing strength of upwelling-favorable winds alone cannot explain the cooling temperatures and lower nutrient availability recorded in planktic $\delta^{18}O$ and $\delta^{13}C$ (Dekens et al.,

2007) because nutrients and associated productivity decreased toward modern, based on trends toward more enriched $\delta^{13}C$ and lower C_{37} total in the western EEP over the Plio-Pleistocene. The EEP subsurface $\delta^{18}O$ (which was presumably out of reach of the winds' influence) cooled prior to and more intensely than the surface, pointing to the temperature signal of upwelled water rather than wind stress controlling zonal SST gradients. The more weakly stratified mixed layer of the Pliocene EEP would have required lower zonal wind stress to upwell the same amount of nutrients as the more stratified Late Pleistocene EEP (**Figure 5**). High latitude cooling and resulting EEP thermocline shoaling manifested as cooler surface alkenone-based temperatures and planktic $\delta^{18}O$ (Fedorov et al., 2006). Progressive eastern EEP subsurface cooling may have led to an increased thermocline tilt via surface wind stresses, producing the possibility of a feedback between thermocline temperature, tilt, and wind strength.

Equatorial Pacific thermocline steepening and shoaling over the Plio-Pleistocene is well documented (Fedorov et al., 2006; Ford et al., 2015; Ravelo et al., 2006; Rickaby & Halloran, 2005; Wara et al., 2005). EEP nutricline evolution is more elusive, with some studies indicating nutricline shoaling toward modern based on benthic (Jakob et al., 2021) and planktic (Cannariato & Ravelo, 1997) $\delta^{13}C$, and others suggesting enhanced productivity accompanied cooler intervals (Bolton, Lawrence, et al., 2010), but most records point to high latitude forcing of surface productivity through the Pliocene. Cannariato & Ravelo (1997) published *T. sacculifer* and *N. dutertrei* stable isotope data spanning the last 5.0 Myr from ODP Site 851 (2°30.47'N, 117°58.18'W, 4,200 m water depth), which sits between Sites 846 and U1338, slightly north and toward the western side of the transect. Site 851 planktic $\delta^{18}O$ reflected surface and subsurface cooling of the same magnitude as we report here and subsurface $\delta^{13}C$ values increased since 3.5 Ma (**Figure 3**), supporting weakened upwelling of less nutrient-rich water in the western EEP.

However, average surface $\delta^{13}C$ was ~0.4 ‰ more enriched at Site 851 during the Pliocene compared to that of Sites 846 and U1338 (**Figure 4**), possibly because Site 851 sat farther north of the EEP cold tongue and received considerably fewer upwelled nutrients.

Dang et al. (2024) reported long-term trends of Western Pacific warm pool (WPWP) thermocline cooling and shoaling based on surface- and thermocline-dwelling foraminiferal $\delta^{18}O$ records. Other WPWP planktic $\delta^{13}C$ and geochemical reconstructions recorded tight couplings of productivity and nutricline depth during the Pliocene, with a deeper nutricline regulating lower surface productivity (Shi et al., 2022). Planktic $\delta^{18}O$ and Mg/Ca ratios from the WPWP and alkenone SST from the EEP indicated that a significant increase in east-west SST gradients across the Pacific occurred during glacial intervals beginning ~1.2 Ma due to cooler upwelled eastern EEP waters (de Garidel-Thoron et al., 2005). Despite the clear Plio-Pleistocene cooling trend, the zonal cross-Pacific SST gradient approached the prior Early Pleistocene values during interglacials, a pattern repeated in the EEP surface and subsurface temperature gradients reported here.

Two scenarios could explain the trends toward more isotopically enriched planktic $\delta^{13}C$ and decreased western EEP biological productivity in the context of Plio-Pleistocene cooling: upwelling strength decreased toward modern, or nutrient concentrations of upwelled waters (evidenced by $\delta^{13}C$ of subsurface foraminifera) decreased since the Pliocene. Marlow et al. (2000) report intensified upwelling and greater surface cooling during the Plio-Pleistocene transition based on diatom assemblages in the southeast Atlantic upwelling zone. The modern El Niño-style pattern of cold water and strong upwelling fueling high productivity did not apply to the average Pliocene EEP, where we recorded warm productive water. The emergence of cold water (enriched surface $\delta^{18}O$ and cooler SSTs) with high nutrient content (depleted surface $\delta^{13}C$)

beginning ~2.72 Ma was coupled to high latitude processes just prior to the intensification of Northern Hemisphere glaciation (**Figures 3, 4**). As meridional temperature gradients increased with Pleistocene cooling, which affected the high latitudes most strongly, zonal SST gradients increased across the EEP (Fedorov et al., 2006), strengthening zonal wind stress through the Bjerknes feedback and boosting eastern upwelling (Dekens et al., 2007).

A more likely scenario is that since 3.5 Ma, nutrient concentrations of upwelled EEP waters decreased due to possible shifts in high latitude source water locations and/or nutrient utilization (Cannariato & Ravelo, 1997). EEP *N. dutertrei* $\delta^{13}C$ values are subsurface tags that reflect surface processes in the high latitude regions where EEP upwelled source water forms. Different nutrient concentrations are associated with the Southern Ocean and the North Pacific because more nutrients accumulate in the Pacific given the relatively older water age (Pondaven et al., 1999; Rippert et al., 2017). Progressive sourcing from more nutrient-deplete regions could explain decreasing western EEP productivity concurrent with enriched subsurface $\delta^{13}C$ indicating lower nutrient availability throughout the Pleistocene (Cannariato & Ravelo, 1997; Ford et al., 2015, 2022; Shankle et al., 2021). In the context of the Pliocene El Padre, the warmer, deeper, and less steeply tilted thermocline reconstructed from different equatorial Pacific sites and geochemical methods (Ford et al., 2015; Ravelo et al., 2006; Wara et al., 2005) is consistent with our reported surface and subsurface $\delta^{18}O$ warmth at ~3.0 Ma, while our depleted Pliocene $\delta^{13}C$ suggests greater EEP nutrient availability relative to modern. The reconstructed Pliocene relationship between temperature and nutrients poses a challenge to the

future of understanding not only the evolution of high latitude temperatures, but also nutrient inventories and biogeochemistry.

4.3 Glacial-interglacial thermocline and nutricline variability

Evidence of high latitude cooling and high nutrient availability cropped up in the eastern part of the equatorial transect in the form of enriched $\delta^{18}O$ and depleted $\delta^{13}C$ excursions, which became particularly apparent beginning with the ~2.72 Ma glaciation and continuing throughout the Pleistocene (**Figures 3, 4**). Glacial-interglacial variability in the planktic $\delta^{18}O$ and $\delta^{13}C$ records exhibited 41-kyr cyclicity during the Early Pleistocene and agrees with reconstructions of the deep-photic species *Florisphaera profunda* abundance, which is associated with nutricline depth (Bolton, Gibbs, et al., 2010). *F. profunda* abundance decreased and the EEP nutricline shoaled during glacials, a pattern repeated in the ~2.53 Ma glacial when planktic $\delta^{18}O$ became more enriched and $\delta^{13}C$ became depleted (**Figure S3**). Decreased upwelling may have been less important than reduced nutrient availability over the long-term trend toward depleted subsurface planktic $\delta^{13}C$, which accompanied Plio-Pleistocene cooling in both the surface (alkenone SST and *T. sacculifer* $\delta^{18}O$) and subsurface (*N. dutertrei* $\delta^{18}O$). Early to mid-Pleistocene glacial excursions of depleted surface $\delta^{13}C$ indicated brief reversals of greater nutrients availability. Glacial intervals accentuated high-low latitude connections through the oceanic tunnel as Southern Ocean and/or North Pacific cold temperatures and nutrients were transmitted through the EEP subsurface.

5. Conclusion

New surface and subsurface foraminiferal stable isotope analyses from two EEP sites demonstrate that upwelled waters became cooler and less nutrient-rich over the last 3.5 Myr. Significant change occurred between the four ~250-kyr windows reported here, so the ultimate question of whether the gradient evolution was punctuated or gradual cannot yet be addressed. Vertical $\Delta\delta^{18}O$ gradients reflect EEP subsurface cooling coincident with high latitude cooling and the intensification of Northern Hemisphere glaciation, which delivered colder waters from high latitudes to the EEP. Vertical $\Delta\delta^{13}C$ gradients decreased toward modern, indicating that oceanic tunnels transported diminishing nutrient supplies to the EEP throughout the Plio-Pleistocene as upwelling strength or nutrient availability decreased at both sites. The flatter and warmer thermocline of the Pliocene EEP supports current interpretations of Pliocene El Padre mean state temperature patterns (Fedorov et al., 2006; Ford et al., 2015; Wara et al., 2005). However, the greater Pliocene upwelling strength or nutrient availability relative to modern implied by subsurface $\delta^{13}C$ contradicts the warm and unproductive waters of modern El Niño events. The demonstrated decoupling between the thermocline and nutricline raises questions about future EEP temperature and productivity evolution. Atmospheric CO_2 concentrations, high latitude ice volume, and global temperatures have changed significantly over the Plio-Pleistocene, but the planktic foraminiferal isotopic data reported here point to the critical role of high latitude oceans in communicating changes to the tropics.

Acknowledgments

This research used samples and data provided by the International Ocean Discovery Program (IODP). The authors would like to thank Steve Clemens for conceptual and technical help preparing the foraminiferal analyses, and Weimin Si for assistance estimating modern

carbonate $\delta^{18}O$. Max Ferguson assisted in preparing and picking foraminiferal samples. Funding for this research was provided by NSF grant 2202760 awarded to TDH and Institute at Brown for Environment and Society Graduate Research, Training, and Travel grant GR500148 awarded to KMK. The authors report no conflicts of interest.

Data availability statement

All planktic foraminiferal $\delta^{18}O$ and $\delta^{13}C$ data generated for this research will be archived at PANGAEA® - Data Publisher for Earth & Environmental Science. For the Gaussian Process code, see http://github.com/SheffieldML/GPy.

Figures

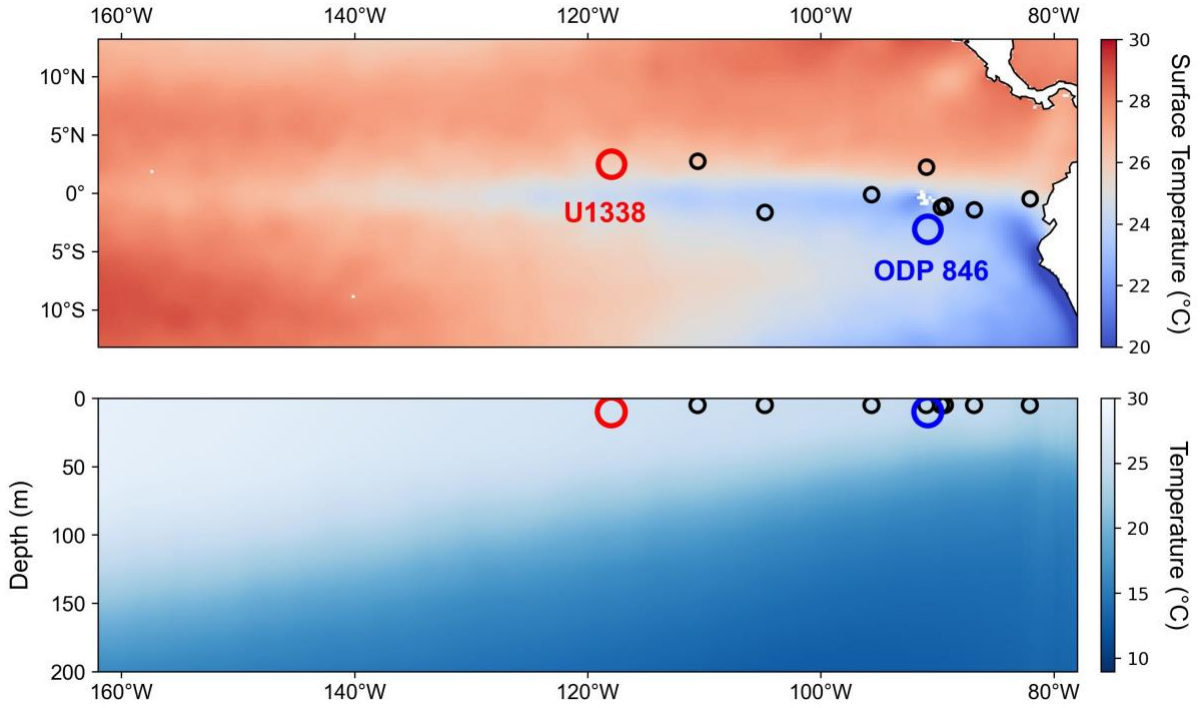

Figure 1. Location of Site 846 (blue), Site U1338 (red), and core top sites (black) in the EEP. The top panel shows modern annual mean SSTs, while the bottom panel shows thermocline depth across the EEP. Note the different color bar scales. Data are from the World Ocean Atlas 2018 (Boyer et al., 2018; Locarnini et al., 2019).

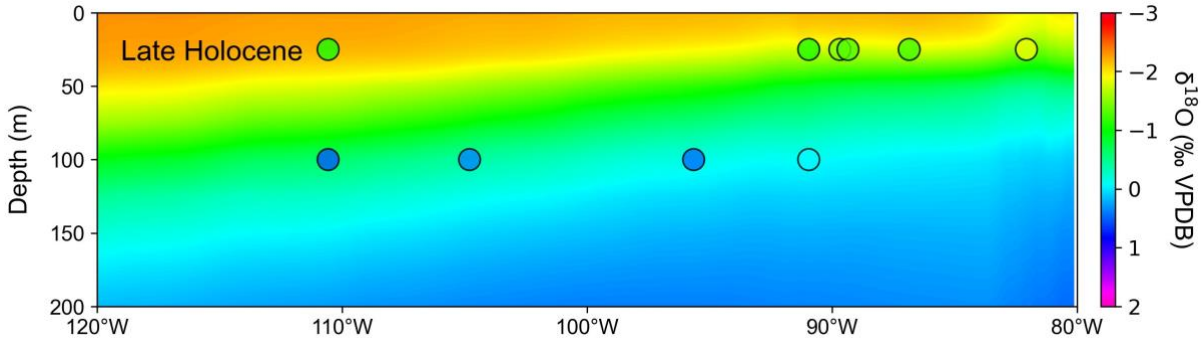

Figure 2. Modern depth profile of the EEP transect with $\delta^{18}O$ values of *T. sacculifer* and *N. dutertrei* (colored circles at water depths of 25 m = *T. sacculifer* and 100 m = *N. dutertrei*). Background colors are expected foraminiferal $\delta^{18}O$ corrected for the temperature effect using alkenone SST using the Bemis et al. (1998) equation. Temperature data are from the World Ocean Atlas 2018 (Boyer et al., 2018; Locarnini et al., 2019) and $\delta^{18}O_{seawater}$ data are from the Global Seawater Oxygen-18 Database (Bigg & Rohling, 2000; Schmidt, 1999; Schmidt et al., 1999).

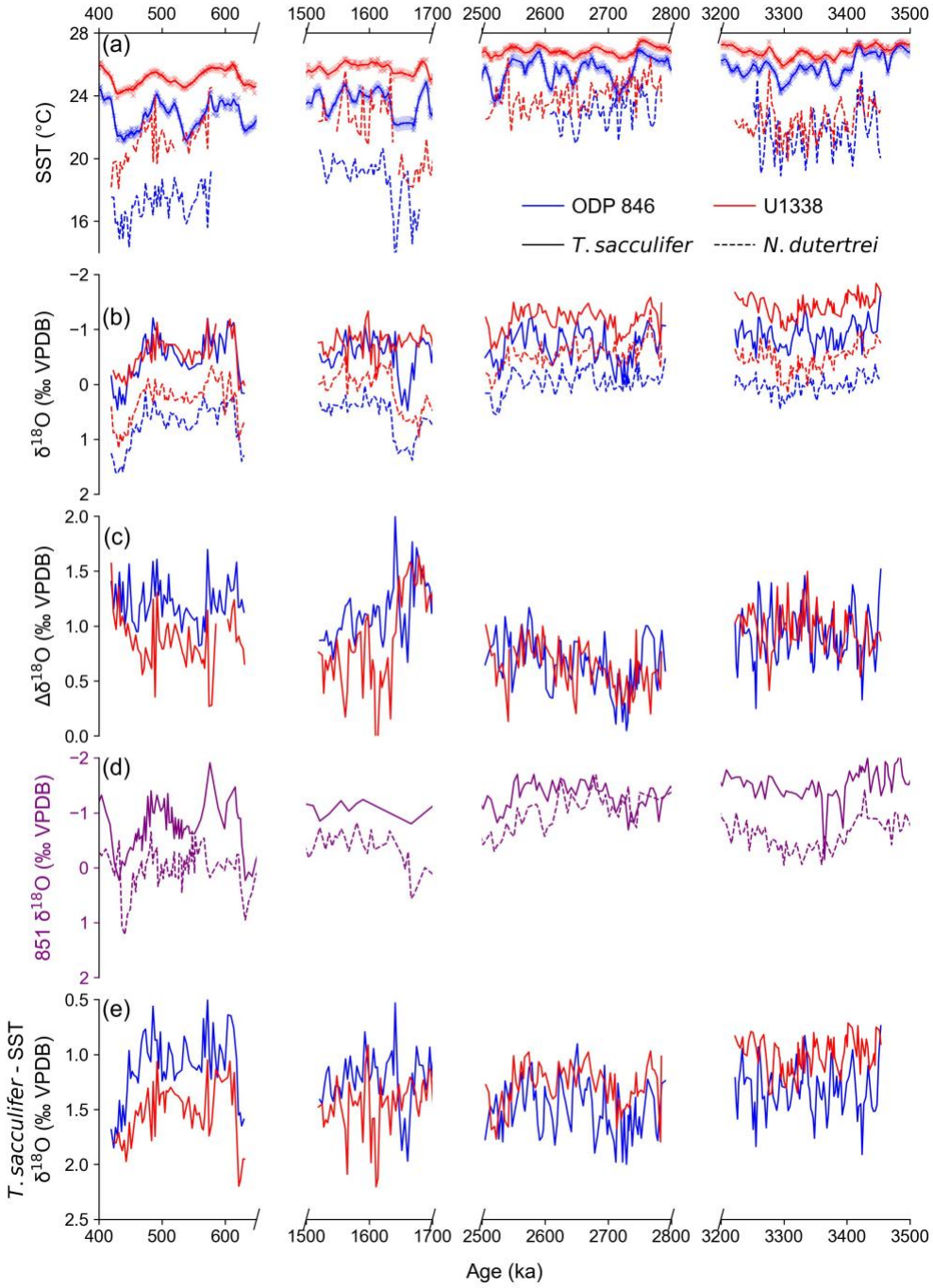

Figure 3. Time series of (a) Sites 846 and U1338 alkenone SST (solid lines) and subsurface temperature (dashed lines) estimated by converting the difference between *N. dutertrei* and *T. sacculifer* $\delta^{18}O$ to °C (1‰ $\delta^{18}O$ change = ~4.5°C) and subtracting from alkenone SST at each time step, (b) Sites 846 and U1338 *T. sacculifer* and *N. dutertrei* $\delta^{18}O$, (c) vertical $\Delta\delta^{18}O$ gradient, (d) Site 851 *T. sacculifer* and *N. dutertrei* $\delta^{18}O$, (e) and residual $\delta^{18}O$ attributed to factors other than SST, calculated by subtracting foraminiferal carbonate $\delta^{18}O$ corrected for the temperature effect using alkenone SST (Bemis et al., 1998) from measured *T. sacculifer* $\delta^{18}O$. Values that approach zero in (e) reflect a greater influence of SST in *T. sacculifer* $\delta^{18}O$ variability.

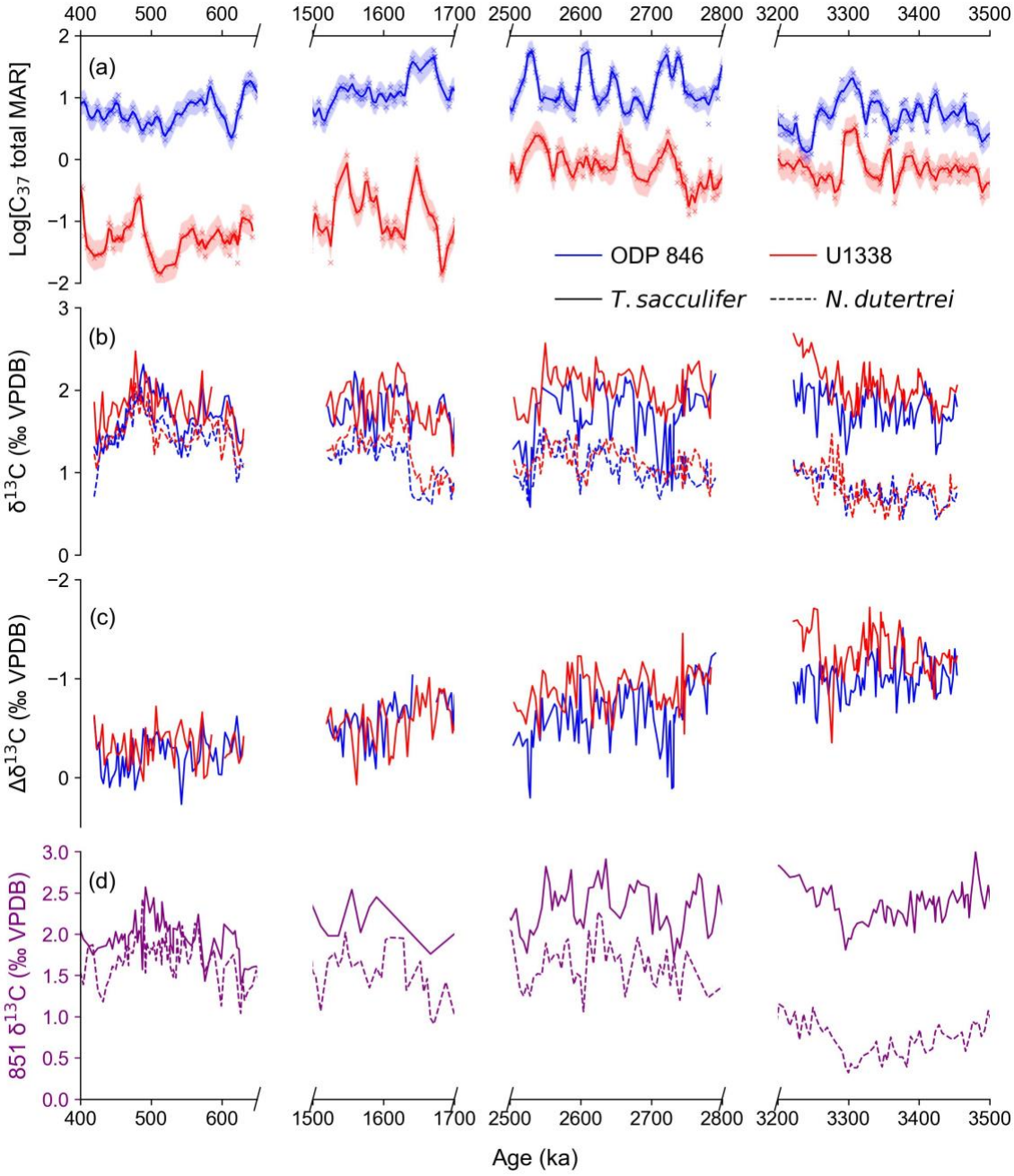

Figure 4. Time series of (a) Sites 846 and U1338 alkenone log[C_{37} total MAR], (b) Sites 846 and U1338 *T. sacculifer* and *N. dutertrei* $\delta^{13}C$, (c) vertical $\Delta\delta^{13}C$ gradient, and (d) Site 851 *T. sacculifer* and *N. dutertrei* $\delta^{13}C$.

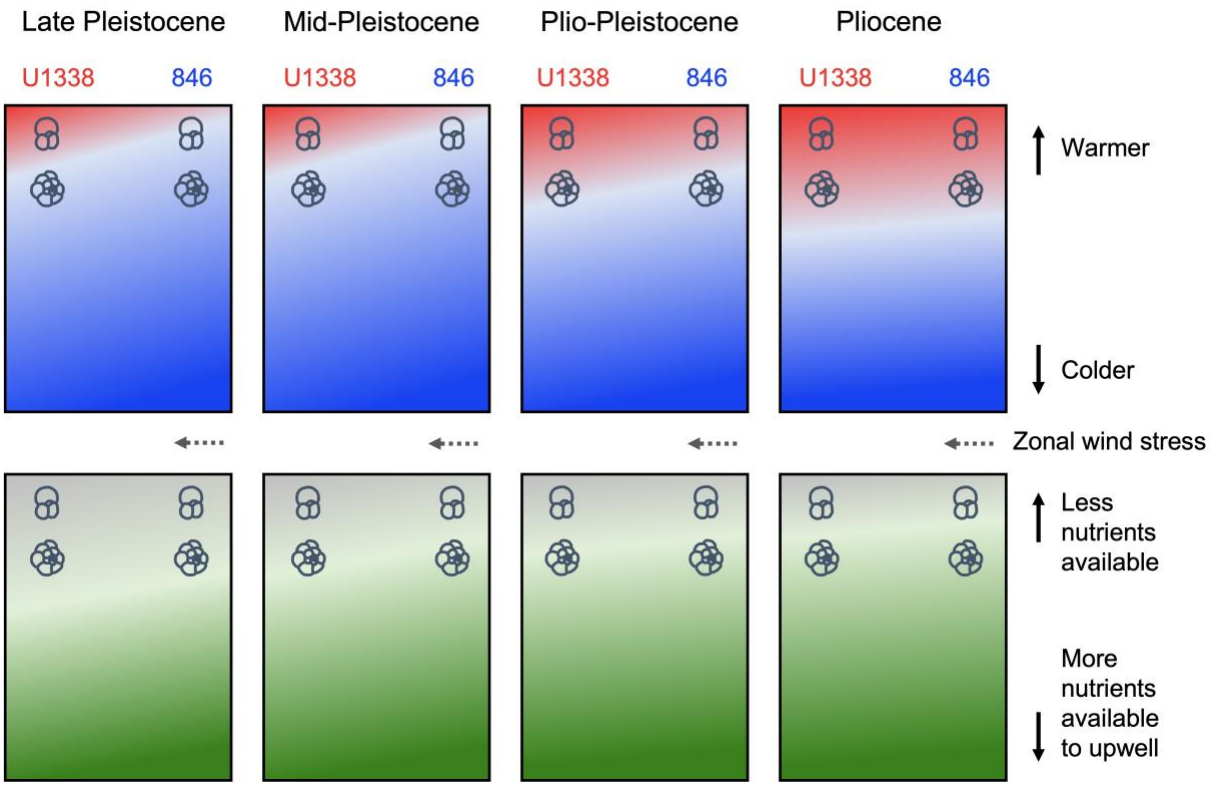

Figure 5. Depth profiles of possible thermocline (top panels) and nutricline (bottom panels) positions relative to Sites 846 and U1338 during four windows over the Plio-Pleistocene. Inferred depth habitats of *T. sacculifer* and *N. dutertrei* are indicated with foraminifera cartoons. The thermocline and nutricline were not strictly coupled and could have evolved independently, so long as they were slightly tilted to allow upwelled water to reach the EEP surface.

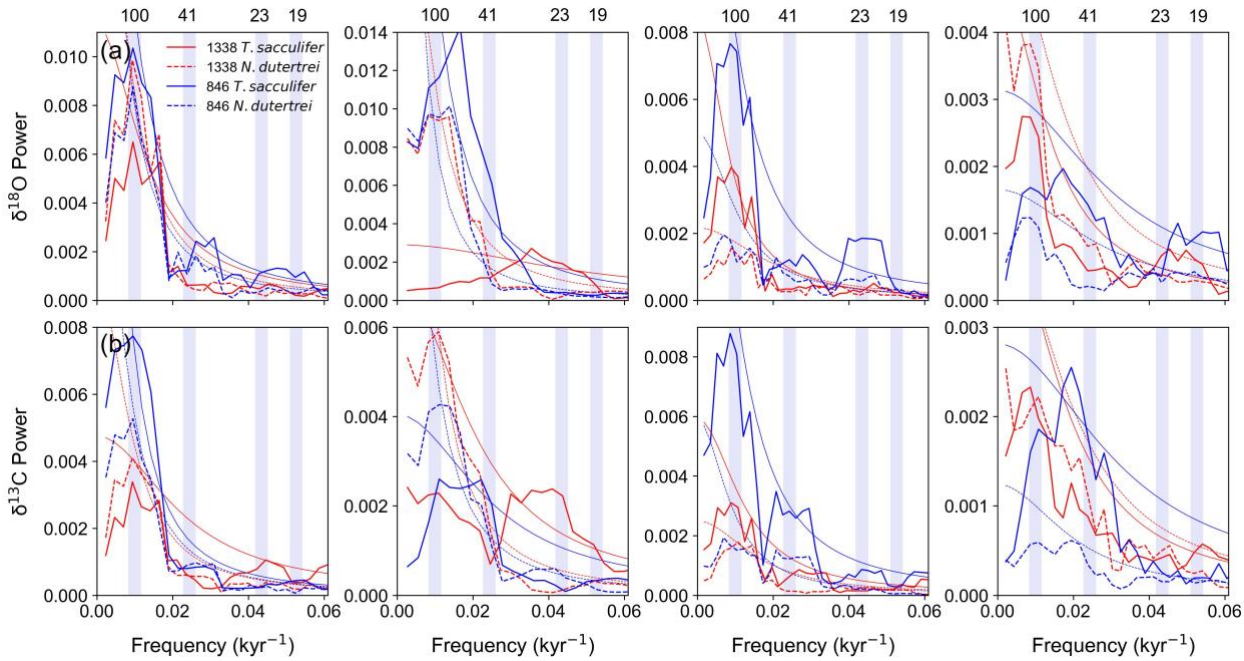

Figure 6. Power spectra of planktic (a) $\delta^{18}O$ and (b) $\delta^{13}C$ at Sites U1338 and 846 showing the influence of eccentricity, obliquity, and precession. The four paired panels reflect the four time windows analyzed in this study: the left panels show the 0.42-0.63 Ma time window, the second-to-left panels show the 1.50-1.72 Ma window, the third-to-left panels show the 2.50-2.78 Ma window, and the right panels show the 3.22-3.46 Ma window. Lavender bands represent orbital cycles at 100-kyr, 41-kyr, 23-kyr, and 19-kyr frequencies.

References

Bemis, B. E., Spero, H. J., Bijma, J., & Lea, D. W. (1998). Reevaluation of the oxygen isotopic composition of planktonic foraminifera: Experimental results and revised paleotemperature equations. *Paleoceanography*, *13*(2), 150–160. https://doi.org/10.1029/98PA00070

Bigg, G. R., & Rohling, E. J. (2000). An oxygen isotope data set for marine waters. *Journal of Geophysical Research: Oceans*, *105*(C4), 8527–8535. https://doi.org/10.1029/2000JC900005

Bolton, C. T., Gibbs, S. J., & Wilson, P. A. (2010). Evolution of nutricline dynamics in the equatorial Pacific during the late Pliocene. *Paleoceanography*, *25*(1). https://doi.org/10.1029/2009PA001821

Bolton, C. T., Lawrence, K. T., Gibbs, S. J., Wilson, P. A., Cleaveland, L. C., & Herbert, T. D. (2010). Glacial–interglacial productivity changes recorded by alkenones and microfossils in late Pliocene eastern equatorial Pacific and Atlantic upwelling zones. *Earth and Planetary Science Letters*, *295*(3–4), 401–411. https://doi.org/10.1016/j.epsl.2010.04.014

Bostock, H. C., Opdyke, B. N., & Williams, M. J. M. (2010). Characterising the intermediate depth waters of the Pacific Ocean using δ13C and other geochemical tracers. *Deep Sea Research Part I: Oceanographic Research Papers*, *57*(7), 847–859. https://doi.org/10.1016/j.dsr.2010.04.005

Boyer, T. P., García, H. E., Locarnini, R. A., Zweng, M. M., Mishonov, A. V., Reagan, J. R., Weathers, K. A., Baranova, O. K., Paver, C. R., Seidov, D., & Smolyar, I. V. (2018). *World Ocean Atlas 2018. Temperature* [Dataset]. NOAA National Centers for Environmental Information. https://www.ncei.noaa.gov/archive/accession/NCEI-WOA18

Brierley, C. M., Fedorov, A. V., Liu, Z., Herbert, T. D., Lawrence, K. T., & LaRiviere, J. P. (2009). Greatly Expanded Tropical Warm Pool and Weakened Hadley Circulation in the Early Pliocene. *Science*, *323*(5922), 1714–1718. https://doi.org/10.1126/science.1167625

Broecker, W. S., Peacock, S. L., Walker, S., Weiss, R., Fahrbach, E., Schroeder, M., Mikolajewicz, U., Heinze, C., Key, R., Peng, T.-H., & Rubin, S. (1998). How much deep water is formed in the Southern Ocean? *Journal of Geophysical Research: Oceans*, *103*(C8), 15833–15843. https://doi.org/10.1029/98JC00248

Cai, W., Santoso, A., Collins, M., Dewitte, B., Karamperidou, C., Kug, J.-S., Lengaigne, M., McPhaden, M. J., Stuecker, M. F., Taschetto, A. S., Timmermann, A., Wu, L., Yeh, S.-W., Wang, G., Ng, B., Jia, F., Yang, Y., Ying, J., Zheng, X.-T., … Zhong, W. (2021). Changing El Niño–Southern Oscillation in a warming climate. *Nature Reviews Earth & Environment*, *2*(9), 628–644. https://doi.org/10.1038/s43017-021-00199-z

Cane, M. A. (1986). *El Niño*. *14*, 43–70. https://doi.org/10.7916/D8NG518N

Cane, M. A. (1998). A Role for the Tropical Pacific. *Science*, *282*(5386), 59–61. https://doi.org/10.1126/science.282.5386.59

Cane, M. A. (2005). The evolution of El Niño, past and future. *Earth and Planetary Science Letters*, *230*(3), 227–240. https://doi.org/10.1016/j.epsl.2004.12.003

Cannariato, K. G., & Ravelo, A. C. (1997). Pliocene-Pleistocene evolution of eastern tropical Pacific surface water circulation and thermocline depth. *Paleoceanography*, *12*(6), 805–820. https://doi.org/10.1029/97PA02514

Chaisson, W. (1995). Planktonic foraminiferal assemblages and paleoceanographic change in the trans-tropical Pacific Ocean; a comparison of west (Leg 130) and east (Leg 138), latest Miocene to Pleistocene. In L. A. Mayer, N. Pisias, & T. Janecek (Eds.), *Proceedings of*

the Ocean Drilling Program, Scientific Results (Vol. 138, pp. 555–597). Ocean Drilling Program.

Claret, M., Sonnerup, R. E., & Quay, P. D. (2021). A Next Generation Ocean Carbon Isotope Model for Climate Studies I: Steady State Controls on Ocean 13C. *Global Biogeochemical Cycles*, *35*(4), e2020GB006757. https://doi.org/10.1029/2020GB006757

Dang, H., Ren, Y., Peng, N., Ma, X., Liu, F., Luo, L., Wang, Y., & Jian, Z. (2024). Long-term changes in the Western Pacific Warm Pool upper-water structure over the last 4 Ma. *Palaeogeography, Palaeoclimatology, Palaeoecology*, *651*, 112396. https://doi.org/10.1016/j.palaeo.2024.112396

de Garidel-Thoron, T., Rosenthal, Y., Bassinot, F., & Beaufort, L. (2005). Stable sea surface temperatures in the western Pacific warm pool over the past 1.75 million years. *Nature*, *433*(7023), 294–298. https://doi.org/10.1038/nature03189

Dekens, P. S., Ravelo, A. C., & McCarthy, M. D. (2007). Warm upwelling regions in the Pliocene warm period. *Paleoceanography*, *22*(3). https://doi.org/10.1029/2006PA001394

Fairbanks, R. G., Sverdlove, M., Free, R., Wiebe, P. H., & Bé, A. W. H. (1982). Vertical distribution and isotopic fractionation of living planktonic foraminifera from the Panama Basin. *Nature*, *298*(5877), 841–844. https://doi.org/10.1038/298841a0

Fedorov, A. V., Burls, N. J., Lawrence, K. T., & Peterson, L. C. (2015). Tightly linked zonal and meridional sea surface temperature gradients over the past five million years. *Nature Geoscience*, *8*(12), Article 12. https://doi.org/10.1038/ngeo2577

Fedorov, A. V., Dekens, P. S., McCarthy, M., Ravelo, A. C., deMenocal, P. B., Barreiro, M., Pacanowski, R. C., & Philander, S. G. (2006). The Pliocene Paradox (Mechanisms for a

Permanent El Niño). *Science*, *312*(5779), 1485–1489. https://doi.org/10.1126/science.1122666

Ford, H. L., Burls, N. J., Jacobs, P., Jahn, A., Caballero-Gill, R. P., Hodell, D. A., & Fedorov, A. V. (2022). Sustained mid-Pliocene warmth led to deep water formation in the North Pacific. *Nature Geoscience*, 1–6. https://doi.org/10.1038/s41561-022-00978-3

Ford, H. L., Ravelo, A. C., Dekens, P. S., LaRiviere, J. P., & Wara, M. W. (2015). The evolution of the equatorial thermocline and the early Pliocene El Padre mean state. *Geophysical Research Letters*, *42*(12), 4878–4887. https://doi.org/10.1002/2015GL064215

Gruber, N., Keeling, C. D., Bacastow, R. B., Guenther, P. R., Lueker, T. J., Wahlen, M., Meijer, H. A. J., Mook, W. G., & Stocker, T. F. (1999). Spatiotemporal patterns of carbon-13 in the global surface oceans and the oceanic suess effect. *Global Biogeochemical Cycles*, *13*(2), 307–335. https://doi.org/10.1029/1999GB900019

Haywood, A. M., Valdes, P. J., & Peck, V. L. (2007). A permanent El Niño–like state during the Pliocene? *Paleoceanography*, *22*(1). https://doi.org/10.1029/2006PA001323

Herbert, T. D. (2014). Alkenone Paleotemperature Determinations. In *Treatise on Geochemistry* (pp. 399–433). Elsevier. https://doi.org/10.1016/B978-0-08-095975-7.00615-X

Herbert, T. D., Caballero-Gill, R., & Novak, J. B. (2021). A revised mid-Pliocene composite section centered on the M2 glacial event for ODP Site 846. *Climate of the Past*, *17*(3), 1385–1394. https://doi.org/10.5194/cp-17-1385-2021

Holden, P. B., Edwards, N. R., Müller, S. A., Oliver, K. I. C., Death, R. M., & Ridgwell, A. (2013). Controls on the spatial distribution of oceanic δ$^{13}C_{DIC}$. *Biogeosciences*, *10*(3), 1815–1833. https://doi.org/10.5194/bg-10-1815-2013

Jakob, K. A., Ho, S. L., Meckler, A. N., Pross, J., Fiebig, J., Keppler, F., & Friedrich, O. (2021). Stable Biological Production in the Eastern Equatorial Pacific Across the Plio-Pleistocene Transition (~3.35–2.0 Ma). *Paleoceanography and Paleoclimatology*, *36*(4), e2020PA003965. https://doi.org/10.1029/2020PA003965

Kimble, K. M., Herbert, T. D., & Jones, C. A. (2024). Pliocene Weakening of Gradients in Temperature but Not in Productivity in the Eastern Equatorial Pacific. *Paleoceanography and Paleoclimatology*, *39*(3), e2023PA004711. https://doi.org/10.1029/2023PA004711

Lakhani, K. Q., Lynch-Stieglitz, J., & Findley, B. (2024). Reconstructing the Tropical Thermocline From Oxygen-Isotopes in Planktonic and Benthic Foraminifera. *Paleoceanography and Paleoclimatology*, *39*(8), e2023PA004794. https://doi.org/10.1029/2023PA004794

Lawrence, K. T., Liu, Z., & Herbert, T. D. (2006). Evolution of the Eastern Tropical Pacific Through Plio-Pleistocene Glaciation. *Science*, *312*(5770), 79–83. https://doi.org/10.1126/science.1120395

Lawrence, K. T., Pearson, A., Castañeda, I. S., Ladlow, C., Peterson, L. C., & Lawrence, C. E. (2020). Comparison of Late Neogene U ^{k'} $_{37}$ and TEX $_{86}$ Paleotemperature Records from the Eastern Equatorial Pacific at Orbital Resolution. *Paleoceanography and Paleoclimatology*. https://doi.org/10.1029/2020PA003858

Lea, D. W. (2003). Elemental and isotopic proxies of past ocean temperatures. In H. Elderfield (Ed.), *The Oceans and Marine Geochemistry* (pp. 365–390). Elsevier-Pergamon.

Lisiecki, L. E., & Lisiecki, P. A. (2002). Application of dynamic programming to the correlation of paleoclimate records. *Paleoceanography*, *17*(4), 1-1-1–12. https://doi.org/10.1029/2001PA000733

Lisiecki, L. E., & Raymo, M. E. (2005). A Pliocene-Pleistocene stack of 57 globally distributed benthic δ ^{18} O records: PLIOCENE-PLEISTOCENE BENTHIC STACK. *Paleoceanography*, *20*(1), n/a-n/a. https://doi.org/10.1029/2004PA001071

Liu, Z., & Yang, H. (2003). Extratropical control of tropical climate, the atmospheric bridge and oceanic tunnel. *Geophysical Research Letters*, *30*(5). https://doi.org/10.1029/2002GL016492

Locarnini, M., Mishonov, A., Baranova, O., Boyer, T., Zweng, M., Garcia, H., Reagan, J., Seidov, D., Weathers, K., Paver, C., & Smolyar, I. (2019). World Ocean Atlas 2018, Volume 1: Temperature. *A. Mishonov Technical Ed.*, *NOAA Atlas NESDIS 81*, 52 pp.

Marlow, J. R., Lange, C. B., Wefer, G., & Rosell-Melé, A. (2000). Upwelling Intensification As Part of the Pliocene-Pleistocene Climate Transition. *Science*, *290*(5500), 2288–2291. https://doi.org/10.1126/science.290.5500.2288

Meyers, S., Malinverno, A., Hinnov, L., Zeeden, C., Liu, H., & Moron, V. (2021). *astrochron: A Computational Tool for Astrochronology*. 144.

Pennington, J. T., Mahoney, K. L., Kuwahara, V. S., Kolber, D. D., Calienes, R., & Chavez, F. P. (2006). Primary production in the eastern tropical Pacific: A review. *Progress in Oceanography*, *69*(2), 285–317. https://doi.org/10.1016/j.pocean.2006.03.012

Pondaven, P., Ruiz-Pino, D., Druon, J. N., Fravalo, C., & Tréguer, P. (1999). Factors controlling silicon and nitrogen biogeochemical cycles in high nutrient, low chlorophyll systems (the Southern Ocean and the North Pacific): Comparison with a mesotrophic system (the North Atlantic). *Deep Sea Research Part I: Oceanographic Research Papers*, *46*(11), 1923–1968. https://doi.org/10.1016/S0967-0637(99)00033-3

Raja, M., & Rosell-Melé, A. (2021). Appraisal of sedimentary alkenones for the quantitative reconstruction of phytoplankton biomass. *Proceedings of the National Academy of Sciences*, *118*(2). https://doi.org/10.1073/pnas.2014787118

Rasmussen, C. E., & Williams, C. K. (2006). *Gaussian processes for machine learning* (Vol. 1, p. 159). MIT press.

Ravelo, A. C., Dekens, P., & McCarthy, M. (2006). Evidence for El Niño—Like conditions during the Pliocene. *Gsa Today*, *16*. https://doi.org/10.1130/1052-5173(2006)016<4:EFENLC>2.0.CO;2

Ravelo, A. C., & Fairbanks, R. G. (1992). Oxygen Isotopic Composition of Multiple Species of Planktonic Foraminifera: Recorders of the Modern Photic Zone Temperature Gradient. *Paleoceanography*, *7*(6), 815–831. https://doi.org/10.1029/92PA02092

Rickaby, R. E. M., & Halloran, P. (2005). Cool La Nina During the Warmth of the Pliocene? *Science*, *307*(5717), 1948–1952. https://doi.org/10.1126/science.1104666

Rippert, N., Max, L., Mackensen, A., Cacho, I., Povea, P., & Tiedemann, R. (2017). Alternating Influence of Northern Versus Southern-Sourced Water Masses on the Equatorial Pacific Subthermocline During the Past 240 ka. *Paleoceanography*, *32*(11), 1256–1274. https://doi.org/10.1002/2017PA003133

Schmidt, G. A. (1999). Forward modeling of carbonate proxy data from planktonic foraminifera using oxygen isotope tracers in a global ocean model. *Paleoceanography*, *14*(4), 482–497. https://doi.org/10.1029/1999PA900025

Schmidt, G. A., Bigg, G. R., & Rohling, E. J. (1999). *Global Seawater Oxygen-18 Database—V1.22* [Dataset]. https://data.giss.nasa.gov/o18data/

Scroxton, N., Bonham, S. G., Rickaby, R. E. M., Lawrence, S. H. F., Hermoso, M., & Haywood, A. M. (2011). Persistent El Niño–Southern Oscillation variation during the Pliocene Epoch. *Paleoceanography*, *26*(2). https://doi.org/10.1029/2010PA002097

Shaari, H. B., Yamamoto, M., Irino, T., & Oba, T. (2014). Nutricline shoaling in the eastern Pacific warm pool during the last two glacial maxima. *Journal of Oceanography*, *70*(1), 25–34. https://doi.org/10.1007/s10872-013-0209-1

Shackleton, N. J. (1987). Oxygen isotopes, ice volume and sea level. *Quaternary Science Reviews*, *6*(3), 183–190. https://doi.org/10.1016/0277-3791(87)90003-5

Shankle, M. G., Burls, N. J., Fedorov, A. V., Thomas, M. D., Liu, W., Penman, D. E., Ford, H. L., Jacobs, P. H., Planavsky, N. J., & Hull, P. M. (2021). Pliocene decoupling of equatorial Pacific temperature and pH gradients. *Nature*, *598*(7881), 457–461. https://doi.org/10.1038/s41586-021-03884-7

Shi, J., Jia, Q., Nürnberg, D., Li, T., Xiong, Z., & Qin, B. (2022). Coupled nutricline and productivity variations during the Pliocene in the western Pacific warm pool and their paleoceanographic implications. *Global and Planetary Change*, *212*, 103810. https://doi.org/10.1016/j.gloplacha.2022.103810

Spero, H. J., Mielke, K. M., Kalve, E. M., Lea, D. W., & Pak, D. K. (2003). Multispecies approach to reconstructing eastern equatorial Pacific thermocline hydrography during the past 360 kyr. *Paleoceanography*, *18*(1). https://doi.org/10.1029/2002PA000814

Thirumalai, K., Partin, J. W., Jackson, C. S., & Quinn, T. M. (2013). Statistical constraints on El Niño Southern Oscillation reconstructions using individual foraminifera: A sensitivity analysis. *Paleoceanography*, *28*(3), 401–412. https://doi.org/10.1002/palo.20037

Thomson, D. J. (1982). Spectrum estimation and harmonic analysis. *Proceedings of the IEEE*, *70*(9), 1055–1096. Proceedings of the IEEE. https://doi.org/10.1109/PROC.1982.12433

Toggweiler, J. R., Dixon, K., & Broecker, W. S. (1991). The Peru upwelling and the ventilation of the south Pacific thermocline. *Journal of Geophysical Research: Oceans*, *96*(C11), 20467–20497. https://doi.org/10.1029/91JC02063

Wang, C., Deser, C., Yu, J.-Y., DiNezio, P., & Clement, A. (2017). El Niño and Southern Oscillation (ENSO): A Review. In P. W. Glynn, D. P. Manzello, & I. C. Enochs (Eds.), *Coral Reefs of the Eastern Tropical Pacific: Persistence and Loss in a Dynamic Environment* (pp. 85–106). Springer Netherlands. https://doi.org/10.1007/978-94-017-7499-4_4

Wara, M. W., Ravelo, A. C., & Delaney, M. L. (2005). Permanent El Nino-Like Conditions During the Pliocene Warm Period. *Science*, *309*(5735), 758–761. https://doi.org/10.1126/science.1112596

Wolf-Gladrow, D. A., Riebesell, U., Burkhardt, S., & Bijma, J. (1999). Direct effects of CO2 concentration on growth and isotopic composition of marine plankton. *Tellus B*, *51*(2), 461–476. https://doi.org/10.1034/j.1600-0889.1999.00023.x

Zhang, J., & Quay, P. D. (1997). The total organic carbon export rate based on13C and12C of DIC budgets in the equatorial Pacific region. *Deep Sea Research Part II: Topical Studies in Oceanography*, *44*(9), 2163–2190. https://doi.org/10.1016/S0967-0645(97)00032-5

Supporting information

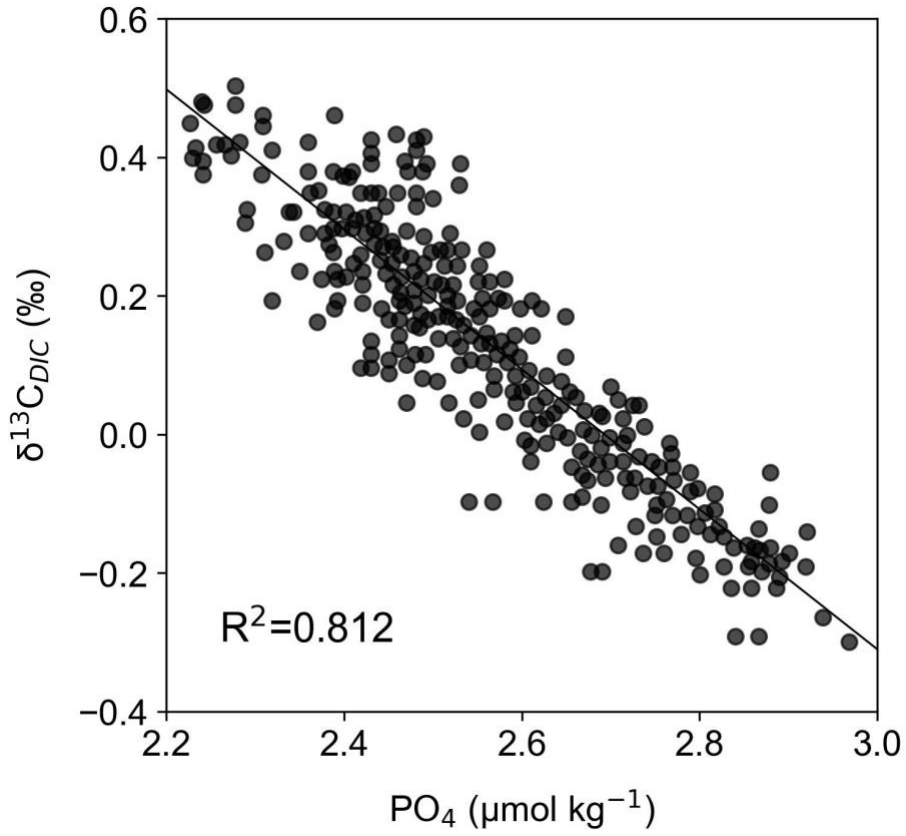

Figure S1: The strong negative correlation between phosphate nutrient concentration (PO_4) and $\delta^{13}C$ of dissolved inorganic carbon ($\delta^{13}C_{DIC}$) in modern Pacific sediments. High surface photosynthesis enriches planktic $\delta^{13}C$ and depletes nutrients like phosphate. Respiration and remineralization at depth result in more depleted planktic $\delta^{13}C$ and greater nutrient concentrations. Data are from Claret et al. (2021).

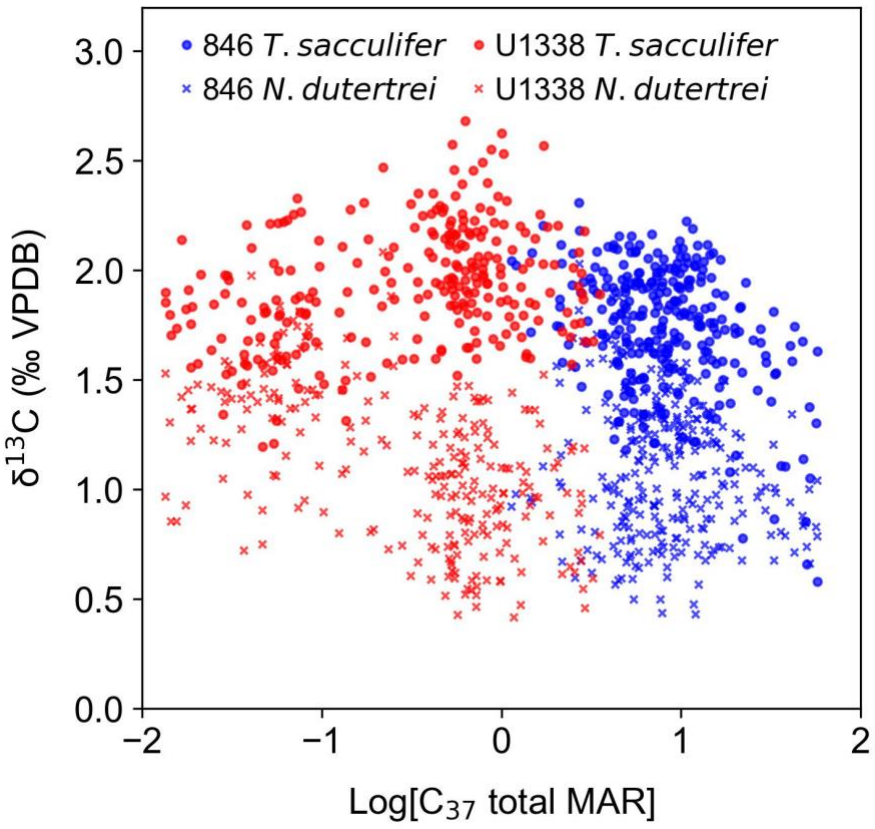

Figure S2: Correlation between log[C_{37} total MAR] and $\delta^{13}C$ of *T. sacculifer* and *N. dutertrei* from Sites U1338 and 846. In general, alkenone productivity and planktic $\delta^{13}C$ are weakly negatively correlated, indicating greater upwelling of available nutrients corresponds to higher alkenone productivity.

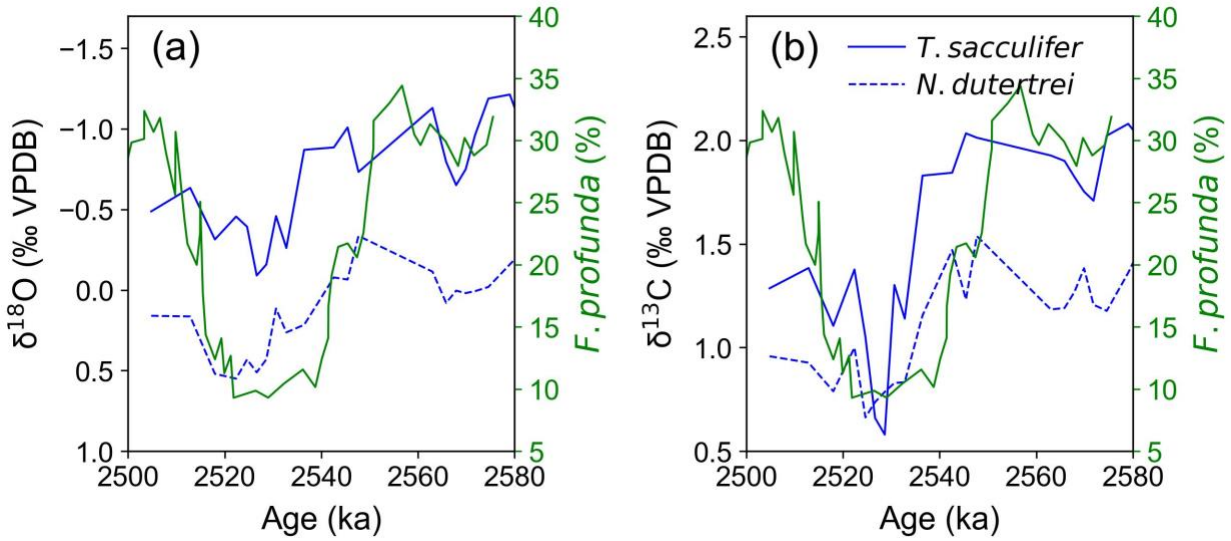

Figure S3: The abundance of the lower photic zone species *Florisphaera profunda* overlayed on (a) planktic $\delta^{18}O$ and (b) planktic $\delta^{13}C$ data from Site 846 during a window in the Early Pleistocene. The *F. profunda* and planktic isotope records are positively correlated and paced by 41-kyr cycles, suggesting that cooler glacial intervals corresponded to a shoaled nutricline and high surface productivity due to greater surface nutrient availability. Site 846 *F. profunda* abundance data are from (Bolton, Gibbs, et al., 2010).

References

Bolton, C. T., Gibbs, S. J., & Wilson, P. A. (2010). Evolution of nutricline dynamics in the equatorial Pacific during the late Pliocene. *Paleoceanography*, *25*(1). https://doi.org/10.1029/2009PA001821

Claret, M., Sonnerup, R. E., & Quay, P. D. (2021). A Next Generation Ocean Carbon Isotope Model for Climate Studies I: Steady State Controls on Ocean 13C. *Global Biogeochemical Cycles*, *35*(4), e2020GB006757. https://doi.org/10.1029/2020GB006757

CHAPTER 5

Revision of a classic: a revised benthic isotope record from the Mio-Pliocene ODP site 846

Kristin M. Kimble[1] and Timothy D. Herbert[1]

[1]Department of Earth, Environmental, and Planetary Sciences, Brown University, Providence, Rhode Island, 02912, USA.

Key Points

- Analytical offsets between preexisting and newly generated benthic isotope records are obstacles to estimates of past global climate states.
- A widely used isotope record appears to suffer significant analytical artifacts in light of newly generated stable isotopic data: carbon isotopes are consistent with new results, but oxygen isotopic values deviate significantly and unpredictably.
- The new Mio-Pliocene benthic record from Ocean Drilling Program Site 846 is consistent with most published stable isotopic data from the same time window and removes a potential large reduction in ice volume and/or deep sea temperature rise from ~5.1-5.5 Ma interpreted from the previous results at Site 846.
- Variability in the updated benthic isotope record can provide insight into global ice volume versus deep ocean temperature change during a period of warmer-than-present climate.

Abstract

Paleoceanographic records from the tropical Pacific Ocean have been instrumental in constraining past climate mean states and variability both locally and globally. Ocean Drilling Program Site 846 in the eastern equatorial Pacific yielded a stable isotope record that spanned 1.8-6.1 Ma, making it one of the longest orbitally resolved isotope records in existence. As such, it has comprised a major portion of global benthic isotope stacks. However, several considerations arose regarding the original benthic isotope record from Site 846 related to analytical advancements, reproducibility, and interspecies isotope offsets. Here we present new benthic oxygen and carbon isotope data generated from a single genus (*Cibicidoides spp.*) at Site 846 over a Late Miocene to Pliocene window (~4.0-6.2 Ma). Our updated benthic oxygen isotope record displayed a variable heavier offset relative to the original record (average +0.18‰ from 5.1-5.5 Ma but < +0.05‰ throughout the rest of the Late Miocene to Early Pliocene), but the two records' carbon isotopic values are within analytical error. At orbital scales, the newly generated oxygen and carbon isotope data agree with Site 846 variability in physical properties and alkenone-derived sea surface temperature estimates and align much better with benthic records spanning various water depths and locations globally than the previous estimates. Our revision suggests that a significant fraction of uncertainty in global isotope reconstructions could result from inter-lab analytical artifacts.

Plain language summary

Ocean sediment cores provide key records of past local and global climate change through microscopic skeletons of deep ocean organisms that recorded surrounding water temperature and chemistry when they were alive millions of years ago. One historically

important record of deep ocean oxygen and carbon isotopes comes from the eastern tropical Pacific Ocean, and it was generated in the 1990s. The record captures significant global cooling and the expansion of permanent ice sheets in the Northern Hemisphere polar regions over the last several million years. However, major advancements in analytical techniques and data reproducibility have occurred since the original oxygen and carbon isotope records were measured, so we re-analyzed geochemical signals trapped in microscopic marine skeletons from the same site and over the same time period to assess the differences between the original and new records. We found variable offsets between the old and new deep ocean oxygen isotopic records with the original record indicating a half-million-year-long interval of deep-sea warming and/or increased sea level that does not appear in the updated data. We looked to other records from around the global oceans and determined that global isotopic variability more closely resembles that captured in the new record. These offsets between the original and newly generated records serve as reminders to revisit historically important sites that influence the interpretation of global climate history.

1. Introduction

Ocean Drilling Program (ODP) Site 846 has been described as a "platinum mine" of continuous, high-resolution, non-destructive records for paleoclimate reconstructions (Mayer et al., 1992). Its location in the heart of the eastern equatorial Pacific (EEP) upwelling zone positions Site 846 to capture both tropical and extratropical changes because cold tongue waters originate in high northern and southern latitudes (Liu & Yang, 2003). Sediment recovered from Site 846 extends to the middle Miocene and tracks a period of significant global cooling (Mayer

et al., 1992). Stable isotopic reconstructions from this site trace the evolution of deep ocean temperature and global ice volume change over Mio-Pliocene cooling (Shackleton, 1987).

Several million-year-long, high-resolution paleoclimate records have been generated for Site 846, including benthic stable oxygen and carbon isotopes (Mix et al., 1995; Shackleton, Hall, et al., 1995), lithological physical properties (Hagelberg et al., 1995), and sea surface temperatures (SST; Lawrence et al., 2006, 2020). The Shackleton, Hall, et al. (1995) benthic isotope record supplied the Pliocene backbone of the Lisiecki & Raymo (2005) and Ahn et al. (2017) global $\delta^{18}O$ stacks, and thus Site 846 stable isotopic records have been influential in age model development and paleoclimate interpretations over the Plio-Pleistocene. However, some questions have been raised as to the appropriateness of the shipboard composite section used (Herbert et al., 2021), the stable isotope data reduction (Shackleton, Hall, et al., 1995), and the benthic foraminiferal interspecies isotopic offsets used to create an integrated record (Shackleton & Opdyke, 1973).

Despite its importance as a pillar of paleoceanographic climate interpretation, the Shackleton, Hall, et al. (1995) record warned of occasionally variable reproducibility, which was attributed to daily to weekly variability in vacuum line contamination. Systematic isotopic fractionation due to valve malfunctioning was also reported in Shackleton, Hall, et al. (1995), although affected data that were caught were rejected. Analytical advancements, such as sample acidification within individual sealed vessels rather than in a common acid bath, have become more widely used over the last 30 years and may yield more accurate stable isotope measurements (Swart et al., 1991). The original Site 846 stable isotope record also relied on over a dozen separate benthic species to generate a continuous record at ~2.5-kyr resolution, so it represents a splice of $\delta^{18}O$ and $\delta^{13}C$ adjusted for vital effect offsets.

If the goal of the measurements was to derive the most likely stable isotope time series on which to perform time series analysis, then it may have been justified to discard visually anomalous data that diverged from surrounding data and from replicate analyses (Shackleton, Hall, et al., 1995). However, this data reduction approach may prove too heavy-handed, and new comparisons of reduced and unreduced data would be informative.

In an effort to improve the original shipboard composite that misidentified the stratigraphy around marine isotope stage M2, Herbert et al. (2021) analyzed benthic foraminifera over equivalent intervals to Shackleton, Hall, et al. (1995) and found a 0.17‰ offset in $\delta^{18}O$ between the new data and the original record (new data heavier). They found no offset between the re-analyzed and original $\delta^{13}C$ values. Whether due to differences in analytical techniques, reproducibility issues, or data reduction methods, the offsets between $\delta^{18}O$ but not $\delta^{13}C$ records that cropped up in the Pliocene may have persisted in older samples.

We revisited the original Site 846 benthic isotope record, incorporating new splices where relevant, to assess the offset between newly generated $\delta^{18}O$ data and the original data over the time span ~4.0-6.2 Ma. We largely followed the same splices and sampled the same cores as Shackleton, Hall, et al. (1995), so offsets between records cannot be attributed to stratigraphy. One goal of this research is to investigate whether the new $\delta^{18}O$ and/or $\delta^{13}C$ data diverge from the original data over discrete time intervals or over the entire Mio-Pliocene record.

Here we present new benthic foraminiferal stable isotope data from ODP Site 846 over the >2-Myr-long interval from 4.0-6.2 Ma at ~3-kyr resolution, generated from *Cibicidoides spp.* and *Uvigerina spp*. Only 35% of the original Shackleton, Hall, et al. (1995) data were from *Cibicidoides spp.* and 45% were from *Uvigerina spp.*, while the other 20% were a mix of a dozen benthic species. Located in the EEP cold tongue but connected to high latitudes through

upwelled waters, Site 846 captured relations in surface temperature change relative to changes in deep ocean temperature, ocean circulation, and high latitude ice volume over the last several million years (Herbert et al., 2010), and an updated benthic stable isotope record addresses oceanographic questions on a global scale.

2. Methods

2.1 Oceanographic setting and chronology

ODP Site 846 (3°5.70'S, 90°49.08'W, 3,296 m water depth) sits in the heart of the EEP cold tongue, where intermediate depth Equatorial Pacific Intermediate Water delivers cool temperatures and nutrients to the surface through the EEP upwelling zone (**Figure 1**). Site 846 was cored to reconstruct the history of the biologically productive Peru Current and its interaction with the South Equatorial Current with regard to global climate change (Mayer et al., 1992). The location of Site 846 in the heart of the EEP upwelling zone accentuates its connections to high latitude and global climate (Liu & Herbert, 2004), as water that is sourced from high northern and southern latitudes upwells at Site 846. The Late Miocene through Pliocene sediments of Site 846 consist of biogenic carbonate (nannofossil ooze) and siliceous ooze (Mayer et al., 1992). Foraminifera are present in sufficient quantities for stable isotope analyses, and sedimentation rates exceeding 40 m/Myr assure high-resolution paleoclimate reconstructions that can resolve orbital variability. A continuous shipboard composite section was developed through the middle Miocene, but more recent composite revisions focused on the mid Pliocene have emphasized the importance of revisiting oceanographically important sites (Herbert et al., 2021).

The Site 846 core composite splices of Shackleton, Crowhurst, et al. (1995) and Herbert et al. (2021) were used to guide sample selection for the newly generated stable isotope data collected in the ~4.0-6.2 Ma time window. Slightly modified versions of the age-depth tunings of Lisiecki & Raymo (2005), Herbert et al. (2021), and Kimble et al. (2024) were used to assign ages to new Site 846 data. Sample labels associated with the Shackleton, Hall, et al. (1995) benthic isotope data were used to update the ages assigned by Shackleton, Hall, et al. (1995) according to the slightly modified age-depth tunings.

2.2 Stable isotope analyses

We analyzed 710 samples from holes 846B, 846C, and 846D to generate new benthic isotopic data at the Brown University stable isotope facility. The new data span the Late Miocene to Early Pliocene (~4.0-6.2 Ma). Samples were wet-sieved using a 150 μm sieve and dried at 40°C. Benthic foraminifera (*Cibicidoides spp.* and *Uvigerina spp.* but predominantly *Cibicidoides wuellerstorfi* and *Uvigerina peregrina*) were dry-sieved and picked from the 150-355 μm fraction. When sample volume was sufficient to yield enough benthic foraminifera for isotope analysis, foraminifera were preferentially picked from the 250-355 μm fraction. Foraminifera were cleaned by cracking open the tests and sonicating in 200 μL ethanol for ~30 seconds, after which excess ethanol was drawn off with a pipette. Paired analyses of cracked open versus uncracked samples (n=22) revealed that anomalously low $\delta^{13}C$ values may be attributed to non-foraminiferal carbonate within the test (**Figure S1**). All new data reported here are from foraminifera that were cracked open, sonicated for ~30 seconds, had ethanol drawn off with a pipette, and dried overnight at room temperature.

Isotope ratios were measured using a MAT253+ coupled to a Kiel IV Carbonate Device at Brown University, where the individual sample was reacted with 70°C H_3PO_4. Results are reported relative to ‰ VPDB with uncertainties of ±0.02‰ for $\delta^{13}C$ and ±0.06‰ for $\delta^{18}O$ of in-house Carrara standard (n=84, 1σ) and ±0.03‰ for $\delta^{13}C$ and ±0.05‰ for $\delta^{18}O$ of in-house BYM standard (n=52, 1σ).

When more than one foraminifera species was analyzed in the Shackleton, Hall, et al. (1995) and Herbert et al. (2021) records isotopic adjustments between each species and *Cibicidoides spp.* were calculated and applied. Although the data include analyses of many species, we limited the Shackleton, Hall, et al. (1995) data shown here to only *Cibicidoides spp.*, *Uvigerina peregrina*, and *Oridorsalis umbonatus*. The reported adjustments between species were *Uvigerina* + 0.90‰ and *Oridorsalis* + 1.00‰ for $\delta^{13}C$ values and *Cibicidoides* + 0.64‰ for $\delta^{18}O$ values (Shackleton, Hall, et al., 1995). However, based on duplicate analyses of the published Shackleton, Hall, et al. (1995) *Cibicidoides* and *Uvigerina* stable isotope data (159 paired samples), we calculated average offsets of 0.86 ± 0.26‰ (1σ) for $\delta^{13}C$ (*Cibicidoides* heavier) and 0.58 ± 0.19‰ (1σ) for $\delta^{18}O$ (*Uvigerina* heavier). Paired analyses of published *Cibicidoides* and *Oridorsalis* (n=41) yielded average offsets of 1.13 ± 0.39‰ (1σ) for $\delta^{13}C$ (*Cibicidoides* heavier) and 0.56 ± 0.24‰ (1σ) for $\delta^{18}O$ (*Oridorsalis* heavier). The species offsets between *Cibicidoides* and *Uvigerina* (n=95 paired samples) reported in Herbert et al. (2021) were similar to those calculated based on the Shackleton, Hall, et al. (1995) data: 0.97 ± 0.02‰ (1σ) for $\delta^{13}C$ (*Cibicidoides* heavier) and 0.64 ± 0.01‰ (1σ) for $\delta^{18}O$ (*Uvigerina* heavier).

This study includes new duplicate analyses of *Cibicidoides* and *Uvigerina* (n=75) spanning 4.0-6.2 Ma. The calculated species offsets were comparable to those reported in Shackleton, Hall, et al. (1995) and Herbert et al. (2021): 0.86 ± 0.26‰ (1σ) for $\delta^{13}C$

(*Cibicidoides* heavier) and 0.49 ± 0.18‰ (1σ) for $\delta^{18}O$ (*Uvigerina* heavier). We found non-negligible linear trends in the species offsets over the 4.0-6.2 Ma interval (**Figure S2**), in agreement with shifts observed in longer records where core top data required larger species adjustments relative to ~5-Myr-old downcore data (Clemens et al., 2008). At 4 Ma, 0.86‰ was added to *Uvigerina* $\delta^{13}C$, while at 6 Ma, 0.82‰ was added to *Uvigerina* to make it consistent with *Cibicidoides* $\delta^{13}C$. At 4 Ma, 0.56‰ was added to *Cibicidoides* $\delta^{18}O$, while at 6 Ma, 0.49‰ was added to *Cibicidoides* to make it consistent with *Uvigerina* $\delta^{18}O$. The same linear adjustments were applied to the Shackleton, Hall, et al. (1995) *Cibicidoides* and *Uvigerina* data over the same Mio-Pliocene interval. For the newly generated data, duplicate *Cibicidoides* values were averaged and *Uvigerina* data were not included in the $\delta^{13}C$ and $\delta^{18}O$ records shown here, so of the newly generated records only data from *Cibicidoides* are displayed.

2.3 Data sources

Physical property data (dry bulk density and reflectance) are from the Janus Web Database (Mithal & Becker, 2006). Alkenone SST and productivity (C_{37} total mass accumulation rate, MAR) data are from Herbert et al. (2021) and Lawrence et al. (2006, 2020). Other global benthic isotope records are sourced from IODP Site U1338 in the EEP (Drury et al., 2016), ODP Site 982 in the North Atlantic (Drury et al., 2018; Hodell et al., 2001), ODP Site 999 in the Gulf of Mexico (Haug & Tiedemann, 1998), ODP Site 1264 in the South Atlantic (Westerhold et al., 2020), IODP Site U1443 (Bolton et al., 2022) and IODP Site U1448 (Jöhnck et al., 2020) in the Indian Ocean, and ODP Site 1146 in the western Pacific (Holbourn et al., 2018).

3. Results

The newly generated Site 846 stable isotope data extend the revised composite record of Herbert et al. (2021) from ~4.0 Ma back to 6.2 Ma (**Figure 2**). Overall, the average offset between the new $\delta^{18}O$ data and the $\delta^{18}O$ record reported in Shackleton, Hall, et al. (1995) was within analytical error (~0.06‰ with the new data more enriched) but jumped to 0.18‰ between 5.1-5.5 Ma (the new $\delta^{18}O$ data were more enriched). Although the average offset is small, there are many instances where the records deviate significantly at the orbital scale. Notably, the new data displayed significantly lower variance over the 4.0-6.2 Myr interval (0.06 for $\delta^{13}C$ and 0.02 for $\delta^{18}O$) relative to the Shackleton, Hall, et al. (1995) stable isotope record (0.11 for $\delta^{13}C$ and 0.05 for $\delta^{18}O$; **Table 1**).

The updated $\delta^{18}O$ record does not follow the warming trend that appears in the Site 846 alkenone SST record spanning ~5.1-5.5 Ma (**Figure 3**), in contrast to the Shackleton, Hall, et al. (1995) $\delta^{18}O$ data over the same interval. Despite this long term SST warming interval that does not emerge in the new record, cooler SSTs were coincident with enriched $\delta^{18}O$ on the orbital scale (**Figure 3c**). Physical properties data including reflectance and wet bulk density did not differ significantly in the 5.1-5.5 Ma window relative to the rest of the Late Miocene through Pliocene (**Figure 4**).

There was no average offset between the updated $\delta^{13}C$ and the Shackleton, Hall, et al. (1995) record (~0.05‰ offset throughout the 4.0-6.2 Ma interval with the original data more depleted than the newly generated data). Several isotopically depleted outliers remain in the original Shackleton, Hall, et al. (1995) $\delta^{13}C$ record, and removing those points for the purpose of statistical comparison reduces the average offset between the original and new $\delta^{13}C$ record to 0.004‰ and the variance of the $\delta^{13}C$ record drops to 0.06 (equivalent to the variance of the newly generated $\delta^{13}C$ data; **Table 1**). Enriched $\delta^{13}C$ values may correspond to younger bottom

waters while depleted $\delta^{13}C$ values indicate older bottom waters that have accumulated more respired ^{12}C over time. There was no discernable trend in bottom water $\delta^{13}C$ becoming more depleted or enriched toward present, but $\delta^{13}C$ data share a stronger correlation with $\delta^{18}O$ in the newly generated record relative to the original (**Figure 2**). There is little resemblance between the alkenone productivity record and the updated $\delta^{13}C$ record at Site 846, but in general, more enriched $\delta^{13}C$ coincided with lower alkenone C_{37} total MAR (**Figure 3**).

Global benthic $\delta^{18}O$ stacks compiled by Lisiecki & Raymo (2005; LR04) and Ahn et al. (2017; Prob-stack) used the Shackleton, Hall, et al. (1995) $\delta^{18}O$ data, so comparing the two global stacks to the original Site 846 record indicates the degree to which the Site 846 data influence the average benthic stacks (**Figure 5**). As LR04 compiled only four other benthic $\delta^{18}O$ records older than 5.0 Ma (Lisiecki & Raymo, 2005), it is likely that the Site 846 data heavily influenced the early Pliocene stack. Subtracting Shackleton, Hall, et al. (1995) $\delta^{18}O$ from the $\delta^{18}O$ of the global stacks yields the residual difference between Shackleton, Hall, et al. (1995) and LR04, and Shackleton, Hall, et al. (1995) and Prob-stack, which highlights anomalies of the Site 846 data in relation to global benthic $\delta^{18}O$ compilations (**Figure 5c**). Although the LR04 record extends to only 5.3 Ma and the Prob-stack ends at 5.0 Ma, the 5.1-5.5 Ma isotope depletion presented in Shackleton, Hall, et al. (1995) appears to influence the oldest segment of the LR04 record, a feature not appearing in the newly generated Site 846 $\delta^{18}O$ data reported here.

Other benthic $\delta^{18}O$ records from around the globe display no trend in ice volume and/or deep sea temperature during the latest Miocene, except possibly Site 982 in the North Atlantic, which experienced a ~0.14‰ $\delta^{18}O$ depletion from 5.1-5.5 relative to the 4.5-5.1 Ma and 5.5-6.2 Ma intervals (**Figure 6**). Overall, a trend of enriched $\delta^{18}O$ likely indicative of increasing global

ice volume (and potentially suggesting deep water cooling) appeared by the Late Pliocene, which is consistent with Site 846 cooling as recorded by alkenone SST and global cooling prior to the intensification of Northern Hemisphere glaciation. Variability in global $\delta^{13}C$ records showed strong agreement with both the preexisting and newly generated Site 846 $\delta^{13}C$ data (**Figure 7**).

Evolutive spectral power analysis of the preexisting and updated $\delta^{18}O$ records indicated significant obliquity pacing and no significant eccentricity cycles from ~4.0-6.2 Ma (**Figure 8**). This 41-kyr pacing appears to have strengthened after 5 Ma. In comparison to the original $\delta^{18}O$ data, spectral peaks corresponding to obliquity and precession are more distinctly resolved in the new records (note that both data sets were analyzed on the same age model). Significant 41-kyr obliquity cycles were present in the updated Site 846 $\delta^{13}C$ record but were absent from the preexisting record during the Late Miocene to Pliocene interval. Many Pliocene glacial intervals (recognized by enriched $\delta^{18}O$) corresponded with more depleted $\delta^{13}C$ and older bottom water signatures (**Figure 2**).

4. Discussion

Oceanographic and climate factors that could influence benthic foraminiferal stable oxygen isotope ratios include bottom water temperature, oxygen isotopic composition of sea water, and perhaps most importantly, global ice volume and resulting sea level (Emiliani, 1955; Shackleton, 1967). Stable carbon isotopes track bottom water dissolved inorganic carbon, which can infer ocean circulation and deep water relative age in addition to carbon cycle processes (Curry & Oppo, 2005; Duplessy et al., 1988).

Explaining variable offsets between the Shackleton, Hall, et al. (1995) and newly generated $\delta^{18}O$ records from the same ODP site cannot be a matter of changing environmental

conditions, because the records were produced using the same sediments, but instead may be a sign of analytical differences. The original and updated $\delta^{13}C$ records are not statistically different, a finding supported by Herbert et al. (2021), pointing to an analytical process that affects $\delta^{18}O$ alone that would generate a ~0.17‰ mid-Pliocene offset and a ~0.18‰ Late Miocene offset. The common acid bath used to acidify carbonate samples measured in Shackleton, Hall, et al. (1995) could allow exchange between CO_2 produced in the reaction and the acid or dissolution of CO_2 in the acid, and both scenarios would preserve the "memory" of previous samples (Swart et al., 1991). Liquid nitrogen continually removed CO_2 from the common acid bath, but accumulated water may have altered $\delta^{18}O$ without affecting $\delta^{13}C$. For the sake of transparency, Shackleton, Hall, et al. (1995) mention occasional data reproducibility and instrumental issues they encountered when generating the Site 846 benthic $\delta^{18}O$ and $\delta^{13}C$ records, but affected data were rejected if caught.

Given the small number of Early Pliocene records included in LR04 (Lisiecki & Raymo, 2005), the original Site 846 $\delta^{18}O$ data exert substantial influence on the benthic stack (**Figure 5**). A revised LR04 or Prob-stack record substituting the updated $\delta^{18}O$ values for the original likely would not show Late Miocene to Early Pliocene (5.1-5.5 Ma) ice volume reduction. Benthic $\delta^{18}O$ records generated since LR04 was published indicate stable global ice volume from 5.1-5.5 Ma (**Figure 6**), lending further support to the updated Site 846 $\delta^{18}O$ record reported here (Bolton et al., 2022; Drury et al., 2016, 2018; Haug & Tiedemann, 1998; Hodell et al., 2001; Holbourn et al., 2018; Jöhnck et al., 2020; Westerhold et al., 2020). The LR04 and Prob-stack global compilations supplied age models and climate interpretations for countless studies, and the variable offset between the original and updated Site 846 $\delta^{18}O$ data is a reminder to revisit historically important isotopic records.

The reduction in global ice volume and sea level rise at 5.1-5.5 Ma recorded in the Shackleton, Hall, et al. (1995) $\delta^{18}O$ data has been used as evidence that apparent deglaciation and sea level rise predated Mediterranean flooding at the Mio-Pliocene boundary and tectonic forcings were responsible instead (van der Laan et al., 2006). Ice volume or sea level rise changes in the Late Miocene may have been smaller than previously predicted using the original Site 846 $\delta^{18}O$, calling into question Mio-Pliocene climate interpretations (van der Laan et al., 2006).

Within the global records spanning ~3.0-6.2 Ma, average $\delta^{13}C$ offsets of up to ~1‰ between sites in the North Atlantic and the EEP, for example, were consistent with Atlantic-Pacific deep water age and circulation (**Figure 7**). Surface and mixed layer water in contact with atmospheric CO_2 has isotopically enriched $\delta^{13}C$ relative to deep water because mixed layer photosynthesis removes ^{12}C. North Atlantic benthic $\delta^{13}C$ records would be expected to be isotopically enriched relative to other regions because subducting surface water transports enriched $\delta^{13}C$ water to the deep ocean (Kroopnick, 1985). As deep water travels from its source in the North Atlantic to the other deep ocean basins it accumulates respired ^{12}C and remineralized nutrients, resulting in a progressively depleted $\delta^{13}C$ signature by the time the water arrives in the EEP (Duplessy et al., 1984). Water depth also influences the global benthic isotope records because shallow sites may not reflect deep water conditions. For example, Sites 982 (water depth = 1134 m) and U1448 (water depth = 1098 m) may be bathed in intermediate water, which would make them too shallow to capture changes in deep water $\delta^{18}O$ and $\delta^{13}C$ (**Figure 1**).

5. Conclusion

Newly generated Late Miocene through Pliocene benthic foraminiferal stable isotope data from the historically important ODP Site 846 in the EEP display considerable (0.18‰) offsets in $\delta^{18}O$ values relative to the record reported in Shackleton, Hall, et al. (1995), but statistically negligible offsets in $\delta^{13}C$. The common acid bath used to acidify samples prior to analysis may have accumulated water or preserved memory from prior samples, which would have altered $\delta^{18}O$ while leaving $\delta^{13}C$ unchanged (Swart et al., 1991), but the variable nature of the 0.18‰ $\delta^{18}O$ offset indicates more intermittent disagreement. The updated Mio-Pliocene benthic record is consistent with both local and global isotope records collected from a variety of water depths, as well as reflectance and wet bulk density data generated at Site 846, arguing for coherence of various climatic signals. Site 846 SST records indicate warming from ~5.1-5.5 Ma coincident with an interval of depleted Shackleton, Hall, et al. (1995) $\delta^{18}O$, which disagree with the stable ice volume and/or deep water temperatures implied by the updated $\delta^{18}O$ record. Substituting the newly generated record for the original Shackleton, Hall, et al. (1995) data in the global benthic $\delta^{18}O$ stacks generated by Lisiecki & Raymo (2005) and Ahn et al. (2017) would substantially reduce the uncertainty in LR04 and Prob-stack. The oversized influence of Site 846 data in creating age models and interpreting paleoceanographic data emphasizes the importance of addressing analytical uncertainty. If paired with planktic stable isotope data, the updated benthic isotope record presented here can provide insight into the degree to which global ice volume versus deep ocean temperature influenced benthic $\delta^{18}O$ variability during a period of warmer-than-present global temperature (Shackleton, 1987).

Acknowledgments

This research used samples and data provided by the International Ocean Discovery Program (IODP) and its previous iterations. The authors would like to thank Steve Clemens for conceptual and technical help preparing the foraminiferal analyses. Brown University undergraduate students J. B. Novak, Veronica Gordon, Duncan Jurayi, Anjali Shah, Max Ferguson, Rocky Mattos-Canedo, Jonathan Zhao, Liam Johnson, and Claire Xu diligently prepared and picked foraminiferal samples. Funding for this research was provided by NSF grant 2202760 awarded to TDH and Brown University Undergraduate Teaching and Research Awards. The authors report no conflicts of interest.

Data availability statement

All benthic foraminiferal $\delta^{18}O$ and $\delta^{13}C$ data generated for this research will be archived at PANGAEA® - Data Publisher for Earth & Environmental Science.

Figures

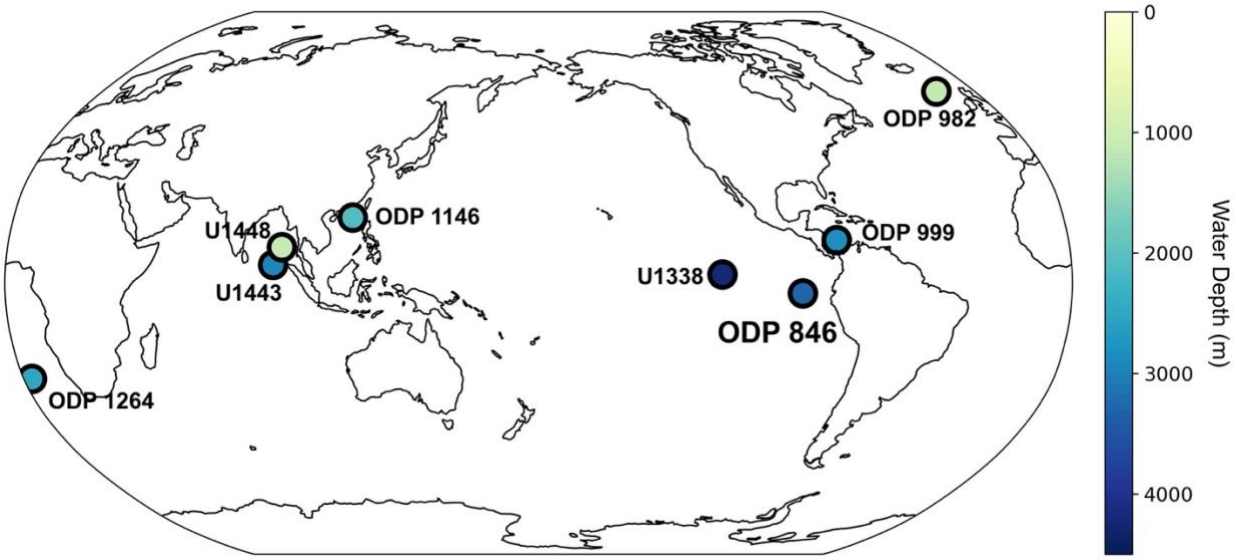

Figure 1: Location of ODP Site 846 in the EEP in relation to other ODP and IODP sites with benthic isotope records. Water depth at each site is indicated with the color scale to provide context for whether the site captures deep water masses.

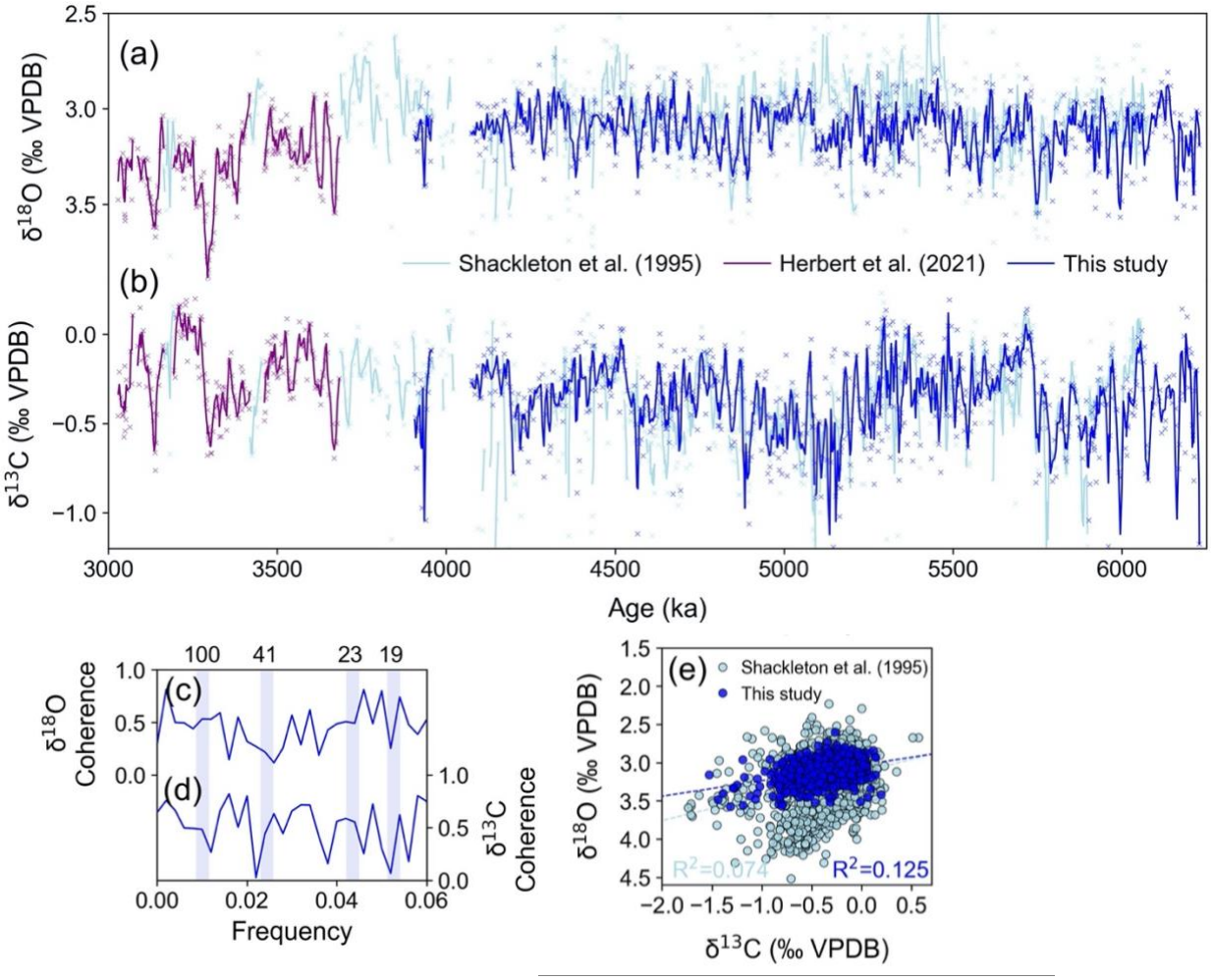

Figure 2: Time series of (a) benthic $\delta^{18}O$ and (b) benthic $\delta^{13}C$ showing the newly generated data in the context of the Shackleton, Hall, et al. (1995) data and the Herbert et al. (2021) data. The time series data are smoothed with a 6-kyr running average with original data plotted as crosses. Coherence between the Shackleton, Hall, et al. (1995) data and the updated data reported here for (c) benthic $\delta^{18}O$ and (d) $\delta^{13}C$ show general agreement between the records (lavender bands represent orbital cycles at 100-kyr, 41-kyr, 23-kyr, and 19-kyr frequencies). Correlations between (e) $\delta^{13}C$ and $\delta^{18}O$ for the Shackleton, Hall, et al. (1995) and newly generated data suggest a tighter correlation exists between the new data.

Table 1: Average, standard error, and variance calculations for the $\delta^{13}C$ and $\delta^{18}O$ records reported in Shackleton, Hall, et al. (1995) and presented here. The values in parentheses under the Shackleton, Hall, et al. (1995) $\delta^{13}C$ column represent average, standard error, and variance calculations after removing isotopically depleted $\delta^{13}C$ outliers included in the original dataset.

	Shackleton et al. (1995) $\delta^{13}C$	Shackleton et al. (1995) $\delta^{18}O$	This study $\delta^{13}C$	This study $\delta^{18}O$
4.0-6.2 Ma Average	-0.425‰ (-0.372‰)	3.041‰	-0.367‰	3.105‰
4.0-6.2 Ma Standard error	0.013‰ (0.009‰)	0.009‰	0.010‰	0.006‰
4.0-6.2 Ma Variance	0.111 (0.059)	0.053	0.061	0.020

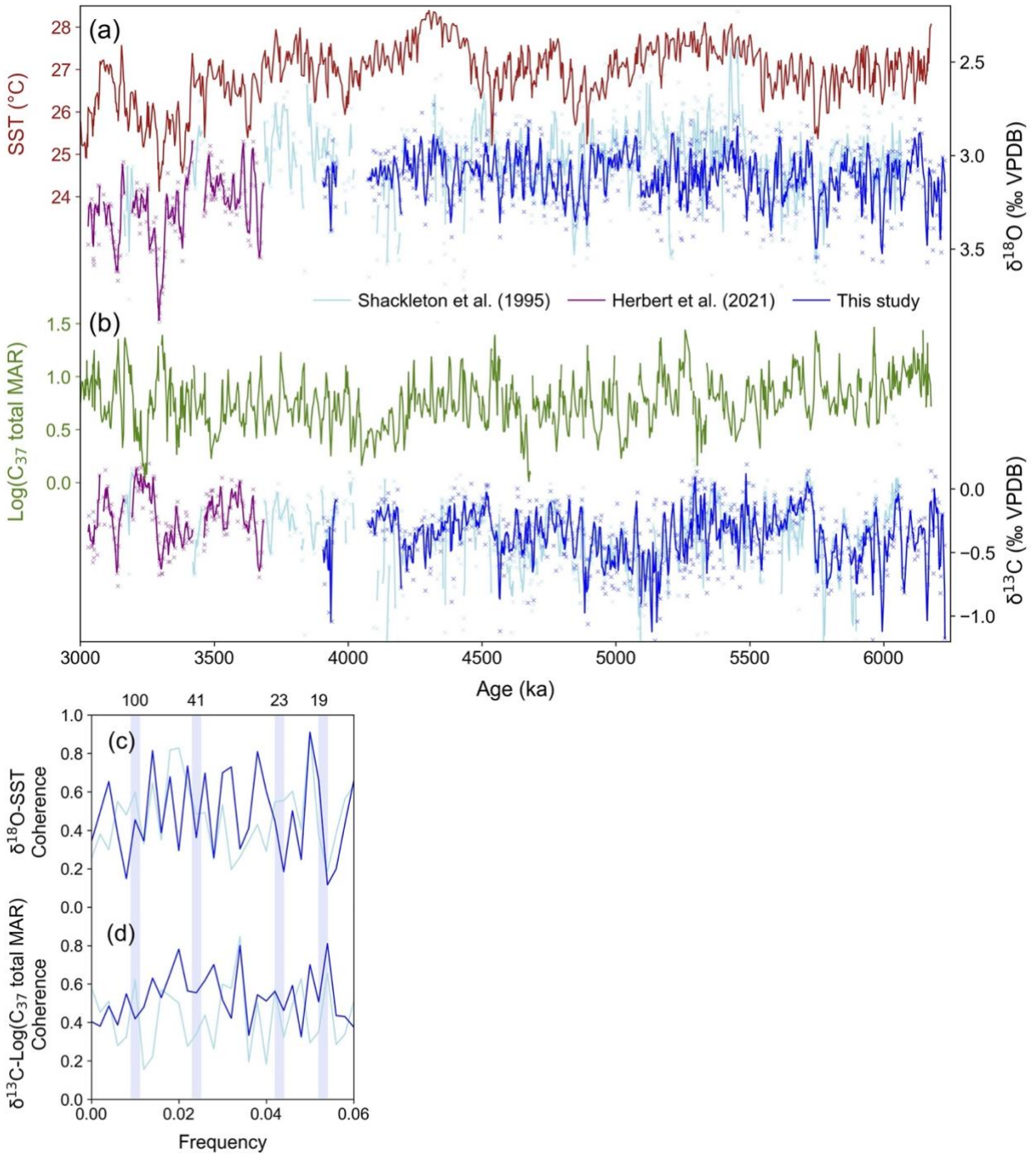

Figure 3: Time series of (a) benthic $\delta^{18}O$ relative to Site 846 SST and (b) $\delta^{13}C$ relative to alkenone productivity. Coherence between (c) SST and benthic $\delta^{18}O$ and (d) alkenone productivity and benthic $\delta^{13}C$ for the original and updated records. Benthic isotope data are smoothed with a 6-kyr running average (crosses are original data). Lavender bands represent orbital cycles at 100-kyr, 41-kyr, 23-kyr, and 19-kyr frequencies.

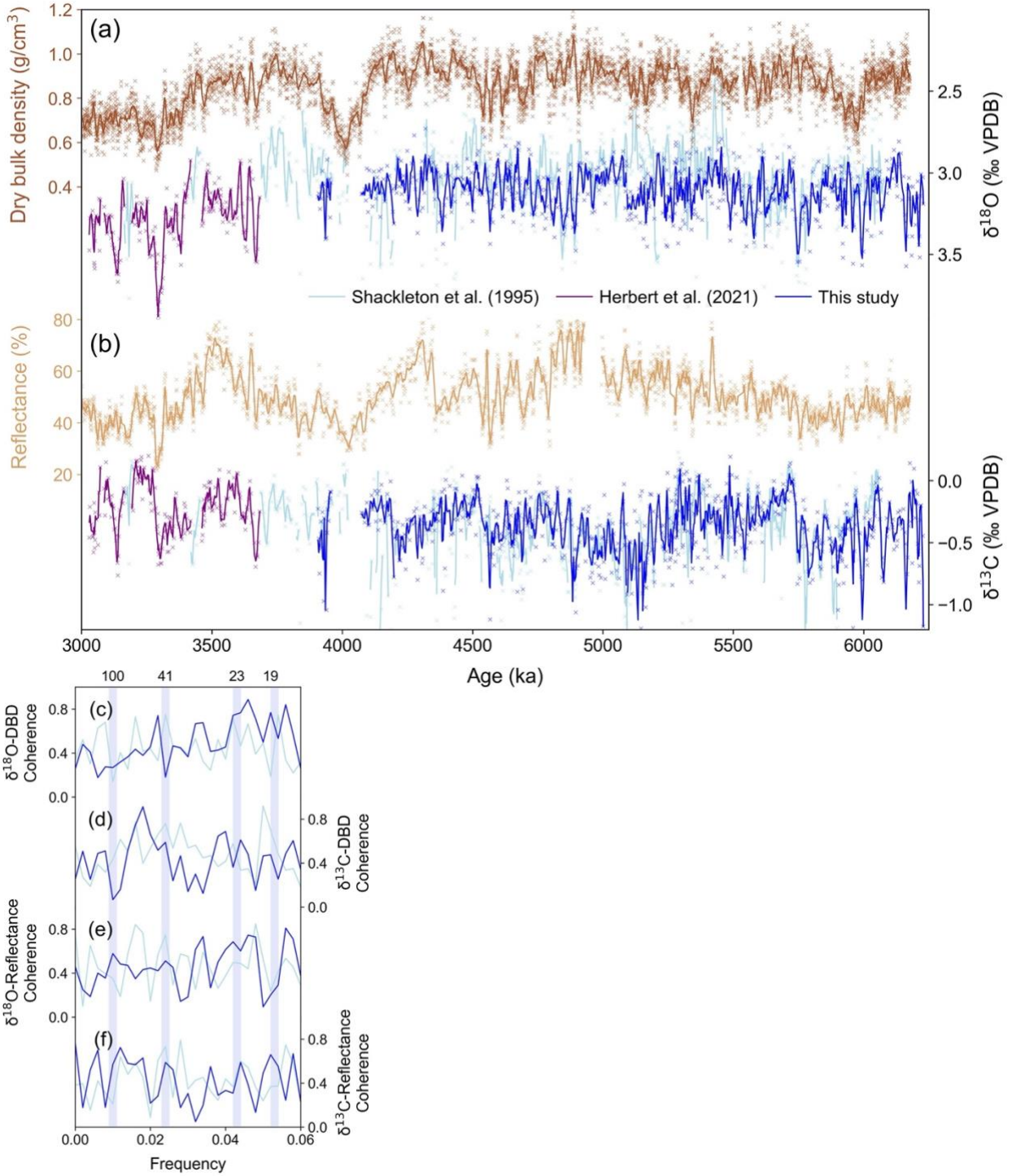

Figure 4: Time series of (a) newly generated $\delta^{18}O$ and (b) $\delta^{13}C$ records relative to the commonly measured sediment physical properties composite (a) dry bulk density (DBD) and (b) reflectance. Benthic isotope data are smoothed with a 6-kyr running average while dry bulk density and reflectance are smoothed with a 10-kyr running average (crosses are original data). Coherence between (c) DBD and benthic $\delta^{18}O$, (d) DBD and benthic $\delta^{13}C$, (e) reflectance and benthic $\delta^{18}O$, and (f) reflectance and benthic $\delta^{13}C$ for the original and updated records. Lavender bands represent orbital cycles at 100-kyr, 41-kyr, 23-kyr, and 19-kyr frequencies.

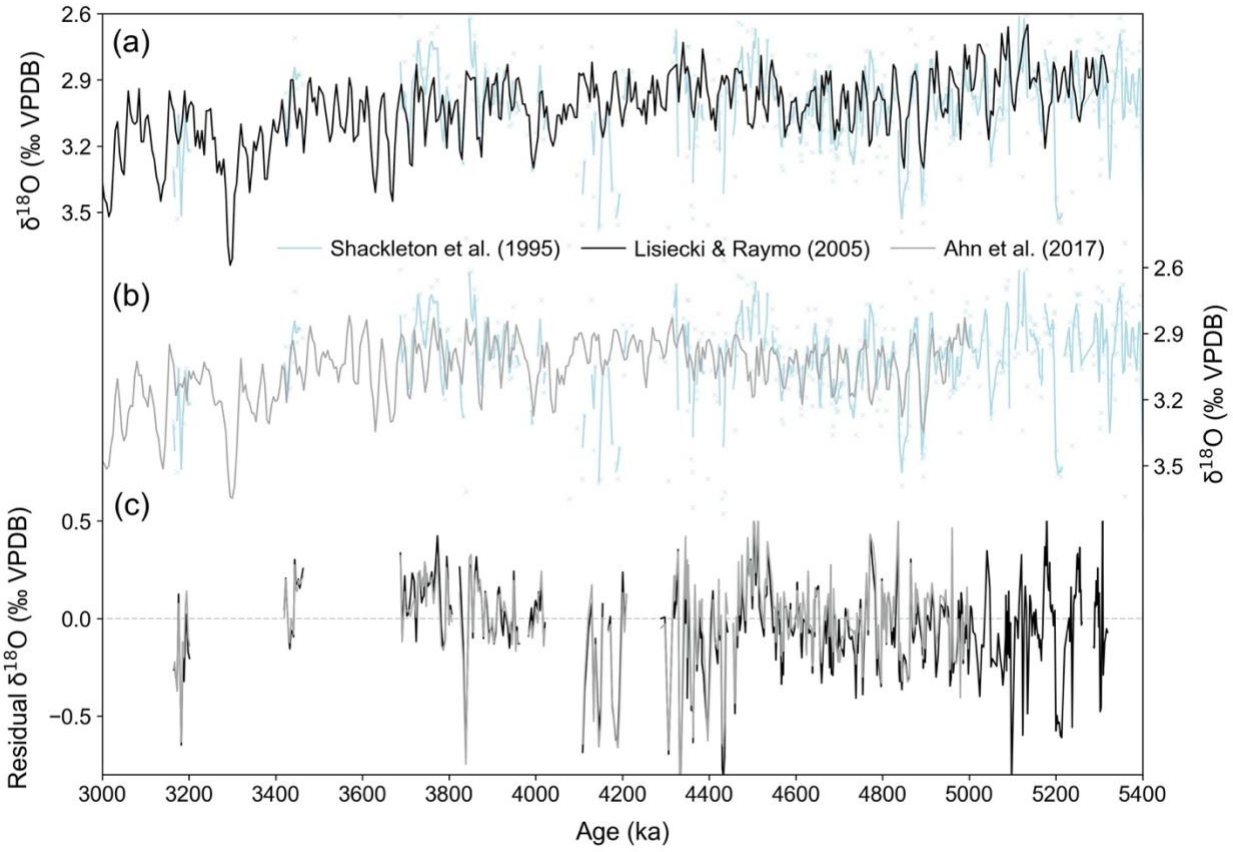

Figure 5: Time series of (a) preexisting benthic $\delta^{18}O$ data from EEP Site 846 and the LR04 global benthic $\delta^{18}O$ stack (Lisiecki & Raymo, 2005) and (b) Site 846 benthic $\delta^{18}O$ and the Prob-stack benthic $\delta^{18}O$ compilation (Ahn et al., 2017). Both benthic stacks heavily relied on the Site 846 oxygen isotope record and (c) the residual after subtracting the Site 846 $\delta^{18}O$ from the $\delta^{18}O$ of the global stacks demonstrates the relative contribution of the Shackleton, Hall, et al., (1995) record. The dashed line in (c) represents no residual. Site 846 benthic $\delta^{18}O$ data are smoothed with a 6-kyr running average (crosses are original data).

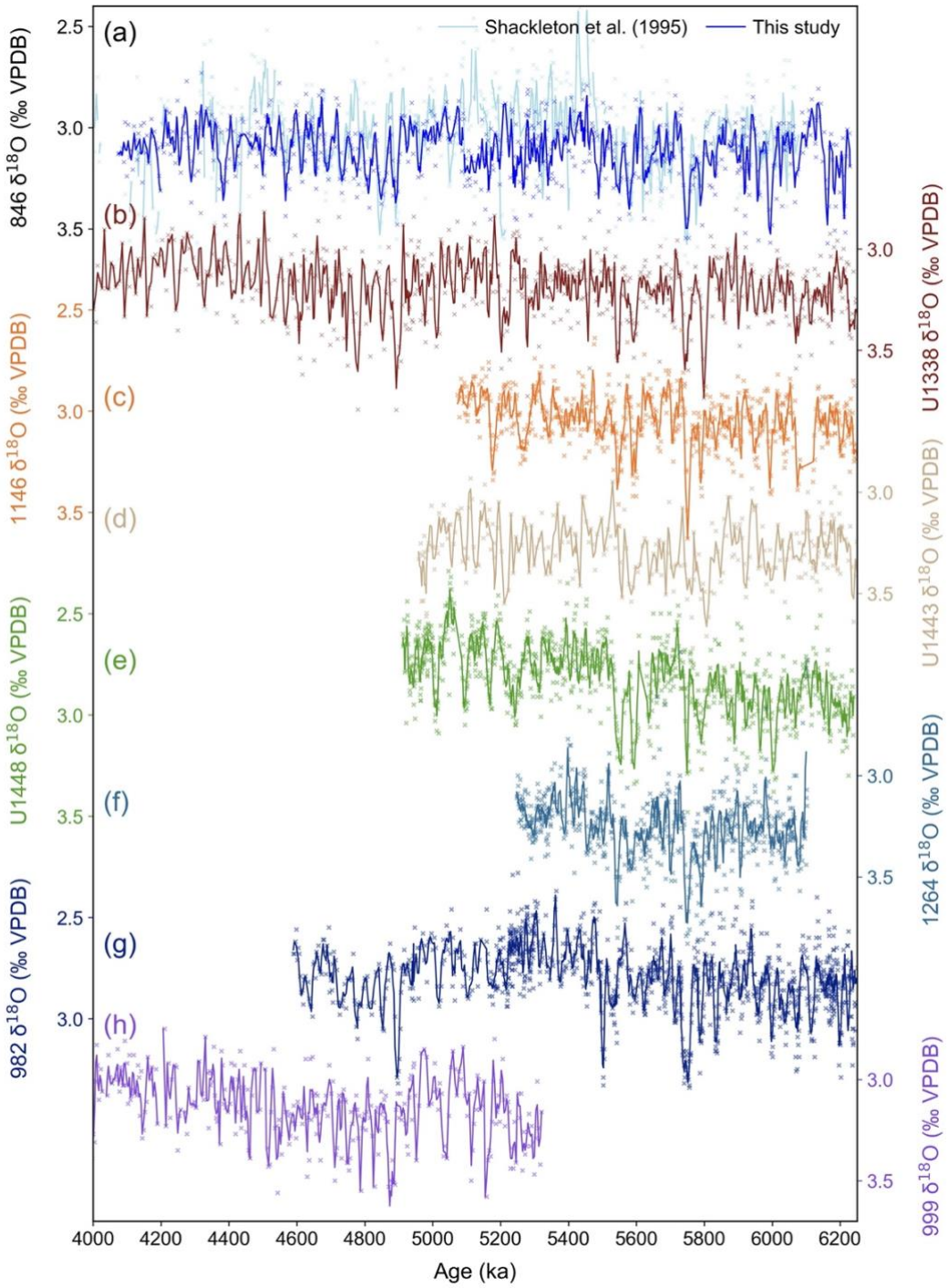

Figure 6: Time series of (a) new and preexisting benthic $\delta^{18}O$ data from EEP Site 846 relative to other benthic $\delta^{18}O$ records spanning the globe, including records from (b) IODP Site U1338 in the EEP (Drury et al., 2016), (c) ODP Site 1146 in the western Pacific (Holbourn et al., 2018), (d) IODP Site U1443 (Bolton et al., 2022), and (e) IODP Site U1448 (Jöhnck et al., 2020), in the Indian Ocean, (f) ODP Site 1264 in the South Atlantic (Westerhold et al., 2020), (g) ODP Site 982 in the North Atlantic (Drury et al., 2018; Hodell et al., 2001), and (h) ODP Site 999 in the Gulf of Mexico (Haug & Tiedemann, 1998). Benthic $\delta^{18}O$ data are smoothed with a 6-kyr running average (crosses are original data).

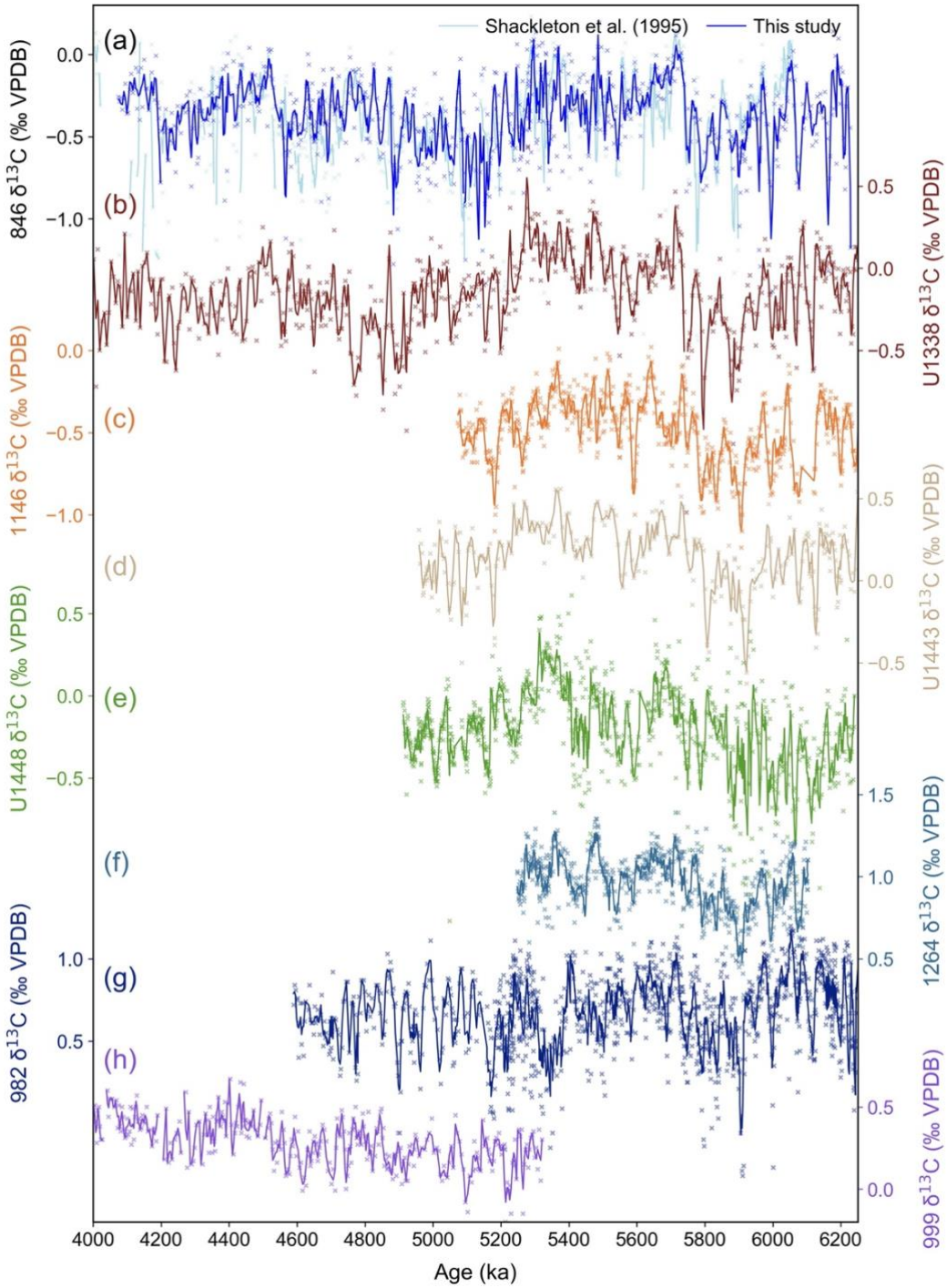

Figure 7: Time series of (a) new and preexisting benthic $\delta^{13}C$ data from EEP Site 846 relative to other benthic $\delta^{13}C$ records spanning the globe, including records from (b) IODP Site U1338 in the EEP (Drury et al., 2016), (c) ODP Site 1146 in the western Pacific (Holbourn et al., 2018), (d) IODP Site U1443 (Bolton et al., 2022), and (e) IODP Site U1448 (Jöhnck et al., 2020), in the Indian Ocean, (f) ODP Site 1264 in the South Atlantic (Westerhold et al., 2020), (g) ODP Site 982 in the North Atlantic (Drury et al., 2018; Hodell et al., 2001), and (h) ODP Site 999 in the Gulf of Mexico (Haug & Tiedemann, 1998). Benthic $\delta^{13}C$ data are smoothed with a 6-kyr running average (crosses are original data).

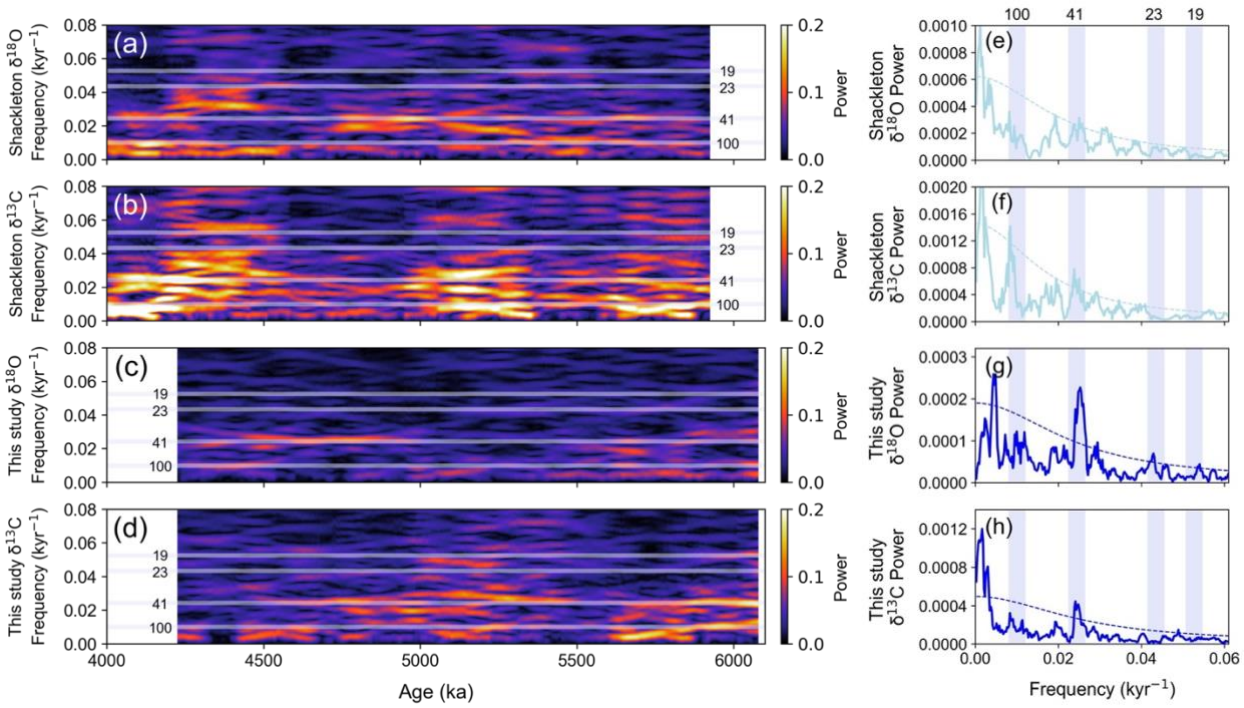

Figure 8: Evolutive power spectra from 4.0-6.2 Ma of (a) preexisting $\delta^{18}O$ and (b) $\delta^{13}C$ Site 846 data from Shackleton et al. (1995), and the new (c) $\delta^{18}O$ and (d) $\delta^{13}C$ records reported here. The right-side panels show non-evolutive power spectra of the entire 4.0-6.2 Ma records for (e) preexisting $\delta^{18}O$ and (f) $\delta^{13}C$, and updated (g) $\delta^{18}O$ and (h) $\delta^{13}C$. Lavender bands in (e-h) represent orbital cycles at 100-kyr, 41-kyr, 23-kyr, and 19-kyr frequencies. Dashed lines in (e-h) reflect the 90% confidence interval.

References

Ahn, S., Khider, D., Lisiecki, L. E., & Lawrence, C. E. (2017). A probabilistic Pliocene–Pleistocene stack of benthic δ18O using a profile hidden Markov model. *Dynamics and Statistics of the Climate System*, *2*(1), dzx002. https://doi.org/10.1093/climsys/dzx002

Bolton, C. T., Gray, E., Kuhnt, W., Holbourn, A. E., Lübbers, J., Grant, K., Tachikawa, K., Marino, G., Rohling, E. J., Sarr, A.-C., & Andersen, N. (2022). Secular and orbital-scale variability of equatorial Indian Ocean summer monsoon winds during the late Miocene. *Climate of the Past*, *18*(4), 713–738. https://doi.org/10.5194/cp-18-713-2022

Clemens, S. C., Prell, W. L., Sun, Y., Liu, Z., & Chen, G. (2008). Southern Hemisphere forcing of Pliocene δ18O and the evolution of Indo-Asian monsoons. *Paleoceanography*, *23*(4). https://doi.org/10.1029/2008PA001638

Curry, W. B., & Oppo, D. W. (2005). Glacial water mass geometry and the distribution of δ13C of ΣCO2 in the western Atlantic Ocean. *Paleoceanography*, *20*(1). https://doi.org/10.1029/2004PA001021

Drury, A. J., John, C. M., & Shevenell, A. E. (2016). Evaluating climatic response to external radiative forcing during the late Miocene to early Pliocene: New perspectives from eastern equatorial Pacific (IODP U1338) and North Atlantic (ODP 982) locations. *Paleoceanography*, *31*(1), 167–184. https://doi.org/10.1002/2015PA002881

Drury, A. J., Westerhold, T., Hodell, D., & Röhl, U. (2018). Reinforcing the North Atlantic backbone: Revision and extension of the composite splice at ODP Site 982. *Climate of the Past*, *14*(3), 321–338. https://doi.org/10.5194/cp-14-321-2018

Duplessy, J. C., Shackleton, N. J., Fairbanks, R. G., Labeyrie, L., Oppo, D., & Kallel, N. (1988). Deepwater source variations during the last climatic cycle and their impact on the global

deepwater circulation. *Paleoceanography*, *3*(3), 343–360. https://doi.org/10.1029/PA003i003p00343

Duplessy, J. C., Shackleton, N. J., Matthews, R. K., Prell, W., Ruddiman, W. F., Caralp, M., & Hendy, C. H. (1984). 13C Record of benthic foraminifera in the last interglacial ocean: Implications for the carbon cycle and the global deep water circulation. *Quaternary Research*, *21*(2), 225–243. https://doi.org/10.1016/0033-5894(84)90099-1

Emiliani, C. (1955). Pleistocene Temperatures. *The Journal of Geology*, *63*(6), 538–578. https://doi.org/10.1086/626295

Hagelberg, T. K., Pisias, N. G., Shackleton, N. J., Mix, A. C., & Harris, S. (1995). Refinement of a high-resolution, continuous elementary section for studyign equatorial Pacific Ocean paleogeanography, leg 138. *Proceedings of the Ocean Drilling Program*, *138*, 31–46. https://doi.org/10.2973/odp.proc.sr.138.1995

Haug, G. H., & Tiedemann, R. (1998). Effect of the formation of the Isthmus of Panama on Atlantic Ocean thermohaline circulation. *Nature*, *393*(6686), 673–676. https://doi.org/10.1038/31447

Herbert, T. D., Caballero-Gill, R., & Novak, J. B. (2021). A revised mid-Pliocene composite section centered on the M2 glacial event for ODP Site 846. *Climate of the Past*, *17*(3), 1385–1394. https://doi.org/10.5194/cp-17-1385-2021

Herbert, T. D., Cleaveland Peterson, L., Lawrence, K. T., & Liu, Z. (2010). Tropical Ocean Temperatures Over the Past 3.5 Million Years. *Science*, *328*, 1530–1534.

Hodell, D. A., Curtis, J. H., Sierro, F. J., & Raymo, M. E. (2001). Correlation of Late Miocene to Early Pliocene sequences between the Mediterranean and North Atlantic. *Paleoceanography*, *16*(2), 164–178. https://doi.org/10.1029/1999PA000487

Holbourn, A. E., Kuhnt, W., Clemens, S. C., Kochhann, K. G. D., Jöhnck, J., Lübbers, J., & Andersen, N. (2018). Late Miocene climate cooling and intensification of southeast Asian winter monsoon. *Nature Communications*, *9*(1), 1584. https://doi.org/10.1038/s41467-018-03950-1

Jöhnck, J., Kuhnt, W., Holbourn, A., & Andersen, N. (2020). Variability of the Indian Monsoon in the Andaman Sea Across the Miocene-Pliocene Transition. *Paleoceanography and Paleoclimatology*, *35*(9), e2020PA003923. https://doi.org/10.1029/2020PA003923

Kimble, K. M., Herbert, T. D., & Jones, C. A. (2024). Pliocene Weakening of Gradients in Temperature but Not in Productivity in the Eastern Equatorial Pacific. *Paleoceanography and Paleoclimatology*, *39*(3), e2023PA004711. https://doi.org/10.1029/2023PA004711

Kroopnick, P. M. (1985). The distribution of 13C of ΣCO2 in the world oceans. *Deep Sea Research Part A. Oceanographic Research Papers*, *32*(1), 57–84. https://doi.org/10.1016/0198-0149(85)90017-2

Lawrence, K. T., Liu, Z., & Herbert, T. D. (2006). Evolution of the Eastern Tropical Pacific Through Plio-Pleistocene Glaciation. *Science*, *312*(5770), 79–83. https://doi.org/10.1126/science.1120395

Lawrence, K. T., Pearson, A., Castañeda, I. S., Ladlow, C., Peterson, L. C., & Lawrence, C. E. (2020). Comparison of Late Neogene U ^{k'} $_{37}$ and TEX $_{86}$ Paleotemperature Records from the Eastern Equatorial Pacific at Orbital Resolution. *Paleoceanography and Paleoclimatology*. https://doi.org/10.1029/2020PA003858

Lisiecki, L. E., & Raymo, M. E. (2005). A Pliocene-Pleistocene stack of 57 globally distributed benthic δ^{18}O records: PLIOCENE-PLEISTOCENE BENTHIC STACK. *Paleoceanography*, *20*(1), n/a-n/a. https://doi.org/10.1029/2004PA001071

Liu, Z., & Herbert, T. D. (2004). High-latitude influence on the eastern equatorial Pacific climate in the early Pleistocene epoch. *Nature*, *427*(6976), Article 6976. https://doi.org/10.1038/nature02338

Liu, Z., & Yang, H. (2003). Extratropical control of tropical climate, the atmospheric bridge and oceanic tunnel. *Geophysical Research Letters*, *30*(5). https://doi.org/10.1029/2002GL016492

Mayer, L., Pisias, N., & Janecek, T. (1992). Site 846. *Proceedings of the Ocean Drilling Program, Initial Reports*, *138*, 265–333.

Mithal, R., & Becker, D. G. (2006). The Janus database: Providing worldwide access to ODP and IODP data. *Geological Society, London, Special Publications*, *267*(1), 253–259. https://doi.org/10.1144/GSL.SP.2006.267.01.19

Mix, A. C., Pisias, N. G., Rugh, W., Wilson, J., Morey, A., & Hagelberg, T. K. (1995). Benthic foraminifer stable isotope record from Site 849 (0-5 Ma): Local and global climate changes. *Proceedings of the Ocean Drilling Program, Scientific Results*, *138*, 371–412.

Shackleton, N. (1967). Oxygen Isotope Analyses and Pleistocene Temperatures Re-assessed. *Nature*, *215*(5096), 15–17. https://doi.org/10.1038/215015a0

Shackleton, N. J. (1987). Oxygen isotopes, ice volume and sea level. *Quaternary Science Reviews*, *6*(3), 183–190. https://doi.org/10.1016/0277-3791(87)90003-5

Shackleton, N. J., Crowhurst, S., Hagelberg, T., Pisias, T., & Schneider, D. A. (1995). A new late Neogene time scale: Application to Leg 138 sites. *Proceedings of the Ocean Drilling Program, Scientific Results*, *138*, 73–101. https://doi.org/10.2973/odp.proc.sr.138.1995

Shackleton, N. J., Hall, M. A., & Pate, D. (1995). *15. Pliocene stable isotope stratigraphy of site 846*. *138*, 337–355. https://doi.org/10.2973/odp.proc.sr.138.1995

Shackleton, N. J., & Opdyke, N. D. (1973). Oxygen Isotope and Palaeomagnetic Stratigraphy of Equatorial Pacific Core V28-238: Oxygen Isotope Temperatures and Ice Volumes on a 10. *Quaternary Research*, *3*(1), 39–55. https://doi.org/10.1016/0033-5894(73)90052-5

Swart, P. K., Burns, S. J., & Leder, J. J. (1991). Fractionation of the stable isotopes of oxygen and carbon in carbon dioxide during the reaction of calcite with phosphoric acid as a function of temperature and technique. *Chemical Geology: Isotope Geoscience Section*, *86*(2), 89–96. https://doi.org/10.1016/0168-9622(91)90055-2

van der Laan, E., Snel, E., de Kaenel, E., Hilgen, F. J., & Krijgsman, W. (2006). No major deglaciation across the Miocene-Pliocene boundary: Integrated stratigraphy and astronomical tuning of the Loulja sections (Bou Regreg area, NW Morocco). *Paleoceanography*, *21*(3). https://doi.org/10.1029/2005PA001193

Westerhold, T., Marwan, N., Drury, A. J., Liebrand, D., Agnini, C., Anagnostou, E., Barnet, J. S. K., Bohaty, S. M., De Vleeschouwer, D., Florindo, F., Frederichs, T., Hodell, D. A., Holbourn, A. E., Kroon, D., Lauretano, V., Littler, K., Lourens, L. J., Lyle, M., Pälike, H., … Zachos, J. C. (2020). An astronomically dated record of Earth's climate and its predictability over the last 66 million years. *Science*, *369*(6509), 1383–1387. https://doi.org/10.1126/science.aba6853

Supporting information

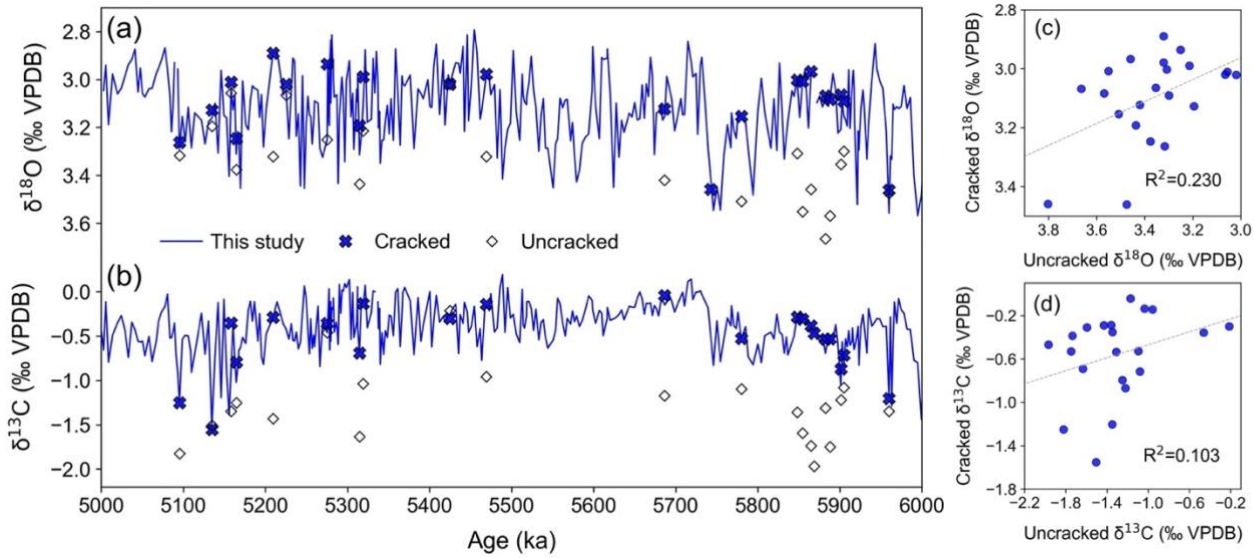

Figure S1: Time series showing benthic records of (a) $\delta^{18}O$ and (b) $\delta^{13}C$ with the uncracked (open diamonds) duplicate analyses not incorporated into the final records, which do include the cracked analyses (blue crosses). Note the anomalously depleted $\delta^{13}C$ values associated with most uncracked analyses. Correlations between uncracked and cracked foraminiferal stable isotope analyses for (c) $\delta^{18}O$ and (d) $\delta^{13}C$.

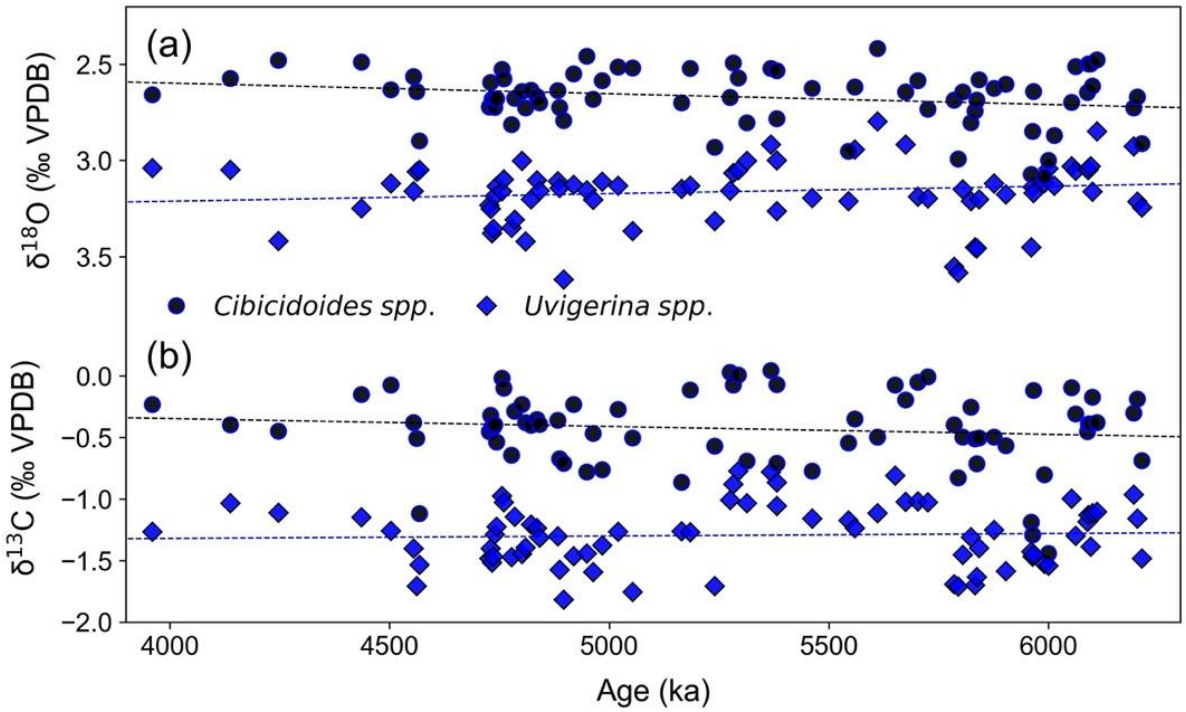

Figure S2: Linear long-term trends in (a) $\delta^{18}O$ and (b) $\delta^{13}C$ values recorded in the two benthic foraminifera species *Cibicidoides spp.* (black circles) and *Uvigerina spp.* (blue diamonds) used for Site 846 analyses. The species adjustments are smaller in the Late Miocene (*Uvigerina* $\delta^{13}C$ + 0.82‰ and *Cibicidoides* $\delta^{18}O$ + 0.49‰ at 6 Ma) relative to the Pliocene (*Uvigerina* $\delta^{13}C$ + 0.86‰ and *Cibicidoides* $\delta^{18}O$ + 0.56‰ at 4 Ma).